
8-2022

Decoding The Tumor And Immune Microenvironment In Pdac And Breast Cancer By Single Cell Sequencing.

Aislyn Schalck

Follow this and additional works at: https://digitalcommons.library.tmc.edu/utgsbs_dissertations



Part of the [Genomics Commons](#)

Recommended Citation

Schalck, Aislyn, "Decoding The Tumor And Immune Microenvironment In Pdac And Breast Cancer By Single Cell Sequencing." (2022). *Dissertations and Theses (Open Access)*. 1197.
https://digitalcommons.library.tmc.edu/utgsbs_dissertations/1197


This Dissertation (PhD) is brought to you for free and open access by the MD Anderson UTHealth Houston Graduate School at DigitalCommons@TMC. It has been accepted for inclusion in Dissertations and Theses (Open Access) by an authorized administrator of DigitalCommons@TMC. For more information, please contact digcommons@library.tmc.edu.

Decoding the Tumor and Immune Microenvironment in PDAC and Breast Cancer by Single Cell Sequencing.

by

Aislyn Schalck, BS

APPROVED:



Nicholas Navin, PhD
Advisory Professor



Ken Chen, PhD



Simona Shaitelman, MD



Cullen Tanaguchi, MD, PhD



Jennifer Wargo, MD

APPROVED:

Dean, The University of Texas

MD Anderson Cancer Center UTHealth Graduate School of Biomedical Sciences

Decoding the Tumor and Immune Microenvironment in PDAC and Breast Cancer by Single Cell Sequencing.

A

Dissertation

Presented to the Faculty of

The University of Texas

MD Anderson Cancer Center UTHealth

Graduate School of Biomedical Sciences

In Partial Fulfillment

Of the Requirements

For the Degree of

Doctor of Philosophy

by

Aislyn Schalck, BS

Houston, TX

August, 2022

Acknowledgements

Throughout graduate school and the completion of the work in this dissertation, I have received a great deal of support and assistance.

First, I would like to thank the graduate school for being so supportive of its students. This is not the case at all schools, but it makes all the difference. Second, I would like to thank my advisor Dr. Nicholas Navin for accepting me into his laboratory and providing invaluable expertise and mentorship. I will forever be grateful for the trust and support you gave me to pursue projects that suited my interests and ideas.

Next, I would like to thank all members of the Navin Lab for making graduate school such a friendly and collaborative environment. In particular, I would like to thank Anna for her mentorship and generosity when I first rotated in the lab. Also, Shanshan, Tran, Jiahong, and Min for their assistance with data acquisition and processing for these projects. I am endlessly grateful for the help you gave me. Finally, I would like to thank Emi for her nonsense as a friend and her no-nonsense as a mentor. Words can't express how much you helped me.

Additionally, I would like to thank my past and current thesis committee and rotational advisors (Dr. Beth Mittendorf, Dr. Keith Baggerly, Dr. Ken Chen, Dr. Simona Shaitelman, Dr. Cullen Tanaguchi, Dr. Jennifer Wargo, and Dr. Jeffrey Chang). Your supportive, yet critical advice and mentorship was pivotal in helping me develop in to the scientist I am today.

Furthermore, I would like to thank my collaborators on the projects in this dissertation and others. Dr. Don Sakellariou-Thompson, my co-author on the PDAC project, and Dr. Chantale Bernatchez, the project's main advisor; thank you for the substantial work you did on this project and for allowing me to collaborate on it. I could not have asked for better collaborators. Also, Dr. Simona Shaitelman who is the driving force behind the radiotherapy work. Thank you for trusting me with the precious samples from your trial, and basically mentoring me as your own grad student. I am so grateful

to be working with you.

Also, I'd like to thank all of the clinicians, pathologists, and clinical staff who made acquiring these samples possible. Moreover, I am so thankful for the generous contributions of the patients who participated in and contributed their tissue for these studies, knowing their contribution would be to help others and not necessarily themselves.

Because nothing is worthwhile without friends and family to share it with, I'd like to thank my lab friends Charissa, Alex, Naveen, Darlan, et al. for the endless sarcasm and shenanigans. Also, I'd like to thank my dog-friends (i.e. friends with dogs) for giving me a hobby and community outside of work. Likewise, I'd like to thank my dogs (Arwen, Parti, and Gimli) and previous foster-dogs (Bindi, Tre, Guster, et al.) for their unconditional love and happiness, and only eating my homework once.

To my parents, sister, grandparents and other family members. I have missed you all these years, and I know you have missed me. I suspect most of you have not understood a single word I've said about my work, but you always supported me nonetheless. I never doubted that you are proud of me for being the first in our family to go to graduate school, and for all I do and all that I am. As promised, this degree cost you \$0.

To my kids, Za'Kari, Zamarion, and Sa'Niyah: You certainly didn't make this finish any faster, but you made doing it worthwhile. I will love and remember and miss you forever.

Finally, I want to thank my wife, Judy Hsiang, for her unconditional support every step of the way. Out of everyone who helped me, you are the one I could not have done it without. This is your accomplishment as much as mine.

Decoding the Tumor and Immune Microenvironment in PDAC and Breast Cancer by Single Cell Sequencing

Aislyn Schalck, BS

Advisory Professor: Nicholas Navin, PhD

This work utilizes single cell RNA sequencing to identify transcriptional populations and gene changes for the purpose of immune-related cancer therapies. First we have characterized the T cell populations of the normal and malignant human pancreas. Furthermore, we utilized single cell TCR sequencing to track transcriptional states of T cell clones from human PDACs into a T cell culture product for adoptive cell therapy. Second, we examined the potential role of radiotherapy in inducing an immune response in hormone receptor positive breast tumors.

Table of Contents

Approval Page	i
Title Page	ii
Acknowledgements	iii
Abstract	v
Table of Contents	vi
Background	1
Chapter 1: T cell populations in PDACs and their culture for adoptive cell therapy	3
Introduction	3
Results	5
Acquisition of T cell scRNAseq data	5
Single Cell T cell clustering	6
T cell cluster characteristics	6
Relative Abundance of T cell populations	13
T cell population abundance by sample type	15
Trajectory-inferred relationship between T cell populations	16
Intra-sample co-occurrence of T cell populations	19
Transcriptional and clonal relationships of T cell populations	20
TCR expansion by cell state	22
TCR overlap by cell state	22
Grown clusters	23
TCR analysis in Grown clusters	26
T cell populations expanded by TIL culture	27
Discussion	29
Methods	30
Patient sample accrual	30
Sample preparation for sequencing	31
TIL culture reagents	31
Expansion of TIL from tumor samples	31

Single-cell RNA/TCR sequencing.....	32
Single-cell data processing and filtering.....	33
Data integration, dimension reduction	33
CD4/CD8 classification, clustering, and marker identification.	34
Pseudotime trajectory analysis	34
Re-assignment in cycling cultured cells	34
TCR analysis and clonotype re-assignment.....	35
Chapter 2: The effects of radiotherapy on the tumor microenvironment in hormone receptor positive breast cancer.....	36
Introduction	36
Results.....	38
Single Cell Characterization Before and After Radiotherapy	38
Changes in T cell populations with therapy.....	39
Changes in myeloid populations with radiotherapy.....	40
Cellular response to radiation in tumor cells.....	41
Clonal selection of DNA copy number sub clones	42
Radiotherapy and DNA damage	43
Clonal selection and the TME	44
Discussion	45
Methods	48
Sample preparation for single cell sequencing.....	48
Single cell RNA and TCR sequencing	48
Single cell RNA data processing.....	49
Single cell RNA TCR analysis.....	49
Single cell copy number sequencing.....	50
Single Cell Copy Number Data Processing and Filtering.....	50
Copy Number subclone clustering and analysis.....	50
Future directions.....	51
Appendices	54
References.....	72
Vitae.....	87

List of Figures

Figure 1.01: UMAP embedding by cluster.....	5
Figure 1.02: Top CD4 population markers.....	6
Figure 1.03: CD4 population marker expression.....	7
Figure 1.04: Fraction PDCD1 expression by cluster and tissue.....	8
Figure 1.05: Top CD8 population markers.....	9
Figure 1.06: CD8 population marker expression.....	10
Figure 1.07: Top cycling population markers.....	12
Figure 1.08: Combined population composition by cohort.....	13
Figure 1.09: Frequencies composition by sample.....	14
Figure 1.10: Frequencies composition by population and tissue	15
Figure 1.11: Patient-matched population frequency	16
Figure 1.12: CD8 Trajectory Map.....	17
Figure 1.13: CD4 Trajectory Map.....	19
Figure 1.14: T cell population correlation frequency	20
Figure 1.15: CD8 circos plot	21
Figure 1.16: CD4 circos plot	21
Figure 1.17: Clonal T cell composition	22
Figure 1.18: CD8 TCR overlap by population	23
Figure 1.19: Grown T cell UMAP.....	24
Figure 1.20: Markers of grown T cell populations.....	25
Figure 1.21: TCR overlap in grown populations.....	26
Figure 1.22: Cell state transition from fresh to grown.....	27
Figure 1.23: Change in clonotype frequency	28
Figure 2.00: Study Overview.....	37
Figure 2.01: Changes in T cell populations with radiotherapy.....	38
Figure 2.02: UMAP of macrophages.....	40
Figure 2.03: Genes expression changes in tumor cells.....	41
Figure 2.04: GSEA cancer hallmarks.....	42

Figure 2.05: Clonal Selection of tumor cells.....	43
Figure 2.06: Number of copynumber breakpoints.....	44
Figure 2.07: Immune fraction post-treatment.....	45
Figure A1.01: UMAP by cohort.....	54
Figure A1.02: CD4 transcription factors.....	54
Figure A1.03: CD8 transcription factors.....	54
Figure A1.04: T cell genes	55
Figure A1.05: Checkpoint genes.....	55
Figure A1.06: Single cell heatmap	56
Figure A1.07: CD4 TCR overlap.....	56
Figure A1.08: Gini index by cluster	57
Figure A1.09: Gini index CD4/CD8.....	57
Figure A1.10: Grown single cell heatmap	58
Figure A2.01: UMAP by major cluster.....	59
Figure A2.03: UMAP by timepoint	59
Figure A2.02: UMAP by patient.....	59
Figure A2.04: UMAP by inferred ploidy.....	59
Figure A2.05: Frequency of major clusters.....	60
Figure A2.06: Frequency of major immune clusters.....	60
Figure A2.07: T cell marker heatmap	61
Figure A2.08: CD4 density	62
Figure A2.09: T cell cluster frequency	62
Figure A2.10: T cell cluster UMAP	63
Figure A2.11: Change in T cell genes.....	63
Figure A2.13: TCR presence	63
Figure A2.12: T cell GSEA	63
Figure A2.14: Top macrophage marker heatmap.....	64
Figure A2.15: Change in myeloid populations.....	65
Figure A2.16: Change in macrophage frequency.....	65
Figure A2.17: Frequency of macrophage populations	65

Figure A2.18: HLA class II expression	66
Figure A2.19: Tumor receptor expression	66
Figure A2.20: Tumor KI67	66
Figure A2.21: DNA damage pathways	67
Figure A2.22: Single cell copynumber profiles	68
Figure A2.23: Single cell copynumber changes	69
Figure A2.24: Selection group expression differences	70
Figure A2.25: Selection group GSEA	70
Figure A2.26: IRDS signature	71
Figure A2.27: IRDS marker genes	71

Background

Therapies directing a patient's immune system to produce and sustain an anti-tumor response have revolutionized the cancer therapy landscape of the past decade. Though it has long been known that the immune system plays a critical role in anti-tumor response¹, the relatively recent successes of immune-related therapies in many cancers has increasingly created a demand for understanding and utilizing the tumor microenvironment states involved in response and resistance to both immune-based and other therapies.

To this end, biomolecules in immune checkpoint blockade (ICB) are used clinically to assist prevention of the immune system shutting off before complete tumor eradication.^{2,3,4,5} Furthermore, adoptive and chimeric antigen receptor (CAR) T cell therapies are used to increase T cell killing of the tumor by exogenous means. Despite the enormous successes of these therapies, responses are heterogeneous with success disproportional among cancer patients and between cancer types. This efficacy discrepancy stresses the need for identifying tumor characteristics indicative of a patient's response. To this end, T cell infiltration, tumor antigen load, and respective checkpoint expression are helpful, but far from perfect predictive biomarkers for immune-based therapy efficacy.^{6,7,8}

To this end, immunohistochemistry, flow cytometry, and bulk RNA-sequencing have long been used to further identify microenvironment cell populations. However, these technologies are not without limitations. Immunohistochemistry and flow cytometry are limited to profiling only a handful of proteins on the same cell. Though modern time-of-flight cytometry techniques can increase the simultaneous profitable panel size to hundreds of markers, *a priori* marker panel creation is still required.⁹ To remedy this bias, the global gene profiling ability of bulk RNA sequencing is appealing. However, bulk sequencing techniques are unable to examine markers at a cellular level, and are thus unable to deconvolute the considerable heterogeneity of transcriptomic states within

immune cell types.¹⁰

Recently, the introduction of single cell RNA sequencing (scRNAseq) has transformed the field of tumor microenvironment profiling.¹¹ Though not without its own challenges (such as gene drop out, high batch effects and high, but improving, cost per cell), scRNAseq addresses many of the limitations of previous cell state profiling techniques by profiling total gene expression at a cellular resolution.¹²⁻¹⁶ With the advent and commercialization of micro droplet-based scRNAseq, and the establishment of single cell atlas initiatives seeking to profile many tissues in large numbers of patients, there has been an explosion of scRNAseq cell type and cell state identifying studies.¹⁷⁻²⁷ These studies have not only aided in the discovery of new immune cell populations, but also expanded and clarified transcriptional markers and relationships for known immune cell states.^{18, 19, 28-30} Furthermore, longitudinal single cell studies have identified specific immune populations and their predictive relationships to therapy response.³¹⁻³³

Due to a lack of universal markers, studying tumor cell expression with bulk RNAseq data has long been a challenge due to the presence of transcripts from stromal and immune cells in the tumor microenvironment (TME).^{34, 35} Though computational deconvolution methods have assisted with this issue, scRNAseq has proven an unparalleled tool in identifying the diverse expression states of tumor cells seen within and between patients. Additionally, scRNAseq has contributed to the ability to trace how tumor cells respond and adapt to therapy providing data suggesting mechanisms of therapy resistance.³⁶⁻⁴⁰

Here we utilize single cell genomics to untangle the tumor ecosystem in the context of two tumor types and immune-related therapies in human patients. First, we examine the transcriptional landscape of T cells in Pancreatic Ductal Adenocarcinoma (PDAC) and determine which populations are favorable for an adoptive cell therapy (ACT) product. Second, we investigate the potential role of radiotherapy to induce an immune response in hormone receptor positive breast cancer.

Chapter 1: T cell populations in PDACs and their culture for adoptive cell therapy

Introduction

Pancreatic ductal adenocarcinoma (PDAC) is a nearly universally fatal tumor type and is the fourth-highest cause of cancer-related death in the United States.⁴¹ Treatment options for this cancer are severely limited and primarily consist of surgery and intense chemotherapy. However, most patients are not eligible for surgery and those that are often experience relapse.^{42,43} The unmet clinical need of this patient population has spurred efforts to expand therapeutic options.

Immunotherapy represents an exciting new therapeutic strategy, in part due to the success of immune checkpoint blockade in melanoma, lung cancers, and renal cell carcinoma.^{2,3,4,5} However, immune checkpoint blockade has seen limited clinical benefit in PDAC thus far, and it is thought that PDACs low T cell infiltration will remain a challenge for using ICB alone in this tumor type. Furthermore, adoptive transfer of T cells engineered to express chimeric antigen receptors (CAR-T) have found success in other, particularly hematologic and highly immunogenic, cancers.^{44,45} Unfortunately, CAR-T therapy has also failed to meet clinical endpoints due to the difficulty of finding a tumor-specific antigen target present across large groups of patients.^{46,47} Understanding the deficiencies from these therapies, it is possible that increasing a patient's anti-tumor lymphocyte count with T cells that recognize a patient's specific tumor antigens could overcome ICB and CAR-T therapy limitations in PDAC. For this reason, here we study an adoptive cell therapy (ACT) product from tumor infiltrating lymphocytes (TIL) for potential clinical use in future studies.

Since the 1980's it's been shown that biopsy-extracted TIL can be expanded ex vivo in high dose IL-2, and reinfused autologously into patients to successfully eliminate their solid tumors.⁴⁸ This form of ACT has been particularly successful in the settings

of metastatic melanoma, where ACT has proven the ability to reduce tumor burden across organ sites, including the bone and the brain, and lead to long-term durable responses through immune surveillance. Later on, the discovery that non-myeloablative lymphodepletion prior to reinfusion could significantly enhance responses, partially due to depleting existing Tregs, and lead to renewed interest in the field.^{49, 50} Furthermore, advances in TIL rapid expansion protocols (REP) have improved the feasibility of creating an infusion product quickly and from few initial TIL.⁵¹ Because of these successes, clinical trials of TIL therapy are currently underway in a variety of tumor types including: TNBC, NSCLC, ovarian, colorectal, and PDAC.

TIL therapy is potentially beneficial for many patients, but as the field expands and diversifies its tumors and protocols, it is critical to understand precisely which populations of T cells from the patient are successfully growing in the infusion product and attacking the tumor post-reinfusion.

Thus far, it appears that less differentiated T cells (such as early memory/effector T cells) are a beneficial population to target in TIL therapy because they persist long term after re-infusion.^{52, 53} However, TIL from early memory populations are usually less likely to be recognizing tumor antigen than other, more differentiated TIL in the microenvironment.⁵³ Unfortunately, these TIL are often found to be more exhausted in the TME, potentially terminally, making them vulnerable to slower proliferation and cell death despite re-stimulation.⁵⁴⁻⁵⁶ Due to this conundrum, as REP protocols advance it will be important to rigorously recognize (at time of biopsy and afterwards) the phenotype of a TIL, if any, which can reactivate, recognize, expand, attack, and persist.

The success of immune based therapies often relies on the nature of immune cells in the tumor to begin with. In fact, presence of TIL has been correlated with better prognosis in a variety of cancers, including PDAC.^{57,58} However, presence alone does not necessarily signify effect. Suppression by regulatory T cells (Tregs) or attenuation of cytotoxic function by entering a dysfunctional state have been identified as mechanisms of tumor immune escape.^{59,60} Conversely, TIL populations such as tissue-resident

memory-like T cells (T_{RM}) have been identified as important for response or improved survival.^{29,61,62} These populations are often defined by a complex combination of surface markers and transcriptional states. T cell repertoire analysis can also provide insight, given that expansion of T cell clones at the tumor site can indicate an immune response and high-frequency clones have been found to be the tumor-reactive clones.⁶³ To profile these heterogeneous populations of T cells, we rely here on combined scRNA and TCR sequencing.

Our goal is to characterize the T cell landscape in PDAC by profiling a large number of patients. Additionally, to be able to identify patients from whose tumor an ACT product can be successfully cultured, it is necessary to understand which T cell populations in the tumor the culture is derived from. To better understand the source of the TIL product, we track T cell clones from tumor to culture product by utilizing their T cell receptor sequence.

Results

Acquisition of T cell scRNAseq data

To identify the transcriptomic landscape of states of T cells in the human pancreas, we performed combined, single cell RNA and TCR sequencing on the T cells from 7 PDAC tumors (cohort MDA1). Additionally, we combined our dataset with the T cells from two external pancreatic scRNAseq cohorts. The first of these cohorts (MDA2), consisted of T cells from 26 PDAC lesions and 10 samples of T cells from PDAC-adjacent, “uninvolved” tissue. The second

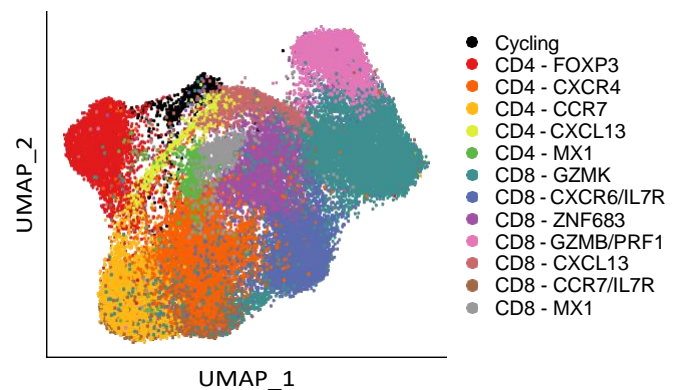


Figure 1.01: UMAP embedding by cluster
Single T cells from all cohorts in 2D UMAP labeled by transcriptional population.

external cohort (PUMCH, published in Peng *et al*) consisted of T cells from 24 PDAC samples and from “normal” pancreas in 11 patients without a PDAC diagnosis. Combining these 3 cohorts, we obtained scRNAseq data on a total of 39,694 T cells from 57 PDAC, 11 uninvolved, and 11 normal samples.

Single Cell T cell clustering

Single cell sequencing across samples is known to be highly sensitive to batch effects. To minimize this confounder we distributed samples into six groups stratified by cohort and size and performed batch integration (see methods). Post-integration samples and cohorts were evenly intermixed in UMAP embedding (Figure A1.01). Clustering of the integrated data revealed 13 pan-sample transcriptional clusters of T Cells; 7 CD8 cluster, 5 CD4 clusters, and

1 cycling cluster (Figure 1.01). Differential expression analysis was performed between clusters within the CD4 and CD8 populations, and the clusters were annotated by top marker genes from this analysis (Figure 1.02, 1.05, A1.06).

T cell cluster characteristics

Many of the clusters closely match single cell T cell clusters described in literature. Each cluster’s transcriptional expression characteristics (Figure 1.02), purported status/

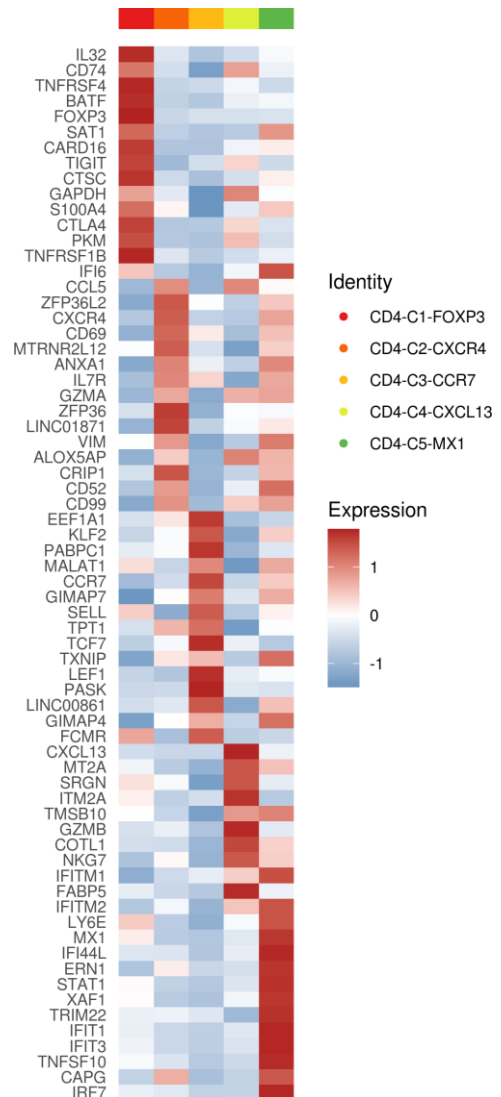


Figure 1.02: Top CD4 population markers
Scaled, average expression of top marker genes for each of the CD4 T cell populations in fresh tumor/pancreas samples.

function, and externally published references are described in detail below. Note that here “expression” refers to gene transcription, not necessarily protein expression.

CD4-FOXP3

Expressing IL2RA (CD25), CD4, several T cell checkpoints, transcription factors IKZF2 (Helios) and IKZF4 (Ikaros), and the authoritative marker FOXP3 (Figure A1.02), this population is with little doubt pro-tumor, regulatory T cells (Tregs).^{64, 65} This population not only matches populations described as Tregs in many other single cell studies, but also the Treg phenotype long established by immunophenotyping techniques long before the existence of single cell transcriptomics. Additionally, Tregs have extensively been confirmed to be present in PDAC and thus were expected to be found prior to this study.⁵⁷

CD4-CXCR4

This CD4 population exhibits several characteristics of CD4 helper T cells, such as expression of the granzyme GZMA and cytokine CCL5.^{66,67} Additionally, this population expresses early activation marker CD69 and lymphocyte migration marker CXCR4. However, low overall expression of both established Th1 and Th2 transcription factors *TBX21* (*Tbet*) and *GATA3* made T-helper cell subtype classification unclear

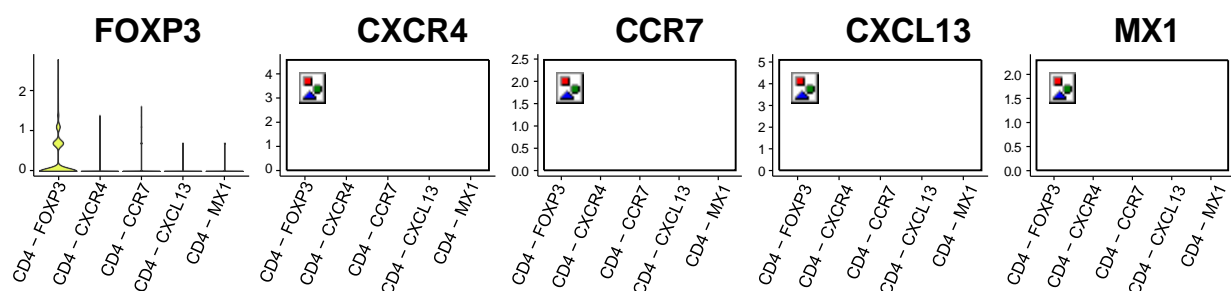


Figure 1.03: CD4 population marker expression
Relative expression of population naming marker genes in the CD4 populations. Plots are colored by mean expression as a percent of maximum expression for each gene

(Figure A1.02). This is somewhat unsurprising because scRNAseq data has recently been challenging the simplicity of the classic Th1 and Th2 helper T cell polarization. Additionally, this population does not consistently match helper T cells from other scRNAseq tumor studies.^{30, 68}

CD4-CCR7 & CD8-CCR7/IL7R

These populations express lymph node homing receptors and canonical Naïve/ Central Memory T cell (Tcm) markers CCR7 and SELL (L-selectin). Additionally, these populations both express the stemness and long-term persistence transcription factors TCF7 (TCF1) and LEF1 characteristic of Naïve and Tcm T cells (Figure 1.02, 1.05). Similar CCR7/SELL/TCF7/LEF1 expressing populations have been discovered almost ubiquitously in single cell studies of PDAC and other tumor types. However, the population with this same phenotype is conflictingly described as “Naïve”, “Central Memory”, or “Naïve/Central Memory” across studies.³⁰ This inconsistent nomenclature is likely due to the lack of definitive markers known to separate Naïve and Tcm cell states, other than the PTPRC isoforms (CD45RA on naïve, and CD45RO on Tcm cells) which

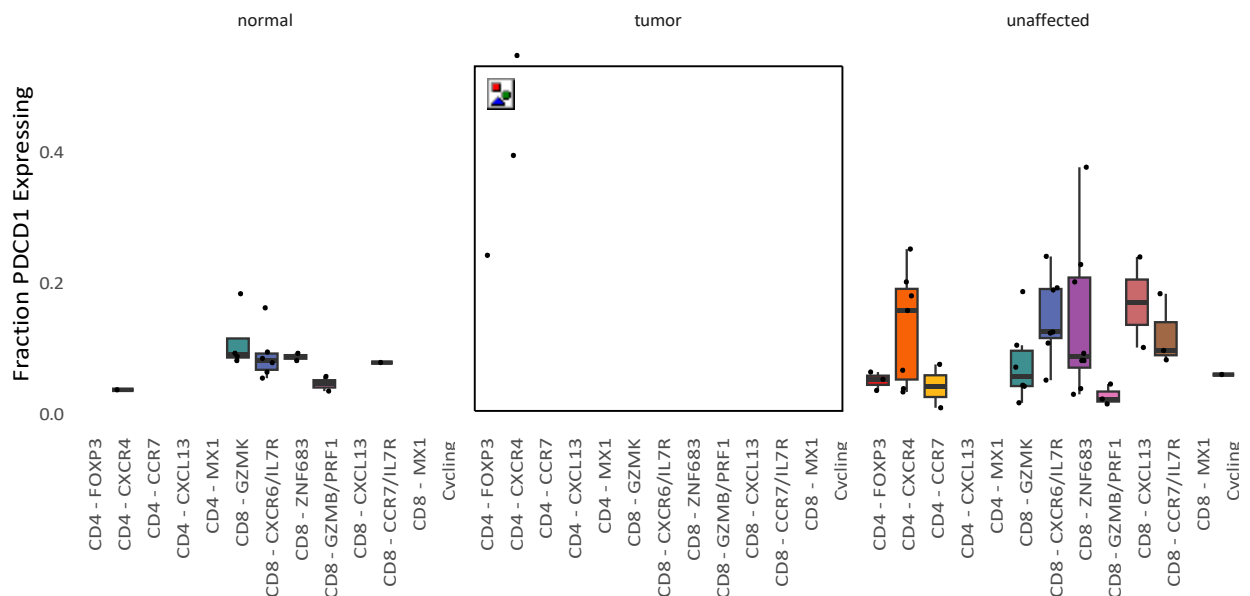


Figure 1.04: Fraction PDCD1 expression by cluster and tissue

Fraction of cells in each cluster for each tissue expressing at least 1 transcript of PDCD1. Each point is an individual sample.

are indistinguishable in sparse coverage scRNAseq.

CD4-CXCL13 & CD8-CXCL13

These populations closely resemble those described in other papers as being an “exhausted” and/or “dysfunctional” population of tumor-recognizing T cells. It’s notable that naming of this cluster with the functional description of “exhausted” is controversial. Unlike the classical definition of exhausted T cells, here and in single cell studies, these populations are often found to be transcribing cytotoxic molecules such as GZMB and NKG7, and are often proliferating when found in vivo. Additionally, these populations express many T cell checkpoint genes: CTLA4, PDCD1 (PD1), HAVCR2 (TIM3), TNFRSF18 (GITR), LAG3, and TIGIT (Figure A1.05). Checkpoint expression (in particular PD1) is an indicator of antigen

recognition by T cells, consistent with the observation that these populations are likely tumor-recognizing (Figure 1.04). For this reason, a prudent, sometimes used descriptor for this population is “experienced T cells.”³² Unsurprisingly, scRNAseq studies have recently shown in other tumor types that the presence of these populations is favorable for a response to anti-PD1/anti-PDL1 checkpoint therapy.

Furthermore, the scRNAseq defining characteristic of these populations, high

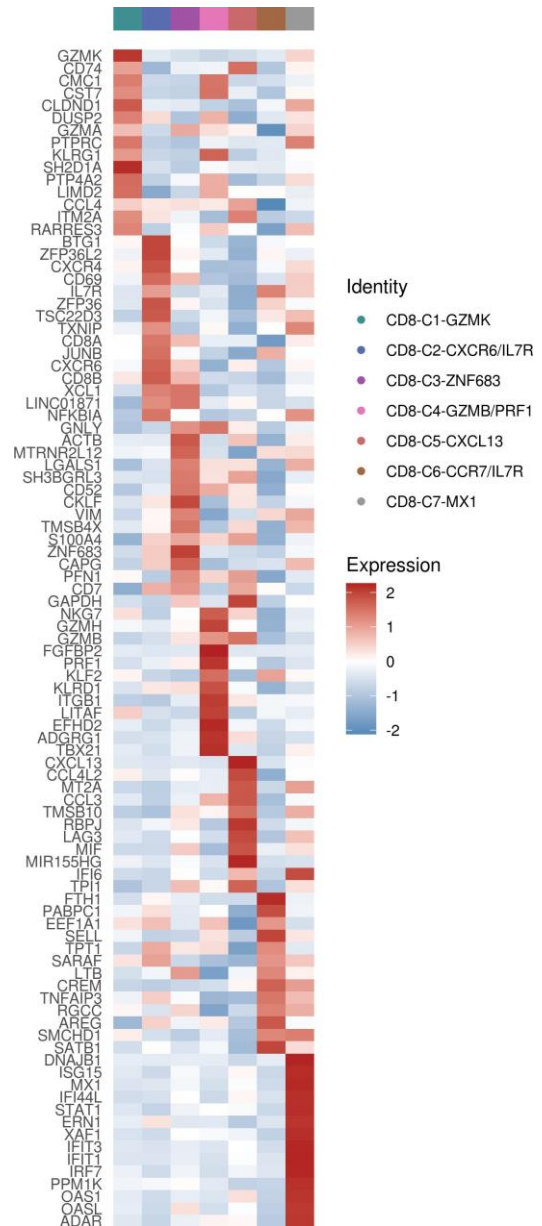


Figure 1.05: Top CD8 population markers
Scaled, average expression of top marker genes for each of the CD8 T cell populations in fresh tumor/pancreas samples.

expression of chemokine and lymphocyte chemoattractant CXCL13 was concordantly observed to be highly expressed in these populations in this dataset. In non-malignant contexts, CXCL13 is characteristically expressed by CD4 T-follicular helper cells in lymph nodes. Considered in total, the aberrant expression of this chemokine and transcription factor RBPJ, and persistent cytotoxic and proliferation despite high checkpoint expression indicate a close resemblance to reputed dysfunctional T cell phenotypes.

CD8-GZMK

Unlike other T Cell populations, GZMK expressing CD8+ T cells have been found in most tumor single-cell studies and are frequent across cancer types.³⁰ This population expresses genes expected in effector memory T cells, such as GZMK (Figure 1.06) and the transcription factor EOMES. As described in other studies, this population has some low expression of PDCD1 indicating previous antigen exposure. Furthermore, it lacks expression of perforin and granzymes other than GZMK and GZMA. This population is known, from experimental and single cell studies, to partially be developmentally related to exhausted/dysfunctional T cells in the tumor persistence setting.^{69,70} For this reason, it is sometimes describe as a “pre-exhausted” or “transitional” T cell population in addition or instead of its common classification as effector memory T cells. Because

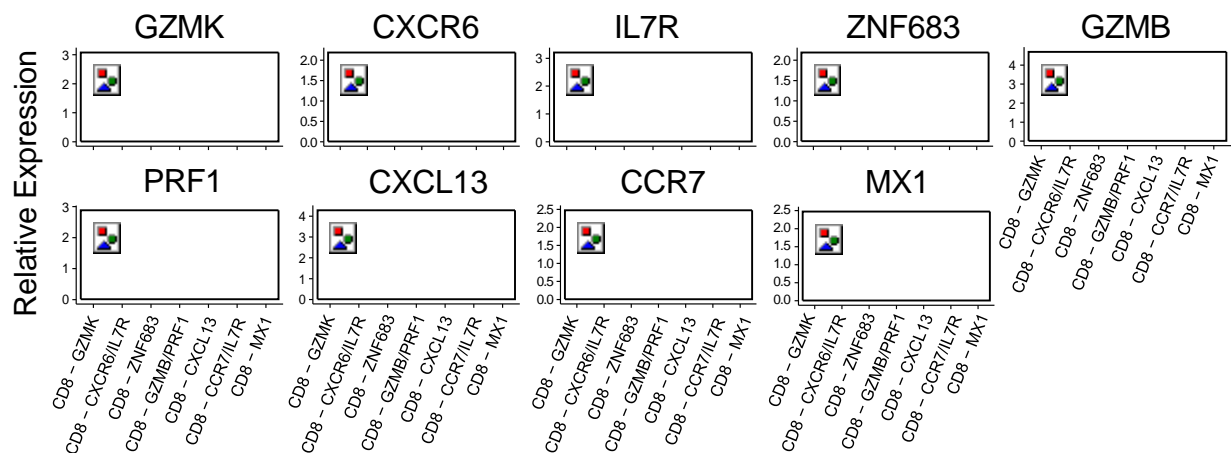


Figure 1.06: CD8 population marker expression
Relative expression of population naming marker genes in the CD8 populations. Plots are colored by mean expression as a percent of maximum expression for each gene

of its likely antigen recognition and purported plasticity, this population is a desirable target for future T cell related therapies.

CD8-ZNF683

This population expresses many characteristics of tissue-resident memory (Trm) T cells. For example, this is the only population in this data strongly expressing the Trm transcription factor ZNF682 (hobit) and lacked expression of T cell migration transcription factor KLF2 (Figure A1.03).^{71,72} Additionally, as expected of tissue resident T cells, it expresses early activation and lymphocyte adhesion marker CD69. Notably, this population almost completely lacked expression of popular Trm marker ITGAE (CD103, αEβ7 integrin subunit). However, this is known to be a tissue-specific and its absence in PDAC is unsuspicious due to the tendency of PDACs to downregulate the αEβ7 ligand E-cadherin.⁷³ Furthermore, this population appears to be cytotoxic as it is transcribing numerous cytotoxic molecules: GNLY (granulysin), PRF1 (perforin), and GZMB.

CD8-CXCR6/IL7R

Similar to the CD8-ZNF683 population, this population expresses Trm marker CD69 and also expresses tissue homing receptors CXCR6 and CXCR4. Additionally, it expresses pro-memory related receptor IL7R, though not at levels as high as the CD8-CCR7/IL7R population. Otherwise this population is transcriptionally similar to the CD8-ZNF683 population, however lacks expression of the previously mentioned cytotoxic molecules suggesting that it is in an inactive state. Further suggesting this inactivity, the CD8-CXCR6/IL7R population expresses T cell activation-restraining RNA binding protein genes ZFP36 and ZFP36L2.

CD8-GZMB/PRF1

Expressing high levels of cytotoxic molecules (GZMB, GNLY, PRF1, NKGZ) and having low to no checkpoint (CTLA4, PDCD1, LAG3) expression, this population has been found across tumor types and also in healthy donor peripheral blood. For this reason, it is usually described as a recently activate effector memory population (Temra), or less-precisely as “cytotoxic” or “effector” T cells. Though this population seems appealing for anti-tumor response, it is controversial whether it is specifically recognizing tumor antigen as it is not clearly associated with favorable responses to immune checkpoint blockade.⁷⁴ Additionally, this state possibly includes a small fraction of gamma-delta T cells (which appear to be too few to form their own cluster) as evidenced by some TRDC expression in this cluster.

Cycling T cells

Expressing many cytoskeletal (ACTB, TUBB) and classical cycling cell marker MKI67, it is clear that these cells are undergoing the cell cycle (Figure 1.07). As this cluster as a whole (but not mutually in a given cell) also expresses genes otherwise exclusive in many of the other clusters, it is likely that “cycling” is a program layered on top of the cell’s ground-state population. Some single cell studies attempt to regress-out the cycling phenotype so as to reassign these cells to their ground state. As they are so few

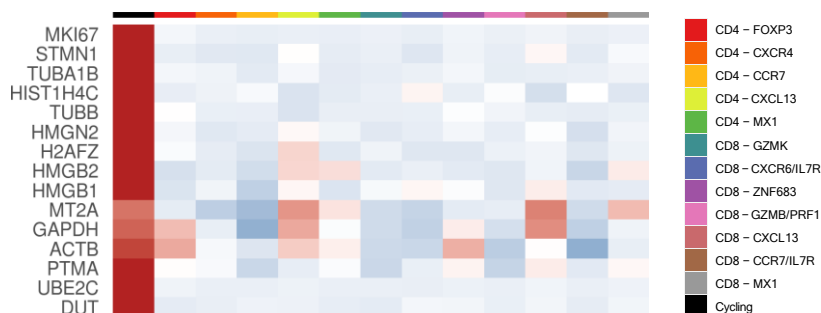


Figure 1.07: Top cycling population markers

Scaled, average expression of top marker genes for each of the cycling T cell population in fresh tumor/pancreas samples.

in our dataset and thus not highly impacting percentages, we chose to refrain from doing so and retain them as their own population (as other studies have).

CD4-MX1 & CD8-MX1

Like the “cycling” cell state, these cell states are plausibly cells from other populations which have been stimulated by interferon(s). They express a number of IFN inducible genes (IFIT1, ISG15, IFIT3, MX1) and are high in the IFN response transcription factor STAT1. Similar to cycling cells, individual cells in this population express marker genes from other populations in addition to this signature. Therefore, it is possible that “interferon stimulated” is a cell state seen on top of a ground-state population and not a true population of its own. ³²

Relative Abundance of T cell populations

All of the previously mentioned T cell populations were seen in tumor samples across all three cohorts at similar cohort-combined frequencies (Figure 1.08). Furthermore, when tumor samples were hierarchically clustered by T cell population frequency composition there appeared to be even mixing of the cohorts, indicating minimal cohort-specific frequency biases. There was, however, inter-patient frequency heterogeneity (Figure 1.09). Though almost all of the identified

T cell populations were present across most of the patients, they were found in varying percentages. In particular, in tumor samples with ≥ 50 T cells detected, the CD8-

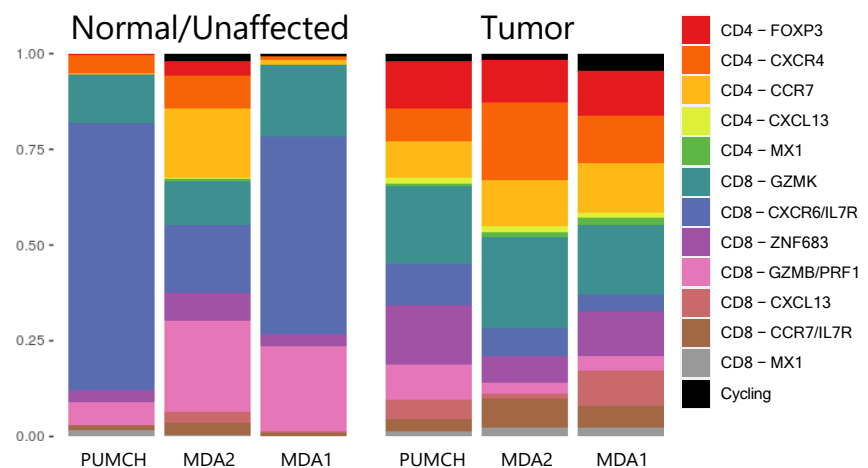


Figure 1.08: Combined population composition by cohort
Frequency of each population in each tissue combining all the T cells in the cohort.

CXCL13 population was observed (at least 1 cell) in 43/53 PDAC samples, but only 7 patients had frequencies $\geq 5\%$ of their total T cell population. However, in 2/7 of these patients, this population comprised over 50% of the T cells. On the other hand, other populations were widely present across patient's tumor samples. For instance, all tumor samples had the CD8-GZMK population present and in 50/53 patients it comprised at least 5% of T cells detected.

Despite these inter-patient differences, tumor samples clustered distinctly from the normal pancreas samples in the PUMCH cohort suggesting, expectedly, strong differences between the tumor and normal pancreas T cell microenvironment. In contrast, samples from “unaffected” pancreas tissue approximately 2cm from the PDAC specimen (predominantly from the MDA2 cohort), did not form a cluster of their own and instead segregated into either the tumor or normal clusters. This mixing is not

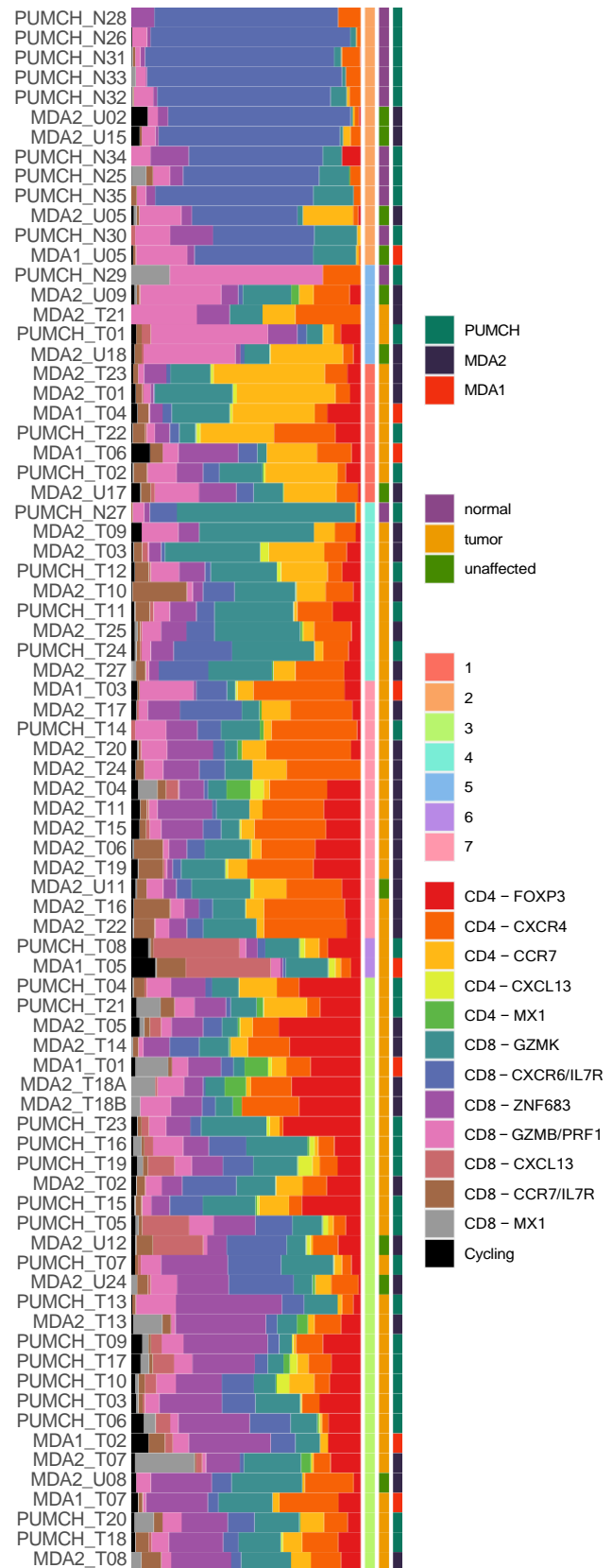


Figure 1.09: Frequencies composition by sample. Each row is a sample. Each annotation is (from left to right) expression population composition, sample hierarchical cluster, tissue type, and cohort.

unexpected, as pancreases affected by PDACs are known to frequently also contain pancreatic intraepithelial neoplasia (PANINs) and therefore the microenvironment of the pancreas in the tumor region can be expected to resemble that of the tumor. In fact, it is for this reason we chose to call these samples “unaffected” instead of “normal.” Nevertheless, some unaffected samples appeared more similar in T cell composition to the truly normal pancreas samples of the PUMCH cohort. This suggests considerable inter-patient heterogeneity exists in pancreas tissue surrounding PDAC lesions.

T cell population abundance by sample type

Though abundance of T cell populations varied by patient, there were several consistent population frequency changes by sample type (i.e. tumor, unaffected, normal)(Figure 1.10). For instance, the CD8-CXCR6/IL7R population was significantly enriched in the uninvolved/normal compared to tumor samples ($P < 0.001$, unpaired wilcox test). In contrast, the tumor samples had higher frequencies of the CD8-ZNF683 cluster ($P < 0.001$). As these populations respectively resemble dormant and activate Trm, their inverse relationship is not surprising, because activation of these cells would be expected to occur in the tumor in response to antigens and inflammation.

Due to the aforementioned inter-patient heterogeneity in the unaffected and tumor

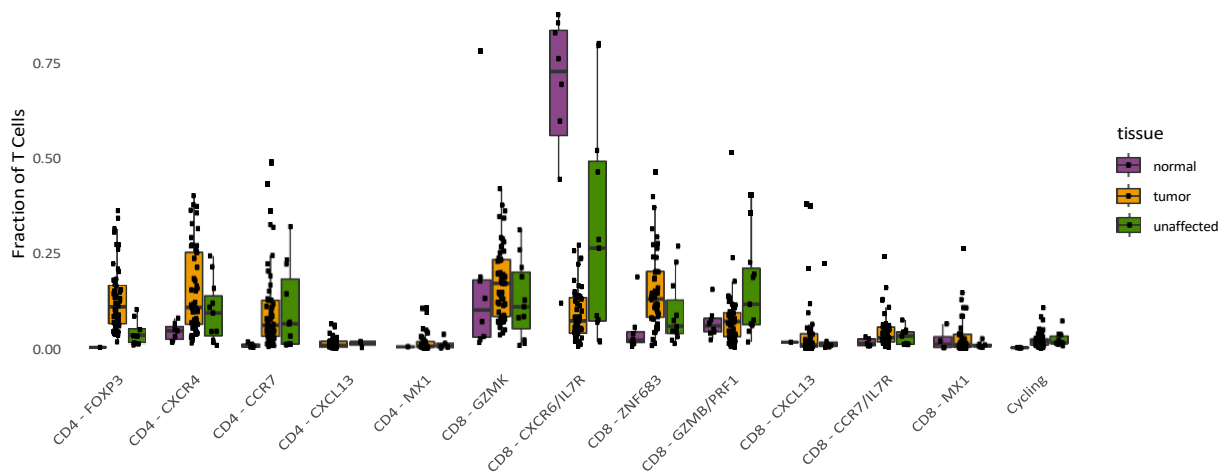


Figure 1.10: Frequencies composition by population and tissue
Each row is a sample. Each annotation is (from left to right) expression population composition, sample hierarchical cluster, tissue type, and cohort.

samples, it is more challenging to obtain the statistical power necessary to distinguish differences between them in a patient-independent manner. To rectify this, we examined the

10 sample pairs in the study which were patient matched (i.e. tumor/uninvolved)(Figure 1.11).

In these matched samples, we found a significant enrichment in the CD4-FOXP3 and CD4-CXCR4 populations in the tumor region over the patients' adjacent, uninvolved tissue. ($P = 0.021$ and $P = 0.035$, respectively. Paired Wilcox test). Additionally, the CD8-CXCR6/IL7R and CD8-GZMB/PRF1 cells were observed in higher relative frequency in the uninvolved tissues versus their matched tumor tissues ($P = 0.041$ and $P = 0.010$, respectively). These results suggest that the T cell microenvironment becomes more suppressive and less cytotoxic as one progresses from adjacent tissue into the tumor. This finding is very much in line with many previous studies of PDAC where this tumor type is well known to usually have a T cell hostile microenvironment.

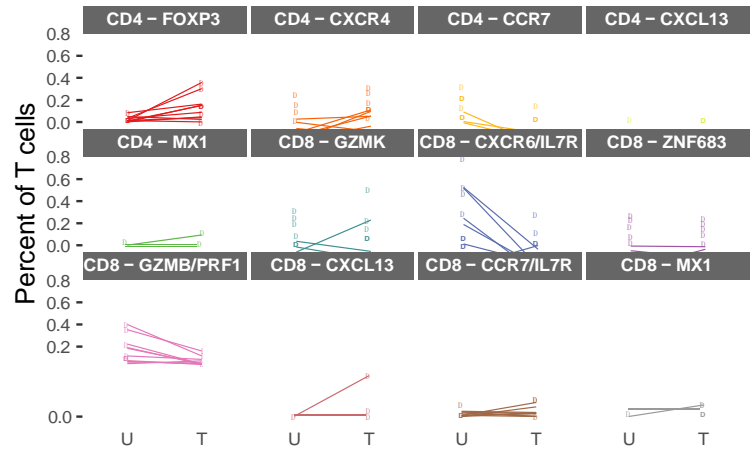


Figure 1.11: Patient-matched population frequency
Frequency of T cell populations in a patient's unaffected and tumor tissue. Each line is a patient (n=10).

Trajectory-inferred relationship between T cell populations

T cells are known for their capacity to transition between many diverse functional and differentiation states. To attempt to unravel these relationships, we performed pseudotemporal trajectory inference in Monocle 3 (one of the few pseudotime tools capable of fitting highly complex relationship structures). Because CD4 and CD8 T cells are known to diverge as separate populations early in T cell development (before leaving the thymus), we performed this analysis on the CD4 and CD8 cell types separately.

Creating this separation is therefore expected to increase the fidelity of the predicted lineages by eliminating relationships inferred from cell programming developed in parallel in both of these cell types (e.g. false relationships inferred between certain CD4 and CD8 populations because they are both in a cytotoxic, memory, naïve, etc. state).

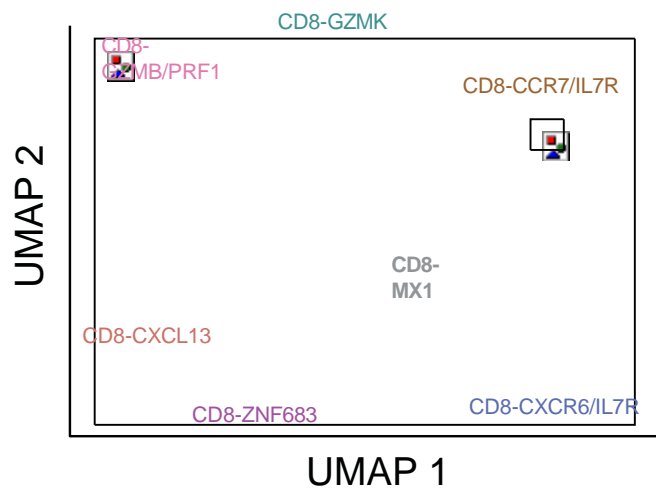


Figure 1.12: CD8 Trajectory Map
Pseudotemporal inference of CD8 T cells using Monocle 3. Cells are colored by population.

CD8 trajectory analysis

For trajectory analysis we extracted non-cycling cells in the CD8 populations and re-embedded them utilizing the Monocle 3 best practices preprocessing workflow. We were pleased to find that the clusters we previously defined were robust to a different processing workflow and still segregated in the trajectory UMAP embedding (Figure 1.12). Furthermore, this analysis strengthened conclusions already apparent in the transcriptional data. For example, the CD8-CXCR6/IL7R and CD8-ZNF683 populations were co-located on the same, long branch of the inferred graph with a high density of cells found continuously along the trajectory. This is highly suggestive of a close developmental lineage between these Trm resembling populations, which are normal and tumor-specific, respectively.

Additionally, the trajectory was highly branching in the CD8-GZMK population, connecting it strongly to several other populations including CD8-GZMB/PRF1, CD8-CXCL13, and CD8-ZNF683. This observation is somewhat unsurprising because the CD8-GZMK Tem-like population is sometimes described in other studies as a “transitional” and therefore would be expected to be centrally located developmentally.

Moreover, this population has been inferred to be less terminally-differentiated/more plastic than the other cytotoxic populations and being connected relationally to several other states is consistent with this postulation. Another finding of note, is that the two GZMB-expressing cytotoxic CD8 populations (CD8-C4-GZMB/PRF1 and CD8-CXCL13) were clearly separately branching from CD8-GZMK in the analysis. Considering both populations express cytotoxic programming, one would expect them to be closely related (similar to the CD8-CXCR6/IL7R and CD8-ZNF683 relation). Instead, both populations exhibited terminal branches of the trajectory. With CD8-CXCL13, the terminality of the branch further insinuates this population's suspected highly-differentiated status. If the CD8-GZMB/PRF1 exhibits the same terminal fate is unclear, but this analysis does not refute that conjecture.

Despite the strong connectivity seen between some clusters in the embedding, CD8-CCR7/IL7R was relatively disjoint from the other clusters. Though Monocle predicted a transition between CD8-CCR7/IL7R and CD8-CXCR6/IL7R, there were very few cells present along the connecting branch, evidencing a tenuous attestation of relationship. As trajectory analysis is known to err towards false positive connections (after all, it is the nature of pseudotemporal analysis to try to make connections), and it is notoriously difficult to accurately predict the entirety of a complex lineage with these methods, we believe this portion of the trajectory in particular should be interpreted cautiously. Moreover, the CD8-MX1 population appeared to be excluded from the trajectory entirely. However, this supports our earlier conjecture that this phenotype is more of a stimulation state than a true population as one would expect a population which is derived from multiple others to behave erratically in trajectory analysis.

CD4 trajectory analysis

Similarly we performed trajectory analysis on the CD4 T cells (Figure 1.13). With fewer populations, the trajectory inferred here was considerably simpler than with the

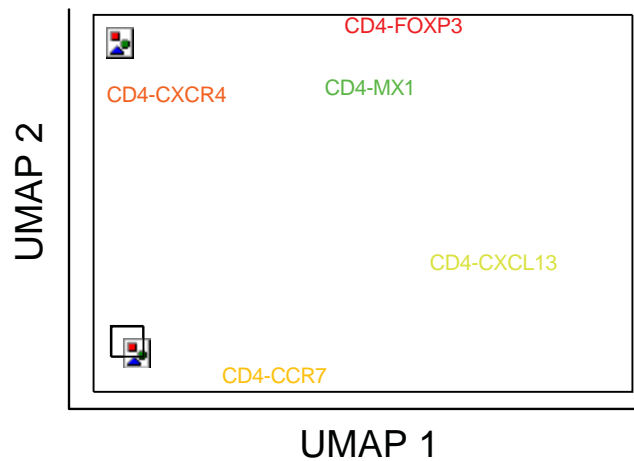


Figure 1.13: CD4 Trajectory Map
Pseudotemporal inference of CD4 T cells using Monocle 3. Cells are colored by population.

CD8 T cells. Here a strong relationship between the CD4-CXCR4 and CD4-CCR7 population was observed with high cell density along the graph. In addition, CD4-CXCL13 was connected to CD4-CXCR4, in the predicted trajectory curve, but with CD4-CCR7 and some CD4-FOXP3 cells distributed in the connecting part of the graph dilute confidence in

this result. Furthermore, though the CD4-CXCR4 population was purportedly joined to the CD4-FOXP3 Tregs though the CD4-MX1 cells in this analysis, the relationship was extremely unsupported by intermediate cells along the lineage suggesting it is another false positive. Supporting this conjecture, is the phenomenon that tumors are known to recruit natural Tregs from peripheral blood (as opposed to induce Treg formation in the tumor). Therefore, it is plausible that the CD4-FOXP3 does not share a recent lineage with the other CD4 populations in the tumor.

Intra-sample co-occurrence of T cell populations

There has long been a desire to classify tumor ecosystems by groups of co-present cells. To this end, we attempted to determine co-occurrence of T cell populations by spearman correlating the pairwise frequency of T cell populations in the tumor samples across patients (Figure 1.14). Unsurprisingly, populations of similar nature but distinguished by CD4 and CD8 tended to be associated with each other. For example, frequency of the CD8-MX1 and CD4-MX1 were significantly correlated ($r = 0.70$, $P = 8.17 \times 10^{-8}$), signifying that if a patient exhibited an interferon stimulated T cell microenvironment, there was a tendency to see this stimulation in both the CD8 and CD4 T cells. The same observation

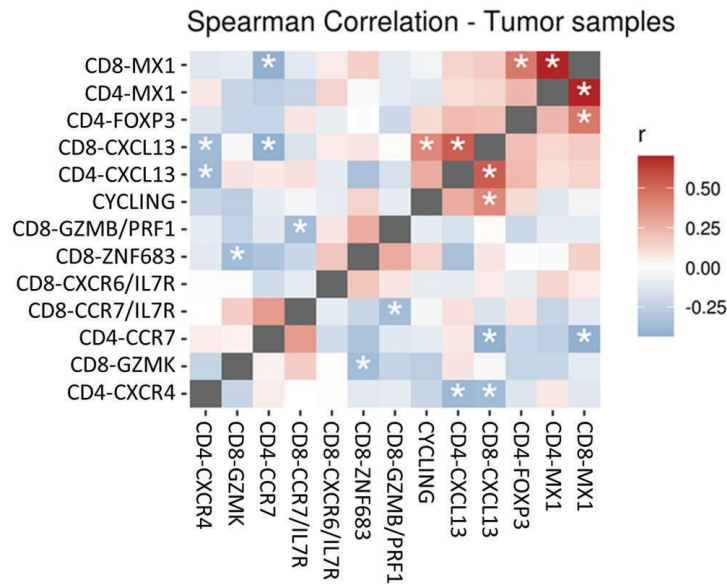


Figure 1.14: T cell population correlation frequency
Spearman rho value for pairwise frequency of T cell populations between tumor samples. Stars mark Benjamini-Hotchberg corrected $p \leq 0.05$.

was made of the CD8 CXCL13 and CD4 CXCL13 populations ($r = 0.53$, $P = 6.71 \times 10^{-4}$) and the CD8-CCR7/IL7R and CD4-CCR7 populations. Furthermore, CD4-FOXP3 and both CXCL13 and MX1 populations tended to jointly co-occur. Since IFN stimulation and suppressive and dysfunctional T cells are all populations expected in the case of persistent antigen recognition,

it is likely that these populations together represent the nature of tumor recognition in PDAC.

Transcriptional and clonal relationships of T cell populations

As previously mentioned, in the samples from the MDA1 we performed single cell TCR sequencing from the same cells as the single cell transcriptomic data. By somatic gene recombination, T cells create essentially unique TCRs early in their development and then later proliferate upon seeing antigen. Therefore, the detection of a TCR in a tumor sample at a high frequency indicates a clonal expansion of that clonotype occurred and suggests that clonotype as being functionally involved in the tumor response. Here we show the frequency of each unique TCR clone present in the cohort (performed separately for the CD8 and CD4 populations). Concurrently, we labeled each clonotype by the patient in which it was observed in and by the population composition of the clonotype. Finally, we hierarchically clustered the clonotypes by their mean transcriptional profile (Figure 1.15).

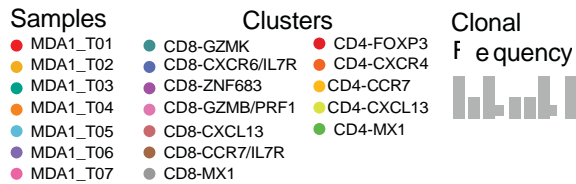
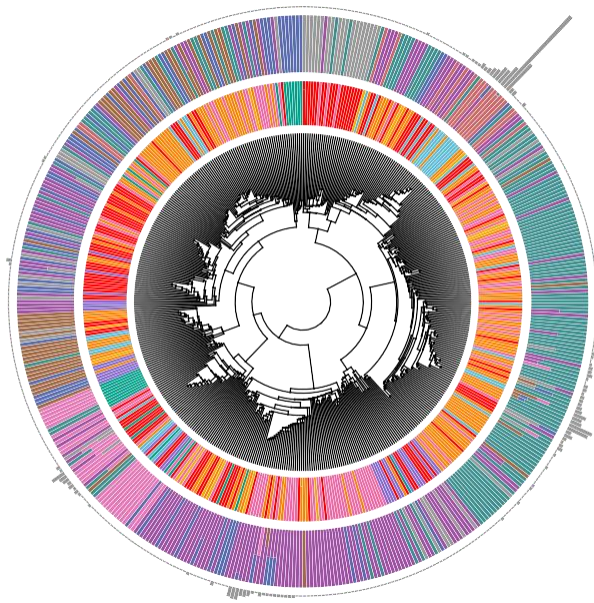


Figure 1.15: CD8 circos plot
From inner to outer ring: hierarchical cluster, patient, population composition, and frequency, respectively for each CD8 clonotype in the MDA1 cohort.

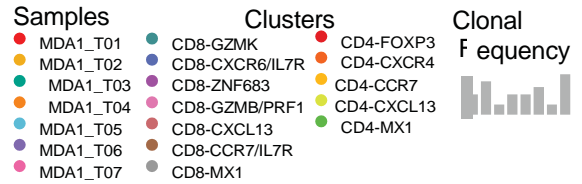
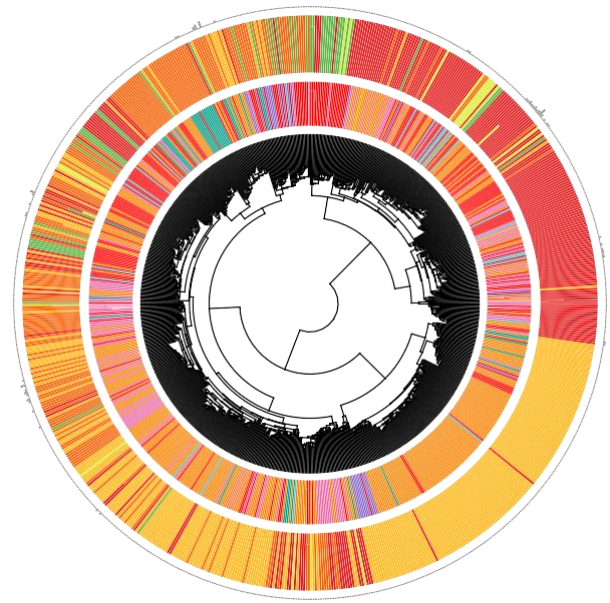


Figure 1.16: CD4 circos plot
From inner to outer ring: hierarchical cluster, patient, population composition, and frequency, respectively for each CD4 clonotype in the MDA1 cohort.

This analysis revealed that several CD8 populations (CD8-GZMK, CD8-ZNF683, CD8-GZMB/PRF1, and CD8-CXCL13) had undergone clonal expansion, though not all clonotypes existing in these populations were expanded. With the exception of CD8-CXCL13 (which was only present frequently in sample MDA1_T05), these expansions were seen across patients. Furthermore, the data as displayed here suggested that most clonotypes (including many expanded ones) exist as a single transcriptional state. However, there were several instances of clonotypes whose cells existed in multiple states. This was particularly the case in the CD8-GZMK population, again reinforcing its central relationship to other clusters. In contrast to the CD8, the CD4 clonotypes were rarely expanded and consequently almost exclusively present as a single transcriptional population within a clonotype (Figure 1.16).

TCR expansion by cell state

Examining expansion status more quantitatively, we summarized the likelihood of a cell belonging to an expanded TCR given its transcriptional population and patient. Unsurprisingly, this enforced the observations from the



Figure 1.17: Clonal T cell composition
Percent of T cells in each patient and population with clonal (n≥2) and non-clonal TCRs.

circus plots. Here, however, it is more clear that some patients saw more diverse clonal expansion than others (e.g. all CD8 populations present in MDA1_T05 contained at least half expanded cells). Furthermore, some populations were more universally expanded across patients, such CD8-ZNF68 which saw expansion in most patients (Figure 1.17). A separate quantification, Gini index (Figure A1.08), which takes into account the unevenness in frequency of the overall clonotype further confirmed higher clonotype unevenness (proxy for clonal expansion) in CD8 clonotypes vs. CD4 clonotypes across patients ($P = 0.034$, paired t-test)(Figure A1.09).

TCR overlap by cell state

To further quantify cell state diversity and similarity within clonotypes we performed upset analysis (similar to a multi-group Venn diagram in bar-plot form) on clonotypes consisting of at least 2 cells (Figure 1.18). This evaluation confirmed that expanded CD8 T cells clonotypes for CD8-GZMk, CD8-ZNF683, and CD8-CXCL13 most often existed with all cells in the same transcriptional population. Additionally, this analysis lends support to the conclusion from the pseudotemporal analysis. The most common population states to share TCR overlap were CD8-ZNF683/CD8-CXCR6/IL7R and CD8-ZNF683/

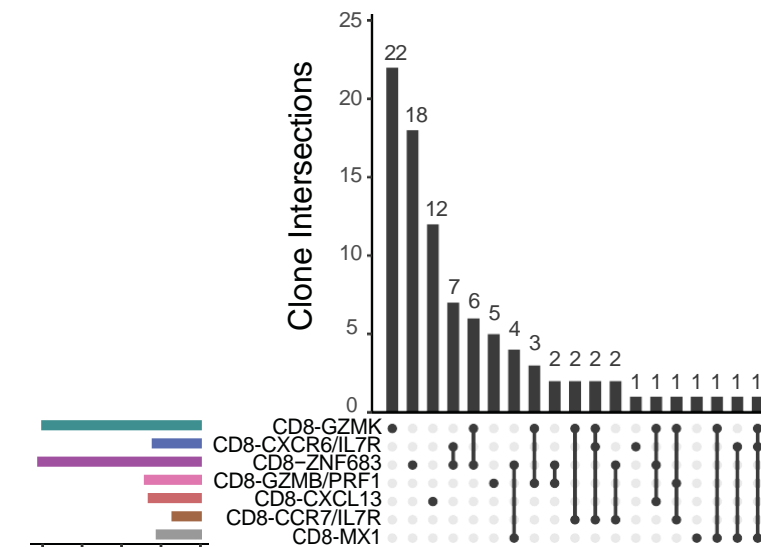


Figure 1.18: CD8 TCR overlap by population
The Frequency of observing expanded ($n \geq 2$) CD8 clonotypes with cells in various combinations of transcriptional states.

CD8-GZMK all of which are inferred to be transcriptionally related in the trajectory analysis. Moreover, clonotypes containing CD8-CXCL13 cells, which was observed as terminal in trajectory analysis, was only observed overlapping with another population only once. This observation supports the conclusion that the CD8-

CXCL13 cells are not recently related to the other populations. Finally, as expected, clonotypes containing CD8-MX1 cells were almost always seen to be overlapping other clusters. Though CD4 cells were rarely observed to be in expanded clonotypes, (and even then are less expanded than the CD8s) cells which were almost entirely consisted of CD4-FOXP3 and CD4-CXCR4 exclusive, non-overlapping clonotypes (Figure A1.07). Though this data cannot add support to the CD4-CXCR4/CD4-CCR7 relationship in the pseudotime analysis (because CD4-CCR7 is rarely expanded and therefore cannot overlap), it does suggest that the CD4-FOXP3 and CD4-CXCR4 populations are not recently related.

Grown clusters

Concurrently, as the tissue samples from the MDA1 cohort were processed for scRNAseq, a piece from each tissue was used for *ex vivo* TIL growth. The cultured TIL was then used for transcriptomic and TCR scRNAseq. These experiments resulted in 40,065 high-quality T cells from six patients, which were then integrated and clustered (Figure 1.19). Though the cultured TIL, as expected, was much less diverse transcriptionally than

the T cells from fresh tumor samples, there were still distinct transcriptomic states present (Figure 1.20, A1.10). The “grown” populations we found were named after key genes in the cluster are briefly described below:

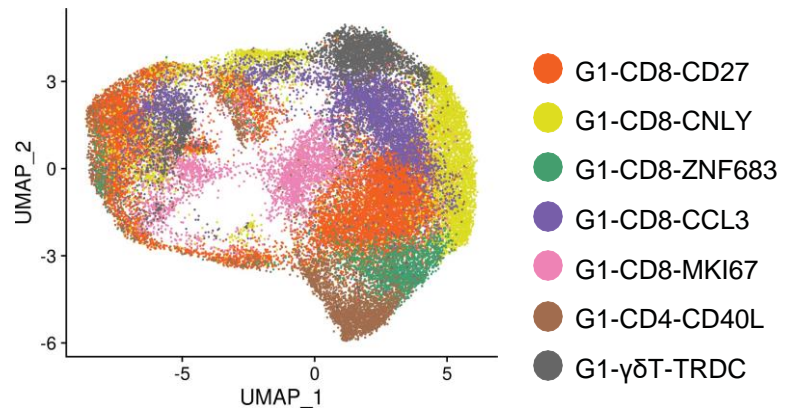


Figure 1.19: Grown T cell UMAP
UMAP embedding of cultured T cells from tumor samples. Cells are colored by assigned transcriptional population.

G1-CD8-CD27

An activated CD8 population expressing early TCR/CD3 stimulation marker CD27 and exhibiting the highest average expression of GZMK of the CD8 populations.

G2-CD8-GNLY

Another activated CD8 population, these cells expressed the highest levels of effectors GNLY, GZMB, and GZMH. Additionally, this population had the highest fraction and level of expression of the cytotoxic lymphocyte associated gene FGFBP2.

G3-CD8-ZNF683

In contrast to the fresh tumor T cells where ZNF683 was population specific, here most of the CD8 populations expressed the gene. However, this population expresses it at the highest level. Additionally, this population expresses the Tem and cell motility associated gene S100A4.

G4-CD8-CCL3

Yet another activated CD8 populations, in addition to expressing cytotoxic genes G4-CD8-CCL3 expressed high levels of T cell-recruiting chemotaxis chemokines CCL3 and CCL4.

G4-CD8-MKI67

This population expressed several glycolysis related genes (PGK1, GPI, etc.) suggesting. T cells are known to increase glycolysis activity (compared to oxidative phosphorylation in dormant cells) upon activation. This metabolic activity is perhaps why it appears to be highly proliferative, expressing MKI67.

G6-CD4-CD40L

The only CD4 population identified in the grown T cells, this population seems to be activated like the CD8 populations. It expresses CD4 T cell-associated activation genes CD40LG and TIMP1 and clearly expresses CD4 over CD8A and CD8B.

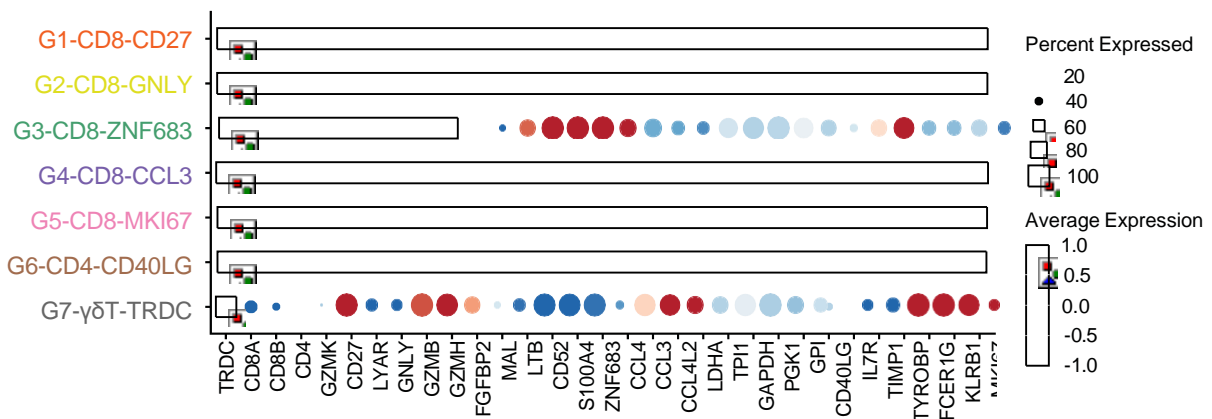


Figure 1.20: Markers of grown T cell populations
Percent of T cells expressing and scaled average mean cluster expression for each of the cultured T cell states.

G7-γδT-TRDC

Though rare in the fresh tumor samples, there was a distinct γδ T cell population in the grown TIL, indicating their ability to be expanded by the culturing process. Only this population expressed the γδ T Cell TCR gene TRDC. Furthermore, it showed high expression of both GZMB and GZMK and γδ T Cell related marker KLRB1.

As expected, a large fraction of the cultured TIL were cycling cells. In order to make use of these cells, we re-classified cycling cells to the established non-cycling profile as described in the methods. Furthermore, by design, the cultured TIL was largely composed of activated CD8 T cells, though effector CD4 and γδ T cells still persisted, albeit at lower fractions.

TCR analysis in Grown clusters

Similar to the CD8 cells in the fresh samples, clonotypes in the cultured TIL existed in a variety of TCR expanded and unexpanded states. Nevertheless, many of the clonotypes in the grown samples saw high degrees of clonal expansion as that is the goal of the culture. However, unlike in the fresh samples, highly frequent clonotypes in the grown samples tended to exist as a mix of transcriptional populations. This was further solidified by the high degree of TCR overlap between

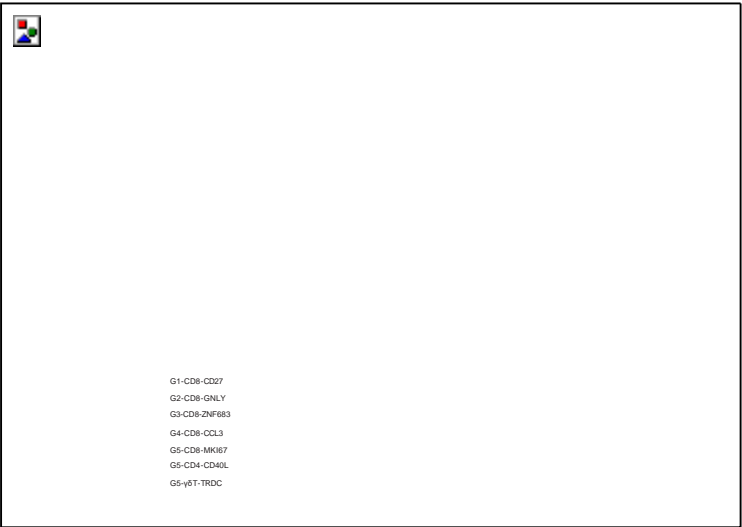


Figure 1.21: TCR overlap in grown populations
The Frequency of observing expanded ($n \geq 2$) clonotypes with cells in various combinations of transcriptional states.

the grown CD8 clusters (Figure 1.21). In contrast to the CD8 clusters, the G6-CD4-CD40L cluster tended to not contain expanded T cells and, expectedly, did not contain clonotypes highly overlapping with the CD8 populations. Overall, this suggests that the CD4 population, though possibly activated, is persisting much more so than it is proliferating.

T cell populations expanded by TIL culture

For several decades, the cellular-based cancer immunotherapy field has been trying to identify and select the best T cell subtypes to provide the most efficacious adoptive cell therapy. To this end, we attempted to distinguish which populations from the fresh tumor samples the T cells in the grown culture product originated from. To do so, we relied on tracing the TCR sequence between the fresh and grown samples, and then examining their transcriptional populations (Figure 1.22). This revealed that the majority of clonotypes present in the fresh tumor were not present in the T cell culture.

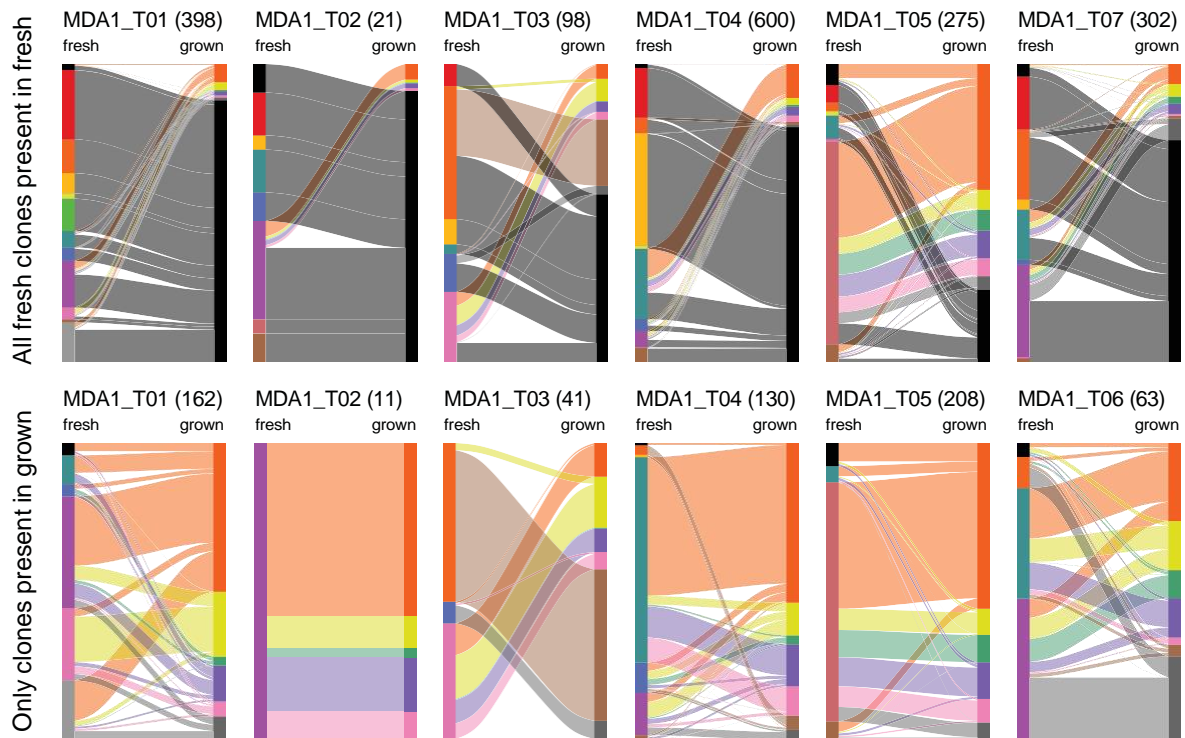


Figure 1.22: Cell state transition from fresh to grown
Clonotype consensus transcriptional state in the fresh compared to its state in the TIL culture product.

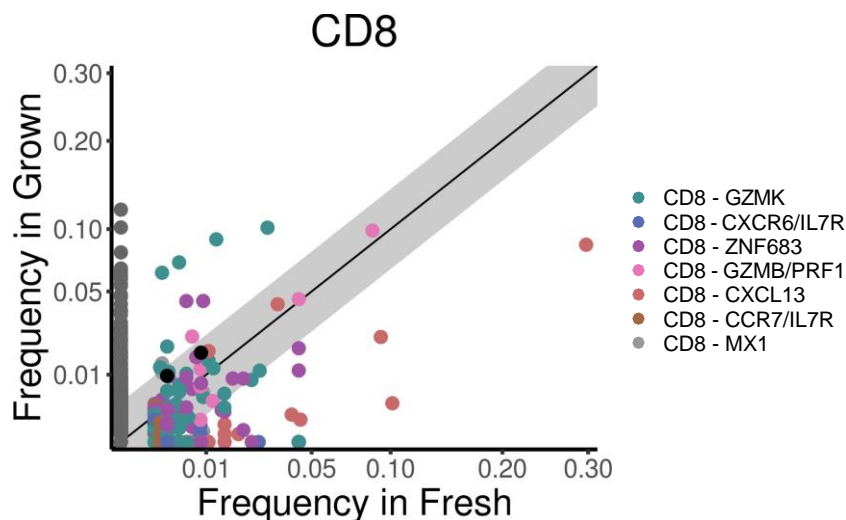


Figure 1.23: Change in clonotype frequency
Change in frequency of clonotypes from the fresh tumor biopsy into the grown ACT product. Clonotypes are colored by consensus population state in the fresh.

Of the fresh clonotypes that did grow in culture, they matched clonotypes coming from any of the CD8 populations in the fresh tumor, and which one predominated varied predominantly by patient. This is suggestive that the TIL culture method used is

highly effective in growing T cells from a variety of cell states. Furthermore, for the CD8 populations, the state a clonotype was found as in the grown product seemingly had little to do with its apparent state in the fresh tumor, again suggests strong reprogramming ability. In contrast, the CD4 population in the grown was found to match TCRs nearly entirely from the CD4-CXCR4. Notably, none of the TCRs found in Treg clusters in the PDAC tumor were observed in the cultured samples. This is a fortunate result, as expansion of pro-tumor T cells is not a therapeutically desirable outcome.

Though presence in the TIL culture was not highly based on CD8 fresh cluster status, there was fresh population dependence for clonotype frequency changes (Figure 1.23). For example, clonotypes whose frequency in the grown samples increased over their frequency in the fresh (indicating stimulation/proliferation) were enriched for CD8-GZMK population clonotypes. Once more, this enforces the potential role for this population as transitional/plastic. Conversely, clonotypes still present in the culture but at a diminished frequency compared to the tumor tended to be from the CD8-CXCL13 population. Due to these results it is unsurprising that, at the gene level, GZMK and NKG7 were overexpressed in CD8 clonotypes that ended up expanding in frequency,

whereas CXCL13 was the most overexpressed gene in clonotypes whose frequency reduced. Once more, this indicated that though the CD8-CXCL13 populations may be tumor recognizing they perhaps have a reduced ability to expand and may be more terminally differentiated as previously suggested.

Discussion

Here, we collected one of the largest scRNAseq studies of pancreas-related T cells to define the T cell populations present in PDAC and uninvolved/normal pancreas tissue samples. Based on these data, and concurrent TCR clonotyping in the same cells, we present a model for the organizational relationship and potential developmental relationship of PDAC TIL as well as their unrestricted expansion into each component population of the *ex vivo* culture.

It is notable that though PDACs are often described as immunologically “cold” and “hostile”, we show in this study a variety of activated and memory T cell states present across patients.^{75, 76} Additionally, many of these states have been reported in single cell T cell studies from other cancers such as melanoma, triple-negative breast cancer, non-small cell lung cancer, colorectal cancer, and liver cancer.

Of particular interest is the CD8-GZMK cluster. Shown in our data and that of other studies, it is purported to be related to several cytotoxic and memory populations. This suggests it may have the ability to be stimulated to multiple cell states, a tempting characteristic for targeting immune based therapies. Likewise, its relationship to dysfunctional CD8-CXCL13, but lack of extensive exhaustion-associated checkpoint expression further suggests its characterization in other studies as “pre-dysfunctional.” If this is indeed the case, it could prove a tempting and possibly tumor recognizing population which could be targeted before it becomes dysfunctional.

Another interesting population identified here is the Trm-like CD8-ZNF683. Interestingly, this population in our study did not express the classic, but not universal, Trm integrin ITGAE (CD103) or, as has been reported, have high expression of checkpoint

markers. It was however, highly associated with tumor presence whereas non-tumor samples contained a similar Trm-like population instead CD8-CXCR6/IL7R. These two clusters were related by transcriptionally similarity and TCR sharing suggesting the CD8-CXCR6/IL7R transitioned to the CD8-ZNF683 during tumor formation. With the transcriptional phenotype of these populations suggesting long-term tumor residence and other studies implicating tumor-recognizing Trm in ICB response, understanding how to stimulate these populations in PDAC could prove useful.

Furthermore, the CD8-CXCL13 population found in this study has been shown in others to be the most predictive of response to ICB and is likely the responding population.⁷⁷ However, it expresses a large number of checkpoints leaving it susceptible to further dysfunction in vivo. Nevertheless, we have shown here that this population can still be stimulated, though its proliferative ability upon stimulation seems to be less prolific than its pre-dysfunctional sister the CD8-GZMK population. Studying this population with the goal of increasing its proliferative capacity in mind, could improve upon available T cell therapies.

Finally, this study exemplifies the ability of ACT culture to re-program a variety of T cells. We have shown here its ability to stimulate a variety of cytotoxic and memory T cells states, though at different efficiencies. Furthermore, it appears to avoid expanding detrimental populations such as CD4-FOXP3 and thus assisting in overcoming issues of pro- and anti-tumor T cell balance in tumors. We hope that future studies can build upon these results to better target T cell populations of interest in PDAC.

Methods

Patient sample accrual

After providing written informed consent, seven patients with primary pancreatic ductal adenocarcinoma underwent surgical resection (Supplementary Table 1). Patients are referred to by their de-identified number. Tissue from surgical resections was used

under protocols (PA 15-0176 and PA17-0793) approved by the Institutional Review Board of The University of Texas MD Anderson Cancer Center. For the MDA1 and MDA2 data sets, tissue from normal pancreas is referred to as “uninvolved” because it came from PDAC patients. For the PUMCH data set, tissue from control pancreases is referred to as “normal” because it came from patients without malignant pancreatic tumors.

Sample preparation for sequencing

Fresh tumor samples were cut into 1-3 mm³ fragments and disaggregated using a Medimachine (BD Biosciences, Franklin Lakes, NJ) to create a single-cell suspension according to manufacturer’s instructions. After disaggregation, CD3⁺ T cells were isolated for sequencing via magnetic bead separation using the EasySep Release Human CD3 Positive Selection Kit (StemCell Technologies, Vancouver, Canada) according to the manufacturer’s instructions. For cultured TIL, previously cryopreserved samples were thawed, washed with 1× PBS, and resuspended at 1×10⁶ cells/mL.

TIL culture reagents

A purified, human IgG4 monoclonal antibody (mAb) against human CD137/4-1BB, Urelumab (663513), was kindly provided by Bristol-Myers Squibb (New York, NY). Human recombinant interleukin-2 (IL-2) (Proleukin) was generously provided by Prometheus Therapeutics & Diagnostics (San Diego, CA). GMP-grade soluble anti-CD3 antibody (OKT3 clone) was obtained from Miltenyi Biotec (Bergisch Gladbach, Germany).

Expansion of TIL from tumor samples

Fresh tumor samples were cut into 1-3 mm³ fragments, and five fragments were placed in G-Rex10 flasks (Wilson Wolf, Saint Paul, MN) containing 20 mL of TIL culture

media (TIL-CM: RPMI-1640 with GlutaMAX [Gibco/Invitrogen], 1× Pen-Strep [Gibco/Invitrogen], 50 μ M 2-mercaptoethanol [Gibco/Invitrogen], 20 μ g/mL gentamicin [Gibco/Invitrogen], and 1 mM sodium pyruvate [Gibco/Invitrogen]) with 6000 IU/mL IL-2, 10 μ g/mL 4-1BB mAb, and 30 ng/mL anti-CD3 (OKT3) as previously described. Four to five days after culture initiation, 20 mL of additional TIL-CM with 6000 IU/mL IL-2 was added for a total volume of 40 mL. Half-media changes were done every 3-4 days with fresh TIL-CM containing 6000 IU/mL IL-2 for up to 35 days or until the cells formed a thick layer completely covering the bottom of the flask. The cell suspensions were collected and cryopreserved in FBS plus 10% DMSO.

Single-cell RNA/TCR sequencing

Single-cell capture and library construction was performed with the 10x Genomics Chromium Single Cell 5' kits v.1.0 (product codes 1000014, 1000020, and 1000151) with TCR enrichment (1000005) according to the manufacturer's instructions. Briefly, cells were loaded into the Chromium Single Cell Chip A for a recovery target of 10,000 cells. Reverse transcription was performed on a BioRad T100 thermal cycler, and the barcoded cDNA was purified with Dynabeads (Thermo Fisher Scientific, 37002D) prior to 14 cycles of cDNA amplification. Of this transcriptome cDNA, 2 μ L was used for TCR enrichment and subsequent TCR library construction. Per the manufacturer's protocol, up to 50 ng (or 20 μ L) of transcriptome cDNA was used for single-cell library construction. Transcriptome libraries were sequenced on a HiSeq 400 (Read 1, 26 cycles; Index 1, 8 cycles; Read 2, 91 cycles), and TCR libraries were pooled and sequenced 150 cycles paired-end on a MiSeq (Illumina). For transcriptome libraries, median sequencing depth for each sample was targeted for a median of 30,000 reads/cell; for TCR libraries, 1,000 reads/cell. Read counts can be found in Supplementary Table 2.

Single-cell data processing and filtering

The 10x Genomics Cell Ranger pipeline (v. 3.1.0) was used to demultiplex and generate unique molecular identifier (UMI) matrices for all samples in the MDA1 cohort. UMI matrices for the MDA2 and PUMCH cohorts were also generated from the provided FASTQ files using this version of the Cell Ranger pipeline. The UMI data were then processed in R (v.3.5.3) using the Seurat package (V.3). Cells with more than 6000 genes, fewer than 200 genes, greater than 20% UMI in mitochondrial genes, or a UMI:gene ratio greater than 10 or less than 1.3 were filtered. To filter out non-T cells from the data sets, all samples were combined, the top 5000 variable genes were reduced to 50 top principal components and clustered using Seurat's SNN clustering function. Clusters with significant average expression (Wilcoxon test) of *CD3* genes (i.e., T cells) were then extracted for further analysis. This gene selection, principal component analysis, and clustering step was performed once more to further remove clusters not expressing *CD3* genes.

Data integration, dimension reduction

To account for library chemistry, and other possible unknown differences between cohorts, the T cells were integrated employing the methods as described in <https://satijalab.org/seurat/v3.0/integration.html>. Briefly, the top 5000 variable features were selected with TCR variable genes (“^TR[ABGD][VDJ]”) excluded. These genes were used to compute 20 “anchors” with the FindIntegrationAnchors function, and subsequently “integrated” with IntegrateData to produce a batch-corrected data set. The first 30 principal components of the integrated expression data were used for subsequent UMAP embedding.

CD4/CD8 classification, clustering, and marker identification

T cells with detectable expression of either *CD4* or *CD8* genes were assigned to their respective clusters. The first 30 principal components (excluding these genes) from a randomly selected training set of 75% of these cells were used to train a random forest classifier (RandomForest package in R) for $CD4^+$ vs. $CD8^+$ T cells. The remaining 25% were used as a validation set. This classifier was then used to classify T cells with no detectable *CD4* or *CD8* expression (likely due to gene dropout) as either $CD4^+$ or $CD8^+$ T cells and then further clustered separately. After CD4/CD8 classification and separation, the top 3000 variable features were re-selected for each group and principal components were computed. The top 30 principal components were used to perform clustering with Seurat's FindNeighbors and FindClusters functions. Top marker genes for each cluster were identified with Seurat's FindAllMarkers function, and *P* values were determined by the Wilcoxon test.

Pseudotime trajectory analysis

Pseudotime analysis was performed on cells in the CD4 and CD8 populations separately using Monocle 3 (version 0.2.2.0; <https://github.com/cole-trapnell-lab/monocle3>). Expression data were UMAP embedded using the Monocle function "reduce_dimension" with the default parameters. The trajectory graph was inferred with the function "learn_graph" with the minimal branch length set to 15 and close_loop = FALSE. The CD4 and the CD8 trajectories were rooted in the clusters CD4-CCR7 and CD8-CCR7/IL7R, respectively.

Re-assignment in cycling cultured cells

Due to the (intentional) highly proliferating state of the cultured T cell samples, a large fraction of the T cells formed a cluster of cycling cells. Non-cycling cell clusters were

used to train a random forest classifier (similar to CD4/CD8 classification in the fresh T cells), which was used to re-classify cycling cells to the most similar non-cycling cluster.

TCR analysis and clonotype re-assignment

TCR calls on the single-cell TCR sequencing data were performed with the “cellranger vdj” function of the Cell Ranger software suite (v.3.1.0). Cells with only a TCR alpha or beta chain detectable whose TCR nucleotide sequence exactly matched that of another clonotype with both the alpha and beta chain detectable were re-assigned to that clonotype.

Chapter 2: The effects of radiotherapy on the tumor microenvironment in hormone receptor positive breast cancer

Introduction

Radiotherapy is a widely used and highly effective treatment for most early-stage tumors, yet much of the biology underpinning its success or failure is rarely studied with the context of a functioning, in vivo tumor microenvironment (TME). Ionizing radiation directly kills malignant and tumor microenvironment cells alike through the induction of various forms of DNA damage. The subsequent cell death instigates the release of DAMPS and cytokines, reprogramming the tumor microenvironment, and potentiating immune-mediated tumor cell killing.^{78,79} Radiotherapy induced interferon expression in tumor cells promotes professional antigen presenting cell activation, encouraging CD8 T cell infiltration and activation.^{80, 81} Additionally, irradiation is known to increase MHC class I expression and alter the expressed antigen repertoire on tumor cells.⁸² For these reasons, there is appreciable interest in exploiting radiotherapy to induce a tumor microenvironment suitable for effective immune checkpoint blockade therapy, in otherwise immune-cold tumors, such as hormone receptor (HR) positive breast cancers.⁷⁶

However, despite this potential immune stimulatory role, radiotherapy induced inflammation is also known to induce pro-tumor function. Inflammatory and IFN signaling often results in upregulation of pro-survival pathways in tumor cells, and increased expression of PD-L1.⁸³⁻⁸⁵ Cytotoxic T cell response is additionally dampened by the increased tumor infiltration of regulatory T cells (Treg) and myeloid derived suppressor cells (MDSCs) in response to prolonged inflammation and antigenicity.⁸⁶

Additionally, the polarity of the radiation induced pro- and anti- tumor

microenvironment response is likely influenced by innate tumor characters, as well as dose and duration of therapy. Because of these complexities, it has become increasingly important to study radiation response in patients while using clinically feasible dose regimens and timeframes. Here we use single cell sequencing to examine the tumor and microenvironment response to radiotherapy in 20 HR+ breast tumors.

Furthermore, intratumoral heterogeneity presents a major challenge to treatment response prediction as tumors may contain multiple genomic subpopulations with varying sensitivity to therapies, including radiotherapy.⁸⁷⁻⁹⁰ In fact, resistant populations of cells pre-existing in the tumor are often responsible for therapy resistance and recurrence.^{36, 37, 40, 91, 92} However, though presenting a major clinical challenge, intratumoral genomic heterogeneity can be utilized to delineate the genomic evolution of subpopulations in tumors and better understand their relationships and growth dynamics.

In the past decade, the advent of single cell genomics has afforded unparalleled ability to resolve intratumoral heterogeneity, and in particular copy number heterogeneity in aneuploid tumor cells. Aneuploidy in tumor cells has long been observable by karyotyping, genomic hybridization array, and bulk next generation sequencing.

However, sequencing of DNA copy number aberrations in single tumor cells, originally by tedious degenerate oligonucleotide-primed PCR, has led to major advances in understanding tumor copy number evolution.⁹³ This

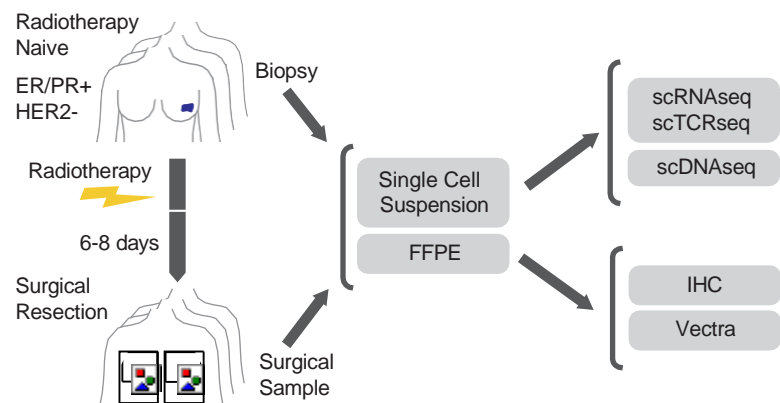


Figure 2.00: Study Overview
Design and sample acquisition for HR+ breast radiotherapy study.

work utilizes a modern, high-throughput single-cell acoustic tagmentation method (ACT)⁹⁴ to profile copynumber profiles in HR+ breast tumors and observe how they respond to radiotherapy.

Results

Single Cell Characterization Before and After Radiotherapy

We conducted a window of opportunity study in early-stage hormone receptor positive breast cancer patients (Figure 2.00). In brief, 7 days before surgical resection, radiotherapy-naïve patients were subjected to a preoperative boost radiotherapy in 1 fraction at 7.5gy or 5 fractions at 2 gy. Tumor material was collected via biopsy just prior to (± 2 days) radiotherapy and from surgical resection. On 11 pairs of these samples, we disassociated the tumor and performed scRNAseq with matched scTCRseq. Additionally, on 8 of these pairs we performed scDNA copy number profiling on nuclear suspensions from the digests.

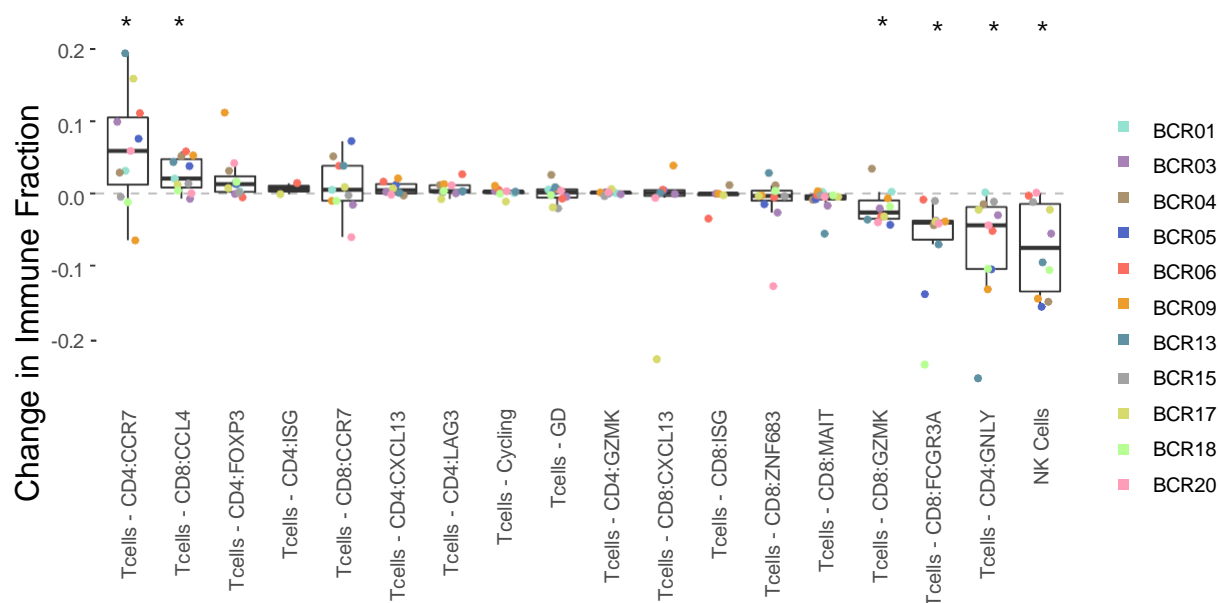


Figure 2.01: Changes in T cell populations with radiotherapy
Difference between post treatment and pre-treatment of T cell populations as a fraction of all immune cells for each patient. Star indicated $p < 0.05$

Changes in T cell populations with therapy

Sub-clustering of the T lymphocytes from the pre- and post-treatment samples (n=22) revealed eight CD8 and seven CD4 subpopulations, as well as gamma-delta T cells, NK cells, and a cycling lymphocyte population (Figure A2.10). Many of these subpopulations displayed marker genes of previously described single-cell defined T cell populations (Figure A2.07) and all populations were present in multiple patients and before/after treatment, albeit in varying frequencies. Notably, the CD4:CCR7 population, which is usually described as being naive and/or central memory-like, considerably increased in frequency with treatment to compose almost half of the post-treatment T cells present between patients (Figure 2.01). IHC confirmed a significant treatment-induced increase of CD4+CD3+ intra-tumor T cell density across patients (Figure A2.08). Patient-level changes of CD4 populations of the subset of these patients with single cell analysis, revealed that the changes in CD4 fraction was repeatedly driven by the CD4:CCR7 fraction and not large increases in Treg (CD4:FOXP3, CD4:LAG3) populations (Fig 2D). Additionally, some patients (6/11) saw small increases in T cell fraction of the corresponding CD8:CCR7 population of T cells (Figure A2.09).

Across patients, fractions of most granzyme-producing populations (CD4:GNLY, NK Cells, CD8:GZMK, CD8:FCGR3A, CD8:CXCL13) decreased with therapy. However, one cytokine-producing cytotoxic population CD8:CCL4 increased in overall fraction among T cells with treatment. Of note, unlike the CD8:GZMK CD8:FCGR3A populations, the CD8:CCL4 expressed T cell effector genes TNF and IFNG, implying that this population exists in an early-reactivation state.

Consistent with the subpopulation changes described above, gene expression changes across all T cells and patients revealed lower overall expression of cytotoxic genes (GZMH, GZMB, GNLY), but higher expression of Naive/Tcm gene (CCR7) and genes associated with tissue-homing and retention (CXCR4, CD69) (Figure A2.11). GSEA analysis confirmed that overall the T cell microenvironment was enriched for

Naive/Memory T cell gene expression post-treatment (Figure A2.12).

Changes in myeloid populations with radiotherapy

Further clustering of the myeloid population indicated six monocyte/macrophage populations (Figure 2.02). Among these, Macrophage:CD52 appeared to be the most recently infiltrating, expressing monocyte tissue-homing gene CD36 and having low antigen presentation. (Figure A2.14) However, all cells in this population belonged predominantly to only one patient in the cohort. Additionally, four of the subpopulations (Macrophage:CPB1, Macrophage:CCL18, Macrophage:CXCL10, Macrophage:CXCL3) were relatively high in expression of class II antigen presenting genes (CD74, HLA-DR, HLA-DP) but expressed distinct cytokine profiles (Figure A2.14). Furthermore, a small TAM-like population of macrophages expressing M2-like TAM markers (SIGLEC15, MMP9) was detected.

The single cell data indicated that the frequency of macrophages in the tumor microenvironment increased markedly with radiotherapy (Figure A2.06). Vectra and traditional IHC analysis further confirmed that CD68+ cells significantly increased in both frequency and density with treatment (Figure A2.16). Though the specific subpopulation nature of the macrophage response to treatment was heterogeneous across patients, almost all patients (9/11) saw an increase in a HLA-II presenting subpopulation (Figure

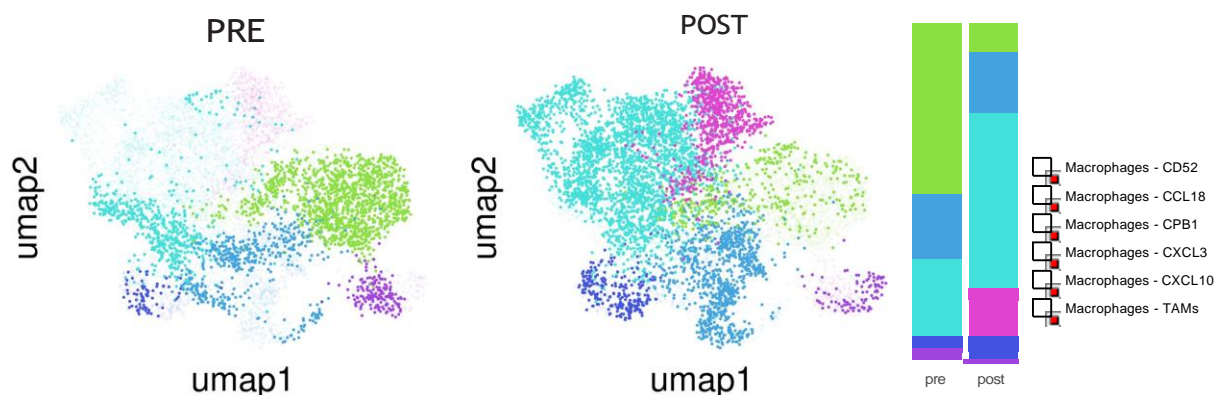


Figure 2.02: UMAP of macrophages
UMAP embedding of macrophages. Cells present in the labeled time point are opaque.

A2.17). Correspondingly, most patients (8/11) saw an increase in total expression of HLA-II presenting genes in their complete myeloid fraction of cells (Figure A2.18). Overall, this analysis indicates that this radiotherapy regime increases not only the frequency of macrophages, but also the degree of class II antigen presentation of macrophages in the TME a week after radiotherapy.

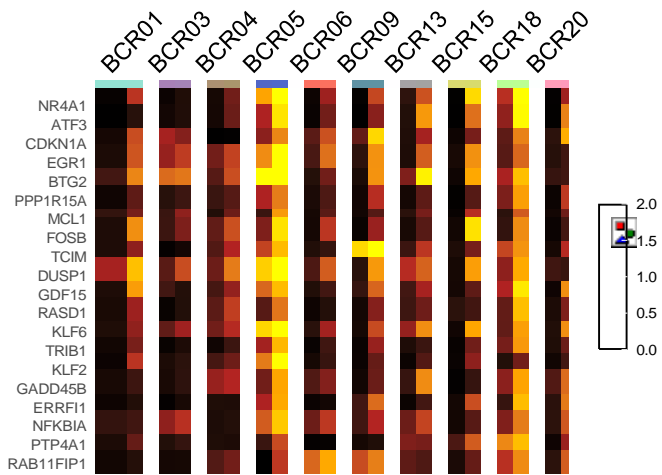


Figure 2.03: Genes expression changes in tumor cells
Average expression pre-treatment (left column) and post-treatment (right column) of genes upregulated in tumor cells across patients after radiotherapy.

Cellular response to radiation in tumor cells

Ten of the 11 patients with single cell data, possessed patient-specific epithelial (EPCAM expressing) clusters where pre- and post- treatment cells remained co-located by patient more so than timepoint in UMAP embedding (Figure A2.02, A2.03). We assumed these clusters to be tumor cells, and confirmed that they were purportedly aneuploid by running the single cell RNA aneuploidy classification tool CopyKat (Fig A2.04). Extracting these cells, we classified these apparent malignant cells by cell cycle status. Surprisingly, there was no significant difference in cell cycle classification post therapy, with this result being confirmed by Ki67 staining (Figure A2.20).

Despite large expression differences in tumor cells between patients, many genes were shared in differential expression across patients in relation to therapy (Figure 2.03). Among these were the multi-faceted tumor-promoting nuclear receptor NR4A1 and anti-apoptotic BCL2 family member MCL1. Additionally, despite inter-patient heterogeneity in tumor cell gene expression response, patient-independent GSEA

analysis of genes differentially expressed in response to treatment converged on several common pathways (Figure 2.04). This included upregulation of several immune-related gene sets including TNF, IL18 and NFKB signaling. Furthermore, across patients, we observed an increased enrichment in hypoxia-related genes and subsequent downregulation in oxidative phosphorylation gene enrichment.



Figure 2.04: GSEA cancer hallmarks
Enrichment by patient for cancer hallmark pathways in tumor cells post treatment.

Furthermore, we examined the transcriptional expression of several key breast cancer-related receptors in the tumor cells. Notably, in over half of the patients ERBB2 (HER2) expression increased transcriptionally with therapy. However, there was no difference in receptor status at the protein level with all the patients remaining HER2 negative. Nonetheless, increased ERBB2 is ominously suggestive of cells poised to acquire a more resistant phenotype in the future.

Clonal selection of DNA copy number sub clones

We performed single cell DNA copy number analysis on nuclear suspensions from 8 paired tumor samples pre- and post- radiotherapy. Though all samples exhibited aneuploid tumor cells, the number of distinct aneuploid profiles observed varied by patient (Figure A2.22). Within each patient, we compared the fraction of each aneuploid population pre- and post- treatment. In four of these patients, we observed drastic changes in subpopulation frequency post-treatment (Figure A2.23). Furthermore,

this observation corresponded to overall frequency changes of genomic regions when comparing all of the cells from each sample combined. Based on these results, we here unto describe these patients as “high selection” and speculate that these patients’ tumor were more sensitive to radiotherapy. Notably, in the tumors exhibiting selection with therapy, the regions and genes selected were specific to each patient.

The remaining 4 patients exhibited smaller clonal frequency changes which were no greater than those that would be observed by chance (Figure 2.05). However, these patients also did not exhibit large changes in frequency in any genomic regions with treatment and thus were labels as “low selection”.

Radiotherapy and DNA damage

Radiotherapy induces cell death by primarily inducing double strand breaks in DNA. Furthermore, it generates reactive oxygen species which can additionally induce single strand breaks. For this reason we expected to see tumor cells after therapy expressing genes enriched for DNA damage response and repair signature. Despite scoring tumor cells for dozens of related signatures we saw no pattern in these pathways changing with therapy, perhaps indicating at this timepoint any DNA damage from therapy has already been resolved (Figure A2.21). Additionally, IHC revealed no increases in γ H2AX foci after treatment. However, γ H2AX is known for being an early responder to DNA damage from radiation and

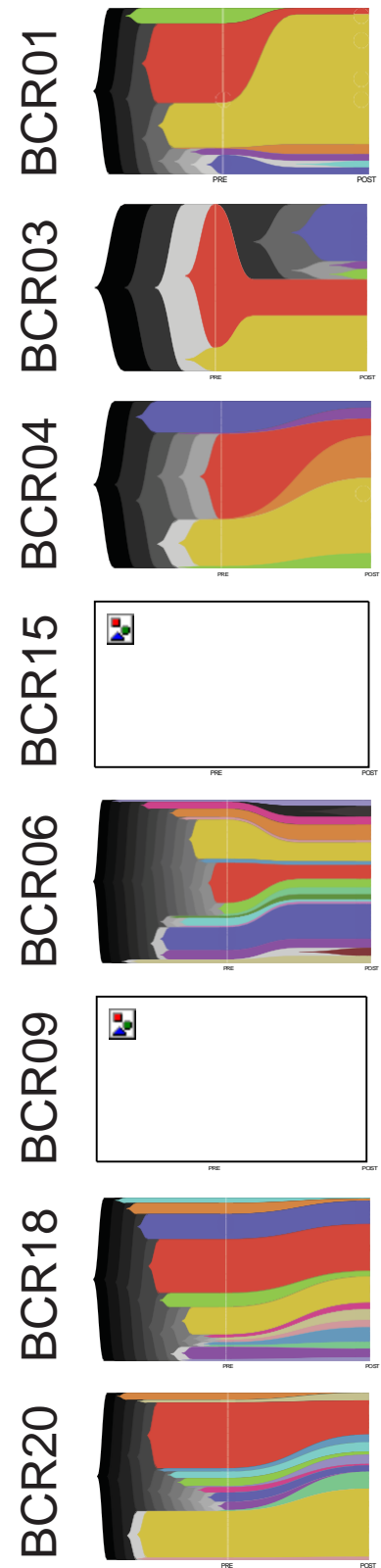
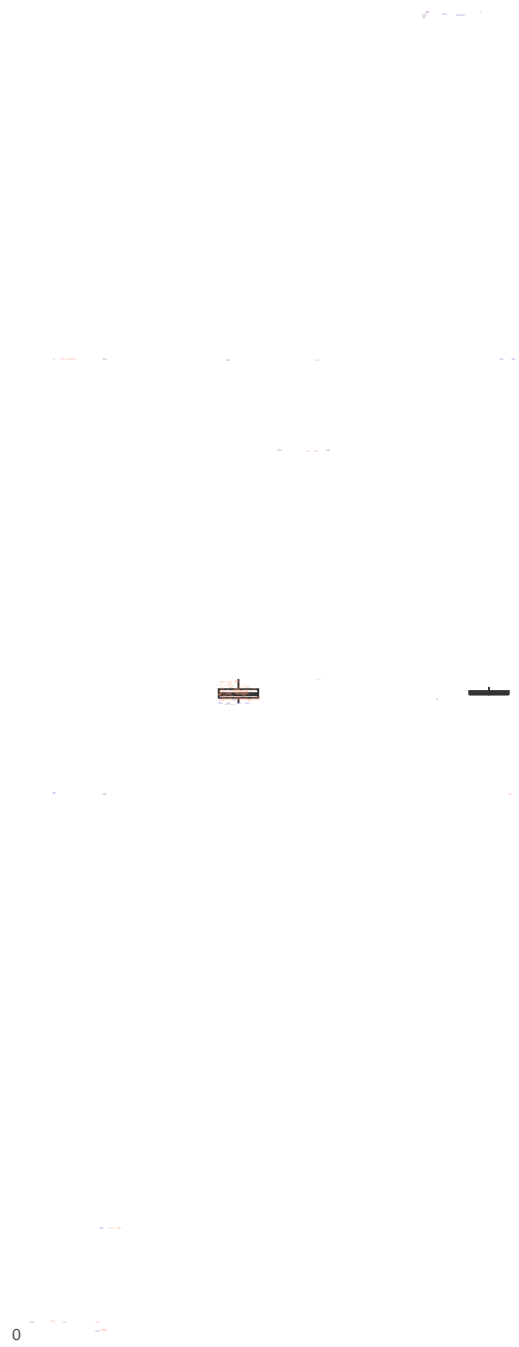


Figure 2.05: Clonal Selection of tumor cells
Change in frequency of tumor copynumber subclones with therapy.

then tapering off over the course of a few days.

Furthermore, we interrogated the scDNA copy number





—

—

—

—

—

—

—

Overdispersion

-

1



...

+

--
--
--

—

.

- - - -

- - - - -

- - - -

1	2	3	4
5	6	7	8
9	10	11	12
13	14	15	16
17	18	19	20
21	22	23	24
25	26	27	28
29	30	31	32
33	34	35	36
37	38	39	40
41	42	43	44
45	46	47	48
49	50	51	52
53	54	55	56
57	58	59	60
61	62	63	64
65	66	67	68
69	70	71	72
73	74	75	76
77	78	79	80
81	82	83	84
85	86	87	88
89	90	91	92
93	94	95	96
97	98	99	100

populations present only after



Figure 2.06: Number of copynumber breakpoints
Number of breakpoints between segments in single cell copynumber data.

therapy, we were underpowered to determine if these populations were truly therapy induced or

just rare before therapy. Additionally, we examined individual single cells for evidence of potential double strand breaks by surrogate of copy-number breakpoints (Figure 2.06). Because it can take several cells to define a population and this analysis is on an individual cell level, we suspected it would be powerful at detecting radiation induced copy number damage. Surprisingly, we found that there was no significant increase in high-breakpoint cells with therapy. This is suggestive of that either radiotherapy at these dosages did not induce DNA damage resulting in copy number changes, or that any cell with aneuploidy induced by therapy were rare and therefore not detected.

Clonal selection and the TME

To distinguish between characteristics of high- and low-selection tumors we performed differential expression analysis on the pre-treatment tumor cells from each of the selection groups. Despite the small number of samples in each cohort, this analysis revealed a surprising number of genes whose overall (Figure A2.24). Additionally, these cohorts shared gene expression patterns in their post-treatment tumor cells.

Gene set enrichment analysis was performed on the median average expression

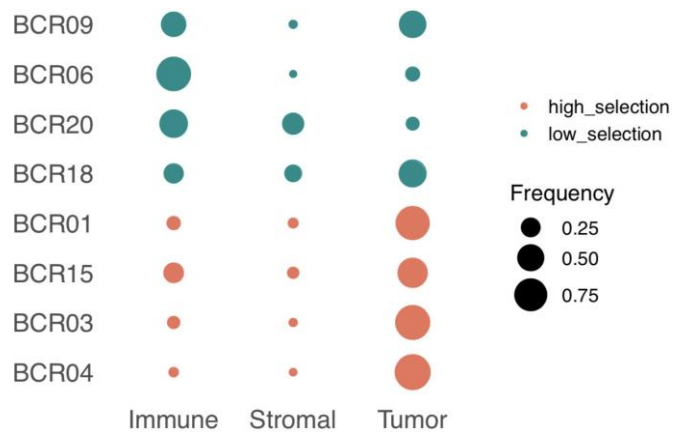


Figure 2.07: Immune fraction post-treatment
Post-treatment fraction of tumor, stromal, and immune cells colored by high and low patient DNA selection.

of gene expression between cohorts pre-treatment. The high-selection cohort was enriched for canonical estrogen related pathways, unsurprisingly because estrogen receptor, ESR1 was among the top DE genes. This is suggestive of the high-selection cohort being more Luminal A-like. On the other hand, the

low selection cohort was enriched for several genes related to interferon signaling, most notably the interferon-induced transcription factor STAT1 (Figure A2.27). Consequently, it was enriched for canonical interferon-related pathways (Figure A2.25).

To better understand the broader implications of our high-selection and low-selection cohorts, we scored our pre-treatment tumor cells for a 45-gene Interferon-Related DNA Damage Resistance Score (IRDS, from Weishelbaum et al. 2008) found to be predictive of clinically favorable outcomes after radiotherapy. We found that median expression in tumor cells of the IRDS gene signature score perfectly separated our genomic selection cohorts, a separation unlikely to occur by chance ($p = 0.028$) (Figure A2.26). Low selection patients scored higher for the signature, further indicating their likely radioresistance.

Though no particular immune sub-population was associated with a patient's genomic selection cohort, low-selection patients had significantly ($p=0.041$) higher fractions of immune cells and conversely lower ($p=0.18$) fractions of tumor cells in their tumors post-radiotherapy (Figure 2.07).

Discussion

Here we examine transcriptional changes in breast tumors and their microenvironment 7 days after radiotherapy. Notably, this is one of the first single cell

studies examining radiation response in patients. Based on this data, we've identified a CD4 central memory/naïve like T cell infiltration to be increased at this timepoint. Frequency of a similar, single cell defined population has already been shown to be predictive of favorable response to anti-PDL1+chemotherapy in a small breast cancer cohort.³² Additionally, we saw treatment-related increases in fraction of an activated, IFNG/TNF-expressing CD8 T cell population suggestive of renewed anti-tumor T cell response. Additionally, this population was expressing high levels of inflammatory cytokine CCL4, likely directing the aforementioned CD4 T cell infiltration. Furthermore, this cytokine is known to attract inflammatory myeloid populations, such as dendritic cells, to the tumor and its presence is known to be associated with favorable outcomes in several tumor types.⁹⁵⁻⁹⁷

In contrast, existing cytotoxic gene expressing T cell populations were often depleted with therapy (Figure A2.13). This includes the CD8 - CXCL13 population which, though only highly present in one patient at the outset, has been shown to be the CD8 population most predictive for response to anti-PDL1 and anti-PD1 therapy in breast cancer.⁹⁸ However, it has been shown that in the long term, the T cell populations sustaining the anti-tumor T cell response to ICB were not highly-present in the tumor beforehand.⁹⁹ Therefore, the long term effects of depleting and replacing this population are unclear.

In addition to changes in the T cell composition, we saw a notable increase in myeloid cell infiltration with therapy. Overall, class II antigen presentation across the macrophage compartment was elevated, indicating a favorable environment for T cell response. However, conflictingly, the population of macrophages which increased with therapy for most patients expressed CX3CR1, which on macrophages is associated with T cell suppression, and unfavorable response to anti-PD1. In contrast, there was no overall increase in inflammatory CXCL9/10 expressing macrophages indicating that they are potentially unnecessary for the observed T cell attraction. All together increases in antigen presentation and T cell activation despite a large suppressive

macrophage presence is difficult to make sense of on its own, suggesting observations at later timepoints are needed. In addition, this result suggests that ablating CXCR3 macrophages would likely increase T cell response further, when combined with radiotherapy.

Further complicating interpretation of the macrophage response were the heterogeneous changes observed in only a few patients. For example, only 2/11 patients saw increases of macrophages expressing CCL18, a cytokine known in several cancers to promote angiogenesis and metastasis.¹⁰⁰⁻¹⁰³ On the other hand, 2/11 patients saw increases of CXCL2, CXCL3, and CCL4 transcribing macrophages. This is the expected phenotype of an IL-1 stimulated macrophage, implying that IL-1 signaling is sometimes involved in the radiation induced inflammatory response. This inter-patient heterogeneity suggests that the macrophage response to radiotherapy is highly multi-faceted and that larger studies are needed to further understand it.

This data overall reveals that though hormone receptor positive breast cancer is generally considered an immunologically “cold” tumor, radiotherapy clearly can still induce significant changes in the tumor microenvironment. In contrast, in tumor cells we did not observe the changes with therapy that one might expect. We saw no evidence, at the transcriptional level, of increased HLA-I antigen presenting genes on irradiated tumor cells. This suggests that therapy at this dose and timepoint is not increasing the amount of antigen presented by tumor cells.

Additionally, we saw no evidence of DNA damage or its response in the tumor cells other than perhaps increases in NFκB signaling. We did however observe transcriptional changes in tumor cells similar across patients, suggesting a consistent molecular response to radiotherapy at this timepoint, despite patient-specific transcriptional and genetic backgrounds. Nevertheless, it is difficult at this timepoint to determine if the radiation induced transcriptional response in tumor cells is pro- or anti-tumor. Some of the genes in the signature, such as the anti-apoptotic MCL1, have clear pro survival functions. Others genes, such as NFκB inhibitor NFKBIA, are markedly hostile to cell

survival. Additionally several genes in the gene set, such as EGR1 and NR4A1, have paradoxically been described as both tumor promoting and suppressing in different contexts.^{104-106,107, 108} Therefore, it is not definitive at this timepoint whether the signaling induced in the tumor will later result in cell death, or successful escape from it. Longer timed observations are likely necessary to determine this.

Methods

Sample preparation for single cell sequencing

Tissue from fine needle aspirates and surgical dissections were minced by scalpel and digested in DMEM with Collagenase A and trypsin for 1hr at 37°C. The resulting single cell suspension was passed through a 40µm filter and red blood cells were lysed. The resulting cell pellet was washed in PBS and frozen in FBS with 10% DMSO. Samples were then thawed for scRNA sequencing preparation and washed in PBS with 5% BSA. Any cells in the suspension remaining after scRNA loading were lysed in NST buffer with DAPI to form nuclear suspension for scDNA sequencing.

Single cell RNA and TCR sequencing

High throughput single cell RNA sequencing was performed with the 10X Genomics Chromium platform's 5' v.1.0 kits (product codes 1000014, 1000020, and 1000151) with TCR enrichment 410 (1000005) according to the manufacturer's protocol. Briefly, a recovery target of 10,000 cells were loaded into the Chromium Single Cell Chip A, and the emulsion was reverse transcribed on a BioRad T100 thermal cycler. The samples were then purified with Dynabeads (Thermo Fisher Scientific, 37002D) and the cDNA was amplified in 24 PCR cycles. Of this amplified cDNA product, 2µL was used to perform TCR enrichment. TCR libraries were only constructed on samples with a visible amplification trace of the expected size. Up to 50 ng (or 20 µL) of the transcriptome cDNA

was used for library construction per the manufacturer's instructions, and the barcoded sample libraries were then pooled for sequencing. The single cell transcriptome library pools Transcriptome libraries were sequenced on an Illumina Novoseq 6000 (Read 1, 26 cycles; Index 1, 8 cycles; Read 2, 91 cycles), to a median targeted sequencing depth of 30,000 read pairs/cell. Pooled TCR libraries were sequenced 150 cycle paired-end on an Illumina Miseq to a targeted depth of 1,000 read pairs/cell.

Single cell RNA data processing

Single Cell transcriptome files were demultiplexed, aligned to the human genome (GRCh38), and processed into gene count using 10X Genomic's Cell Ranger pipeline version 3.1.0. Unfiltered count matrices were analyzed in R version 3.6.2 and the package DropletUtils (v 1.6.1) with default values was used to detect barcodes containing cells. The resulting cells were then processed using the Seurat package (v 3.2.2) and filtered for quality under the following constraints: percent mitochondrial UMI < 20%, percent ribosomal UMI < 40%, number of UMI > 200, number of UMI < 40000, number of genes < 7500. Samples were scaled with the SCTransform function using the top 3000 most variable genes, and regressing for percent mitochondrial UMI. PCA was performed on the scaled values and the top 30 PC's were used for UMAP embedding and SNN clustering (with resolution parameter 0.4). High-level cell types were then labeled based on the cluster's top differentially expressed genes by Wilcox test. Major cell types were then separated for further subtype clustering.

Single cell RNA TCR analysis

Single cell TCR sequences were called using version 3.1.0 of "cellranger vdj" in the Cellranger software suite. Clonotypes with only an alpha or a beta chain called were re-assigned to a clonotype from the same patient with, in this priority, an identical beta or

alpha cdr3 nucleotide sequence.

Single cell copy number sequencing

Single cell copynumber sequencing was performed using direct tagmentation as previously described in Minussi et al., 2021. Briefly, single nuclei suspensions were created in NST buffer with DAPI and single nuclei were sorted into 384 well plates using a BD FACS Melody. The nuclei were then lysed, tagmented, and amplified with barcoded primers in 16 PCR cycles with a labcyte ECHO 525 acoustic liquid handler.

Single Cell Copy Number Data Processing and Filtering

Single cell copy number data was demultiplexed and aligned to hg38. Single cell data was then processed using best practices of the CopyKit package in R. Briefly, reads were binned to a genome scaffold with, on average 200kb bins and each bin's count ratio was calculated relative to the mean bin count ratio. Cells were then marked for filtering with the function *filterCells* and correlation threshold set to 0.8. Cells were additionally marked as Normal/Tumor based on aneuploidy with the function *findNormalCells*. Cells were segmented using circular binary segmentation and segment integer values were calculated using scQuantum via CopyKit's *calcIntegers*.

Copy Number subclone clustering and analysis

Aneuploid cells were clustered by combining cells from both timepoints within a patient and using the k parameter from *FindSuggestedK*, were clustered using *findClusters*. Consensus profiles were then generated from the median integer copy number value for the cluster's segments. Timescape plots were generated using the bioconductor package cellscape, using trees inferred from copykit's *runConsensusPhylo*.

Future directions

Both of the studies mentioned in this dissertation, though extensive, were largely observational and generated numerous avenues to pursue for future study. Notably, we have defined T cell populations present in PDACs at the transcriptional level. However, isolation of these populations at the surface protein level is often necessary for functional studies and potential clinical assays and products. Nevertheless, finding robust surface protein markers for transcriptionally defined cell populations is non-trivial, and likely will entail extensive trial and error. One extensive strategy to do such, could entail repeating the scRNAseq of T cells from additional PDAC samples, but with an added step of profiling a large panel of DNA-barcoded antibodies in the same single cells (i.e. CITE-seq). For at least the more frequent populations, these experiments could possibly identify transcriptomic expression cluster specific, and/or predictive TIL therapy persisting, surface protein markers which could later be validated in smaller FACS panels. Utilizing this strategy to be able to separate distinct, single-cell defined T cell populations could prove beneficial not only for designing future TIL product strategies. Moreover, isolating highly specific transcriptional states of T cells could prove beneficial for functional research experiments, such as identifying cytokines and checkpoints to assist in stimulating and repressing specific populations or development tracts.

Furthermore, we have hypothesized the developmental relationship between these cell states from observational data, but we have not proven experimentally their relationship. Theoretically, it is possible with single cell DNA barcoding methods to track individual population's development proactively. Assuming a particular transcriptional state could be isolated (as described above), barcoded populations could be introduced into mouse models to more directly trace development. However, the applicability of these experiments would be dependent on not only the ability to isolate specific populations, but also to mimic the human tumor microenvironment to direct the same population development. In the context of a TIL product, by barcoding prior to REP, this strategy could be utilized to answer the question: which specific

transcriptional states are responsible for expansion within a given clonotype? Though, in this study we use TCR to track expression states through REP, most but not all cells within a clonotype begin in the same expression state. Re-barcoding could minimize this potential confounder.

Additionally, though we have traced which cell populations persist in the ACT product, we have not yet traced which, if any, transcriptional states from the ACT product persist and mount an anti-tumor response when infused back into patients. Future studies could perform the same scRNAseq/scTCRseq strategy to observe which clonotypes from the TIL product are observed long-term in PBMCs, and potentially the tumor for patients treated with the therapy and profile their expression states.

Secondly, the radiotherapy study, described in this dissertation was intended as an observational hypothesis generating study and as such has several future directions. To start with, we only examined the TME in a single post-radiotherapy timepoint. Because of this, we likely missed some of the early cellular response to therapy such as initial cell death and DNA damage repair. To elucidate mechanisms of these processes in patients at these dosages, future studies should consider observing an earlier timepoint (such as 1 day) after radiotherapy, if feasible. Additionally, cell death and DNA damage response are often protein-based pathways changing through phosphorylation, and not necessarily transcriptional signaling. As such, protein-based analyses should be proactively planned alongside transcriptional ones for future studies.

Additionally, perhaps in a cohort more amenable to serial biopsy, longitudinal data with clearer treatment response metrics would better determine the genomic selection characteristics of therapy. Though we saw genomic selection in some patients a week after radiotherapy, it is unclear if the remaining populations which seem innately insensitive would persist long-term or are exhibiting delayed cell death compared to more sensitive clones. Delineating this is likely only possible in a longer timeframe study. Alternatively, though unlikely, should any of the patients in this study exhibit disease recurrence their tumor cells could be compared genomically to their

tumor cells at other timepoints to infer relation. Furthermore, a timepoint two to three weeks after therapy may be better to measure levels of T cell response to the tumor. Though we observed naive/early memory and early activated T cells in the tumor one week post therapy, it's unclear at this point if these populations would lead to tumor clearance (possibly with the help of a checkpoint inhibitor) or will become exhausted and contribute to long-term inflammation and tumor progression. Examining this warrants future studies in mouse models where Tcell populations can be tracked by serial biopsy or strategically times sacrificing.

Along this tract, the myeloid cell changes seen in patients presents numerous possibilities for enhancing the effects of radiotherapy. Almost all patients in this study saw an increase in inflammatory and tumor-promoting myeloid cells with therapy. This suggests that, similar as to described previously for T cell populations, the myeloid populations found in breast tumors should be isolated and further studies outside of patients. By understanding how these populations are stimulated, inhibited, and developmentally related, it could be possible to identify targets which assist myeloid cells with enhancing T cell response without promoting tumor development. In closing, both of these studies have generated numerous avenues for future functional and translational research.

•

Appendices

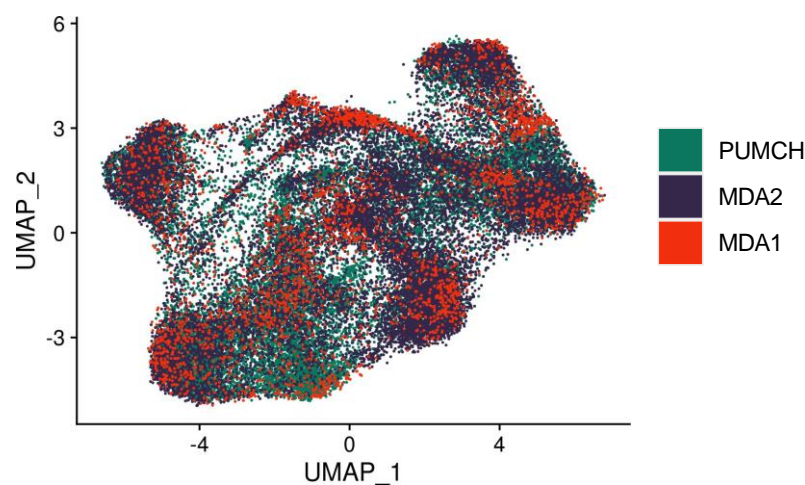


Figure A1.01: UMAP by cohort
UMAP embedding of all T cells colored by cohort

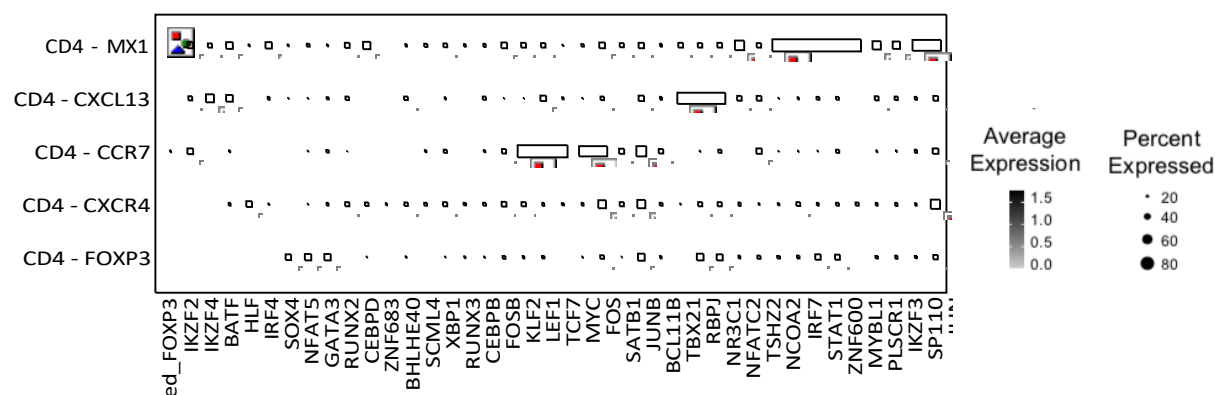


Figure A1.02: CD4 transcription factors
Average and percent expression of top transcription factors for each CD4 cluster

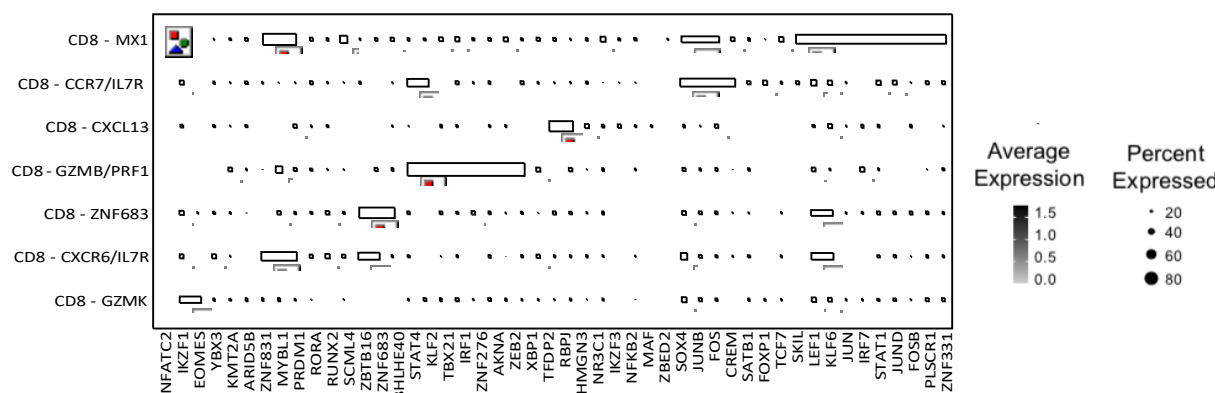


Figure A1.03: CD8 transcription factors
Average and percent expression of top transcription factors for each CD8 cluster

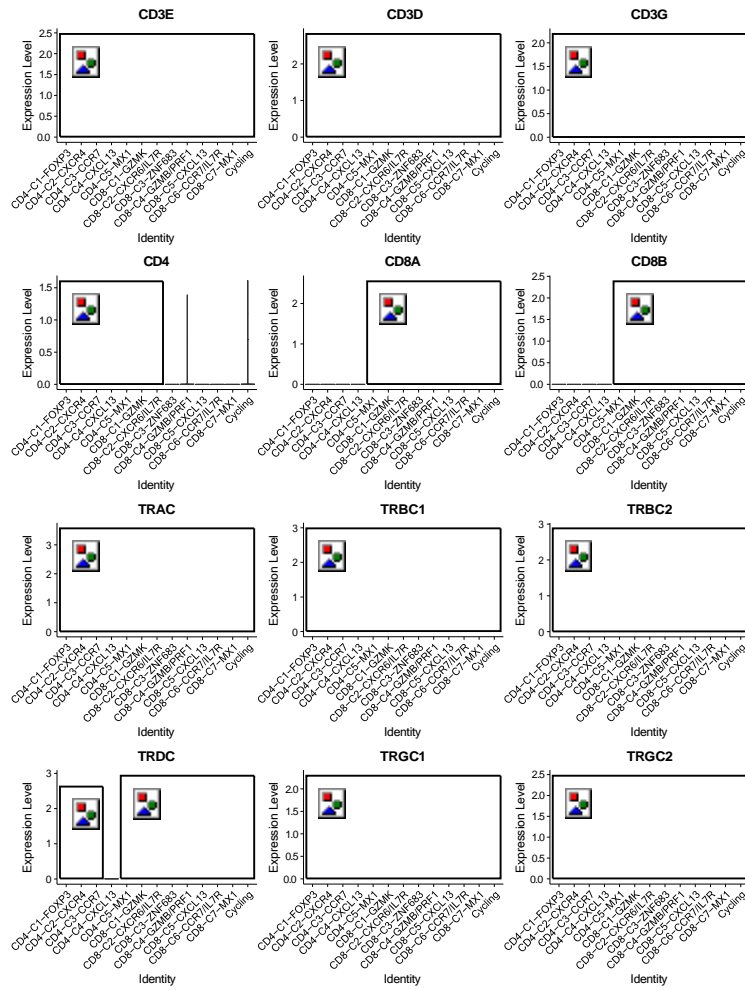


Figure A1.04: T cell genes
Normalized expression of T cell marker genes by cluster

Figure A1.05: Checkpoint genes
Expression of known tumor checkpoint genes by T cell population

Figure A1.06: Single cell heatmap
Heatmap of top markers of each population. Each column is a single cell.

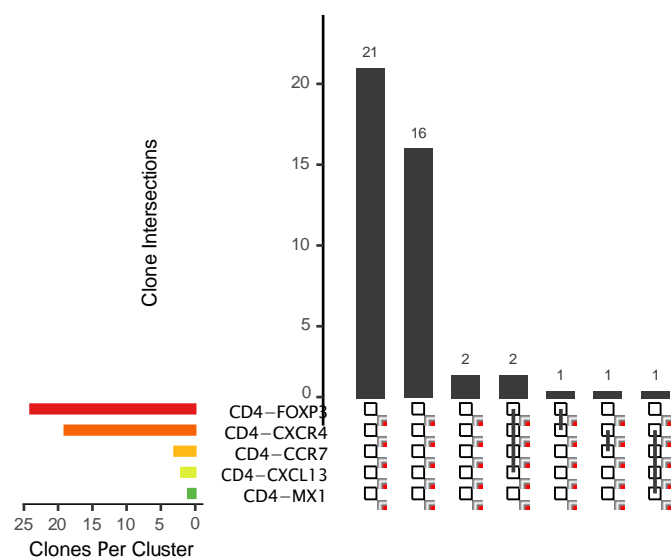


Figure A1.07: CD4 TCR overlap
Overlap of expression states for expanded ($n \geq 2$) clonotypes.

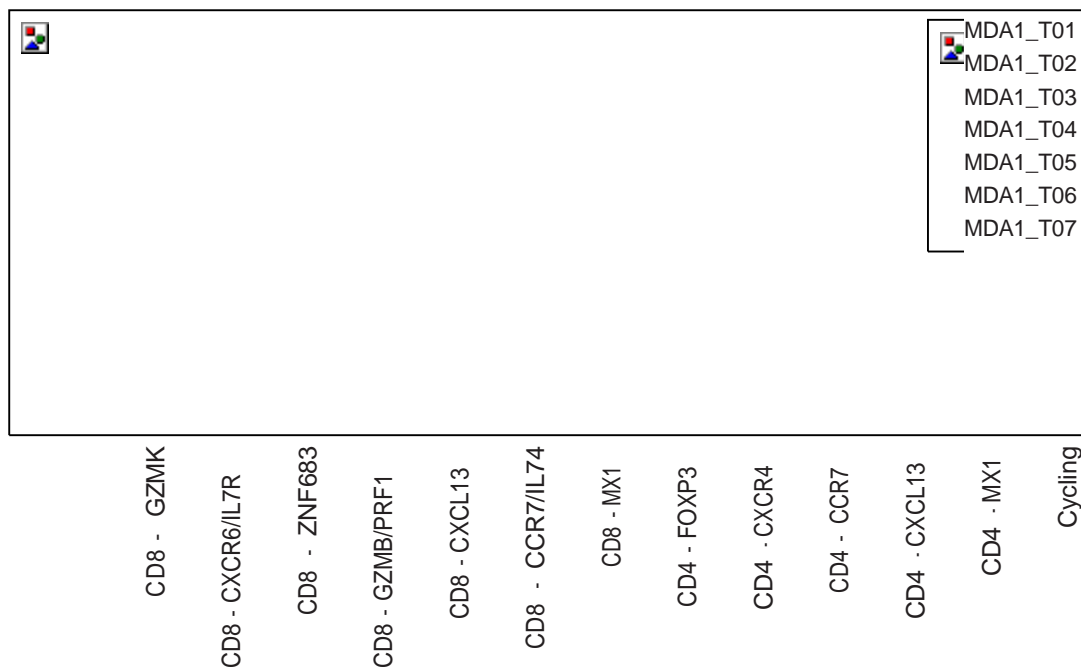


Figure A1.08: Gini index by cluster
Gini inequality of clonotype count for each patient's T cells in each population containing at least 5 cells.

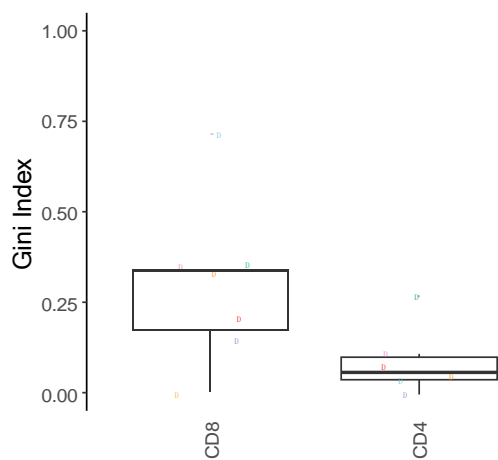


Figure A1.09: Gini index CD4/CD8
Gini index combining CD4 and CD8 populations for each patient.

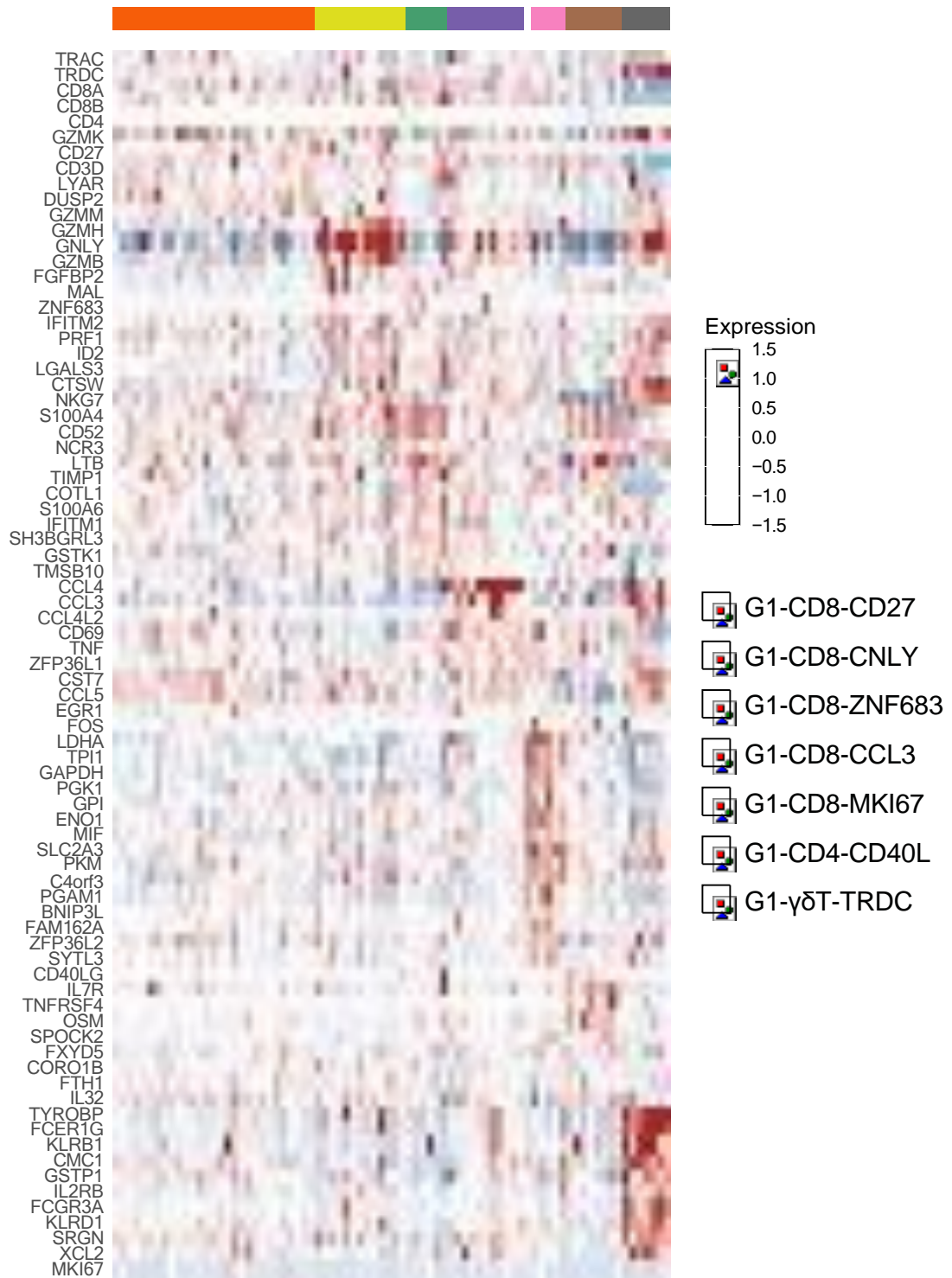


Figure A1.10: Grown single cell heatmap

Top marker genes of each of the grown clusters. Each population was randomly down-sampled to ≤ 1000 cells for plotting.

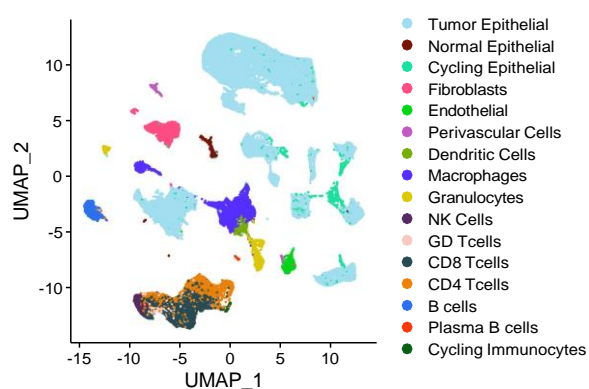


Figure A2.01: UMAP by major cluster
UMAP embedding of all cells labeled by major cell type.

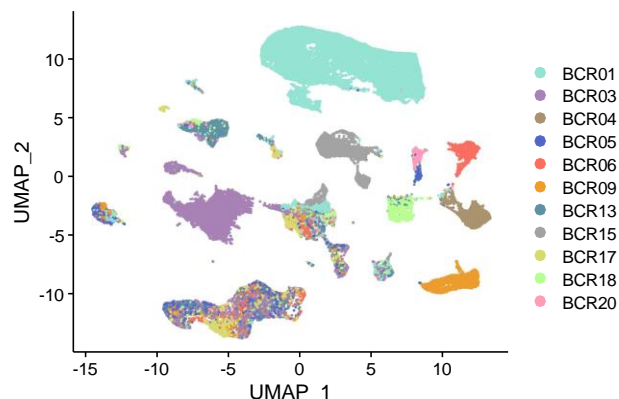


Figure A2.02: UMAP by patient
UMAP embedding of all cells labeled by patient.

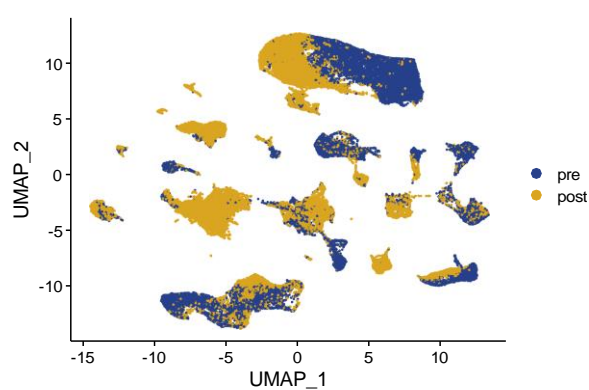


Figure A2.03: UMAP by timepoint
UMAP embedding of all cells labeled by timepoint in respect to radiotherapy.

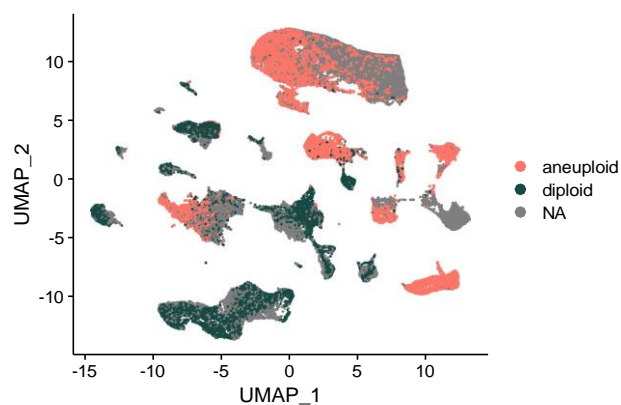


Figure A2.04: UMAP by inferred ploidy
UMAP embedding of all cells labeled by ploidy status as predicted by Copykat.

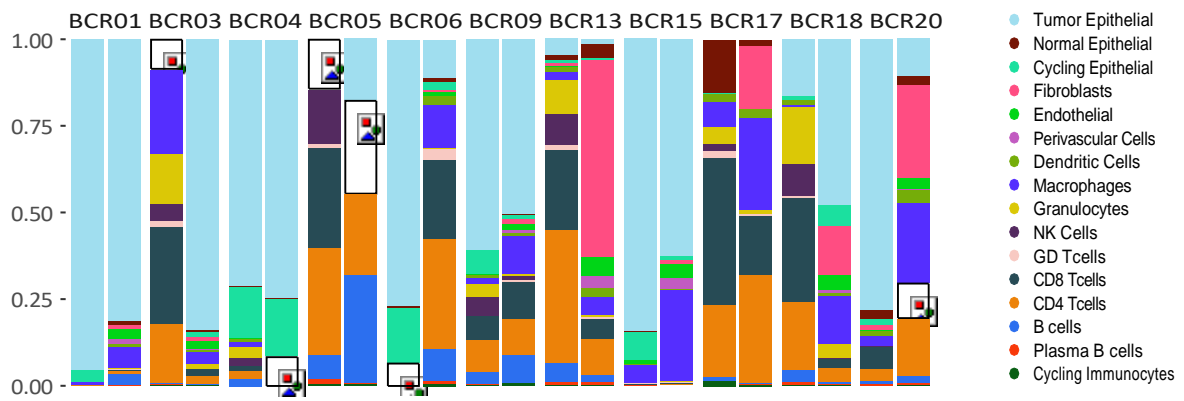


Figure A2.05: Frequency of major clusters
Frequency of major cell types for each patient before (left bars) and after (right bars) radiotherapy.

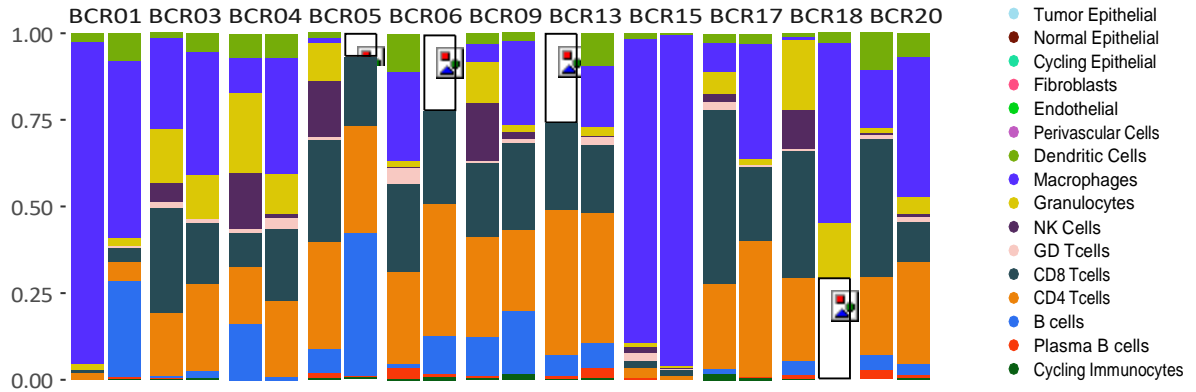


Figure A2.06: Frequency of major immune clusters
Frequency of major immune cell types for each patient before (left bars) and after (right bars) radiotherapy.

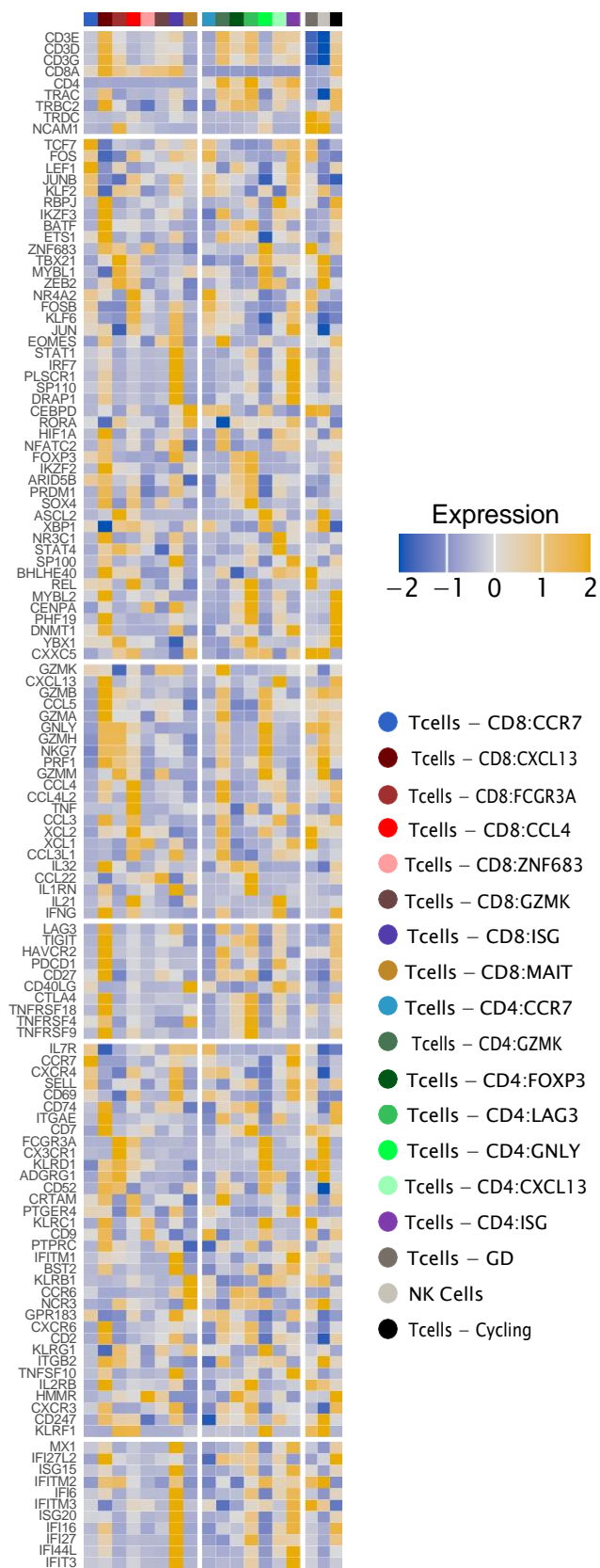


Figure A2.07: T cell marker heatmap
Average, scaled expression of top T cell markers for each cluster.

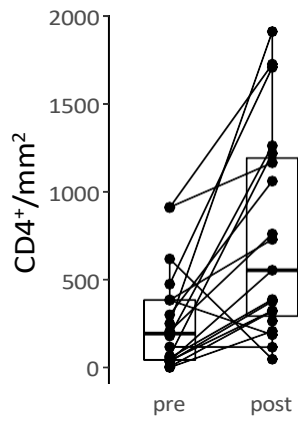


Figure A2.08: CD4 density
CD4+ T cell density of the tumor area pre and post radiotherapy, measured by IHC.

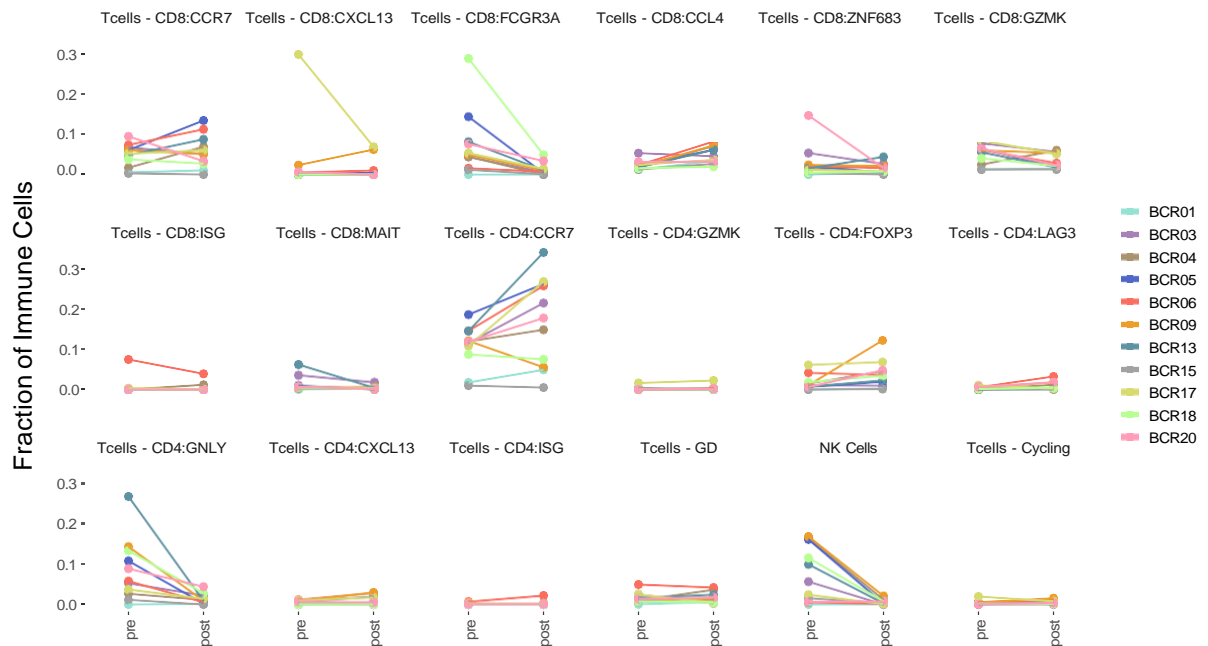


Figure A2.09: T cell cluster frequency
Frequency of T cell populations before and after therapy by patient.

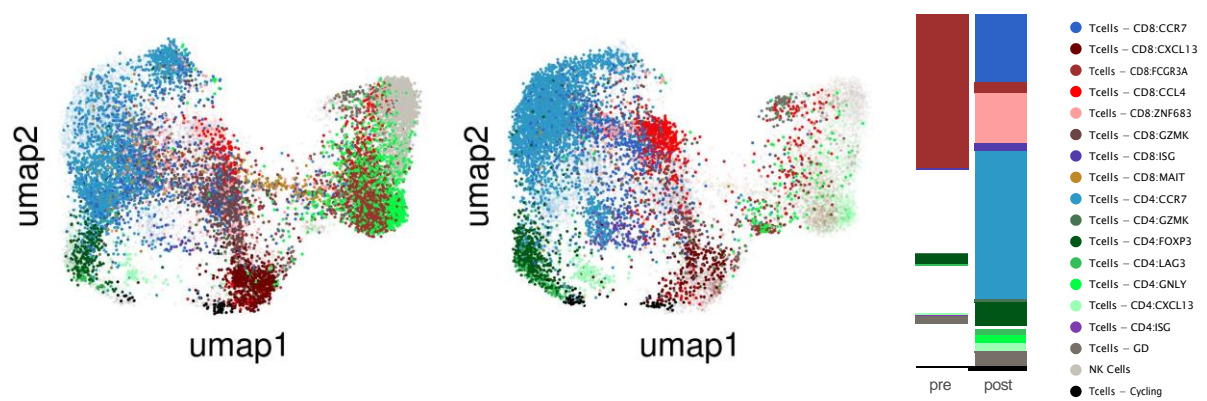


Figure A2.10: T cell cluster UMAP
Left: UMAP embedding of all T cells pre (left) and post (right) radiotherapy. Right: Frequency of patient-combined T cell frequencies.

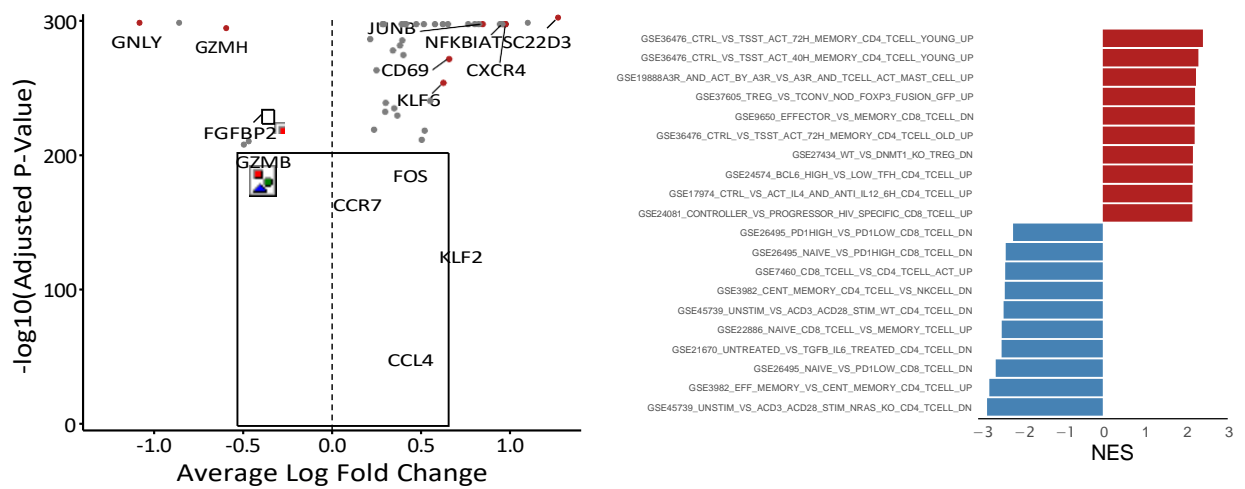


Figure A2.11: Change in T cell genes
Average gene expression changes of T cells with radiotherapy.

Figure A2.12: T cell GSEA
GSEA of Top T cell pathways enriched in T cells with radiotherapy.

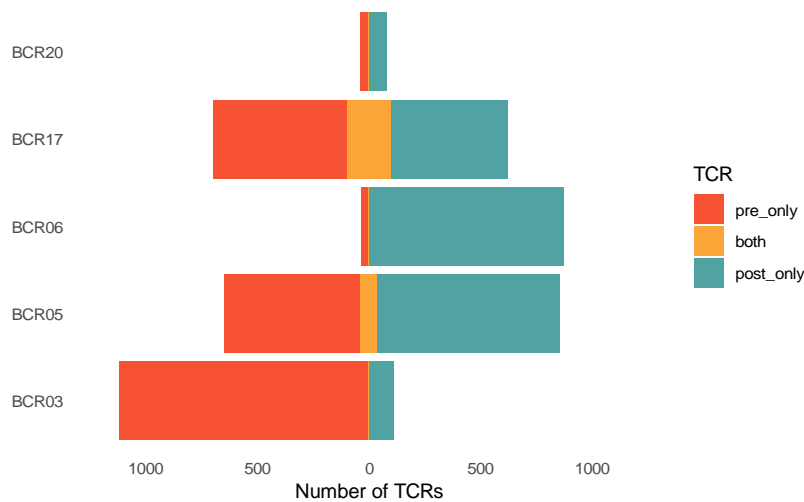


Figure A2.13: TCR presence
Number of T cell clonotypes present pre/post radiotherapy only, or at both timepoints.

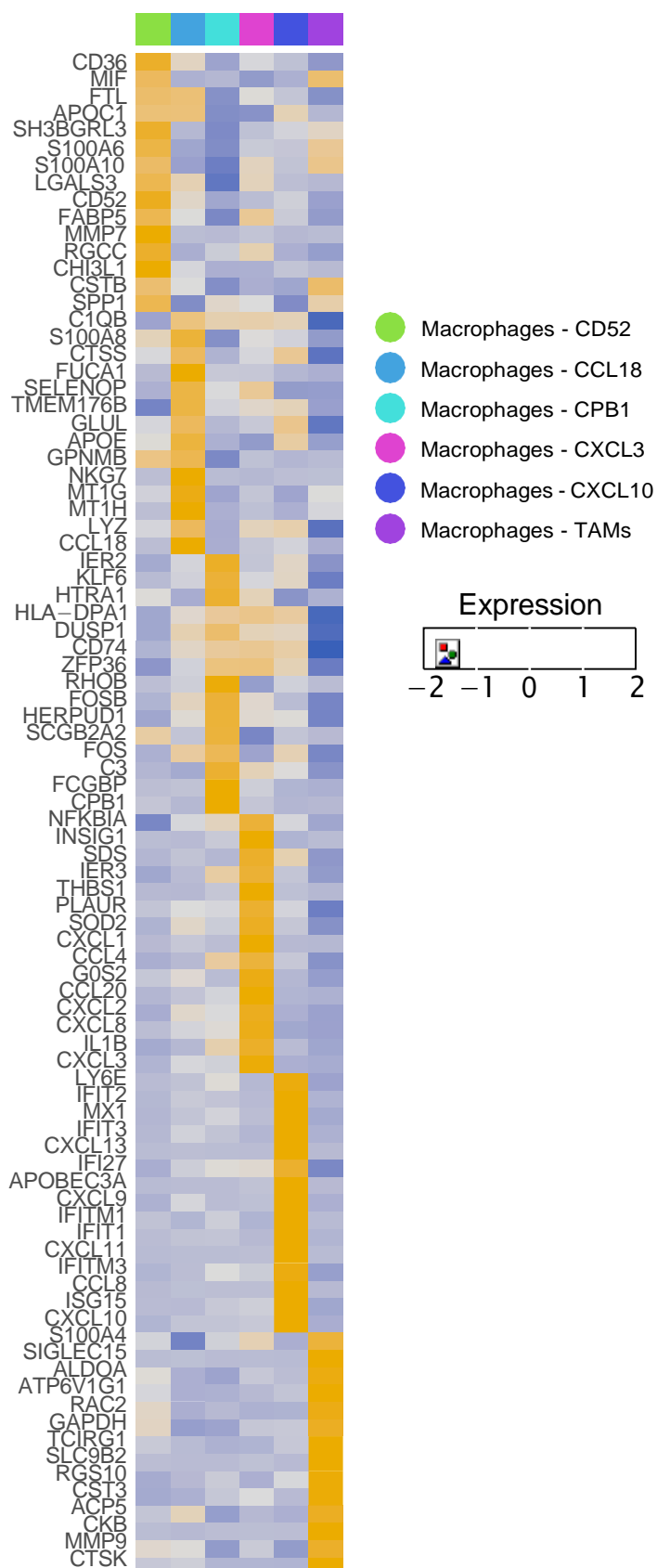


Figure A2.14: Top macrophage marker heatmap
Average scaled gene expression of top macrophage population markers.

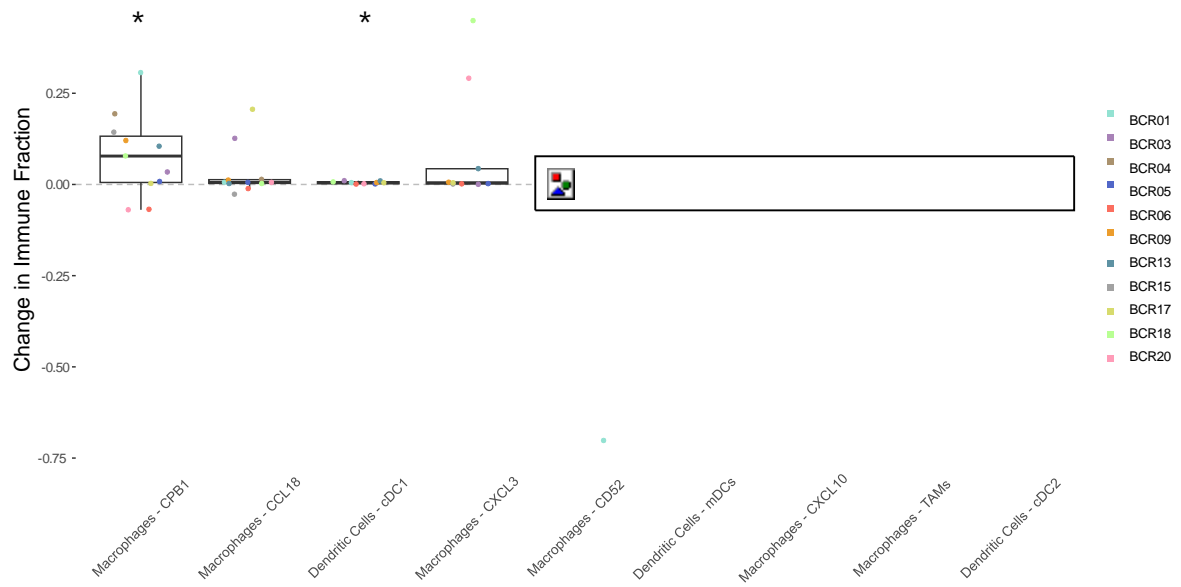


Figure A2.15: Change in myeloid populations
Change in frequency of myeloid populations with therapy.

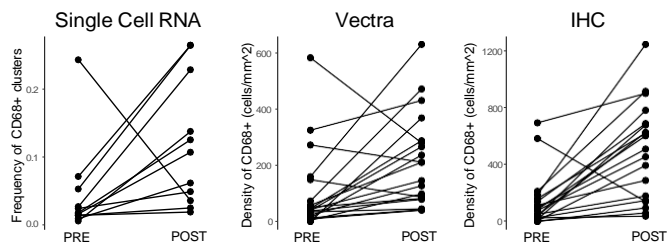


Figure A2.16: Change in macrophage frequency
Change in CD68+ cells as measured by scRNAseq (left),
vectra (center), IHC (right).

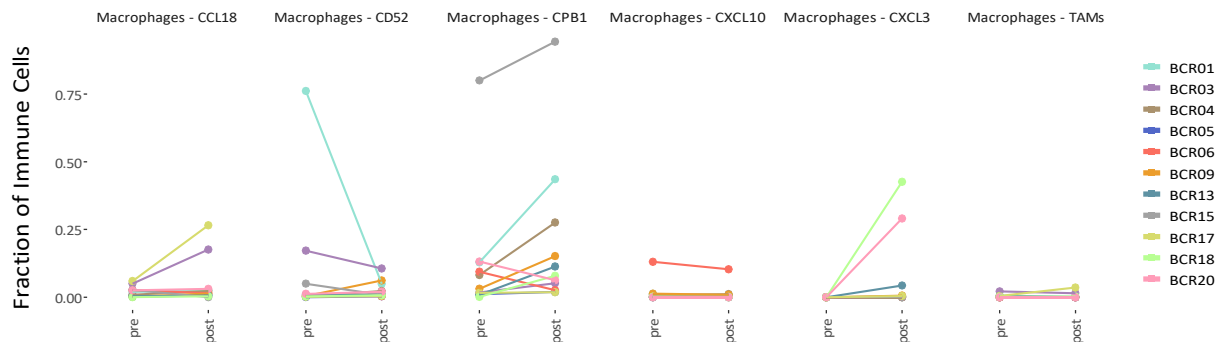


Figure A2.17: Frequency of macrophage populations
Frequency of macrophage populations as a fraction of all immune cells.

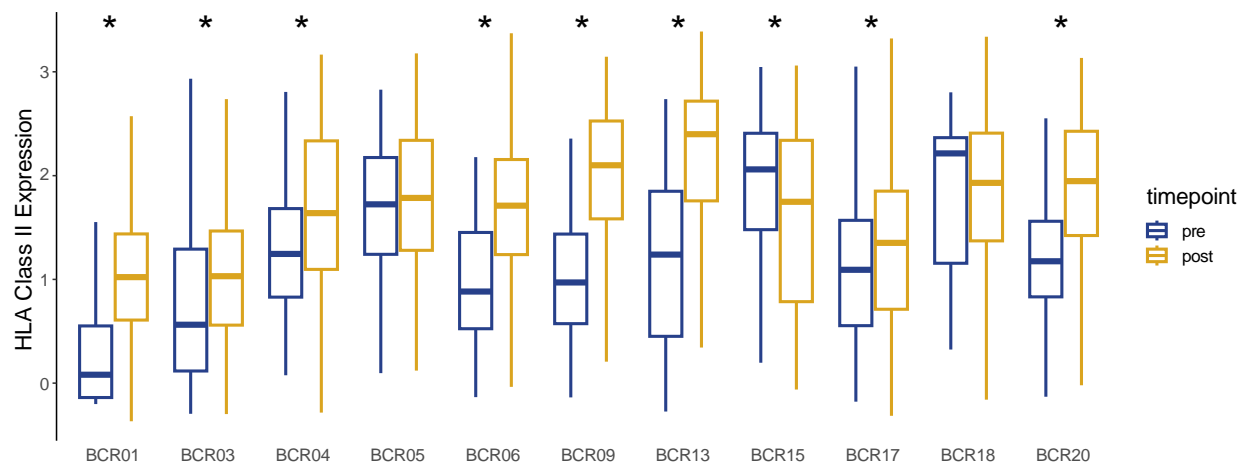


Figure A2.18: HLA class II expression
Expression score of myeloid cells for a signature of HLA II genes.

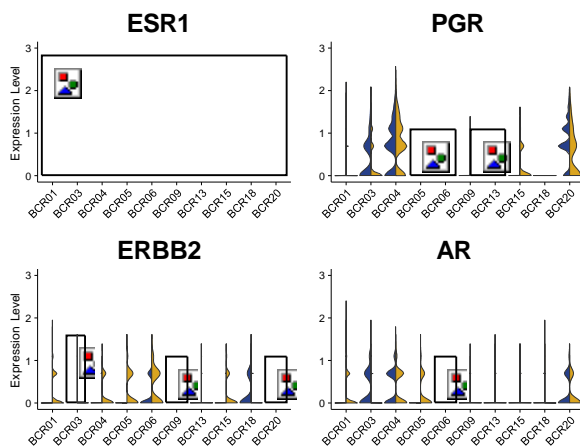


Figure A2.19: Tumor receptor expression
Tumor expression of applicable breast cancer receptor genes in tumor cells before (blue, left) and after (yellow, right) radiotherapy.

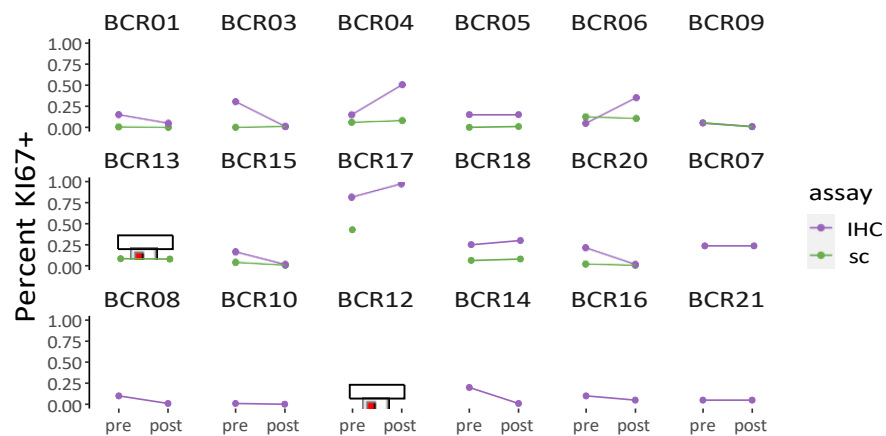


Figure A2.20: Tumor KI67
Percent of KI67 positive tumor cells by single cell analysis and IHC.

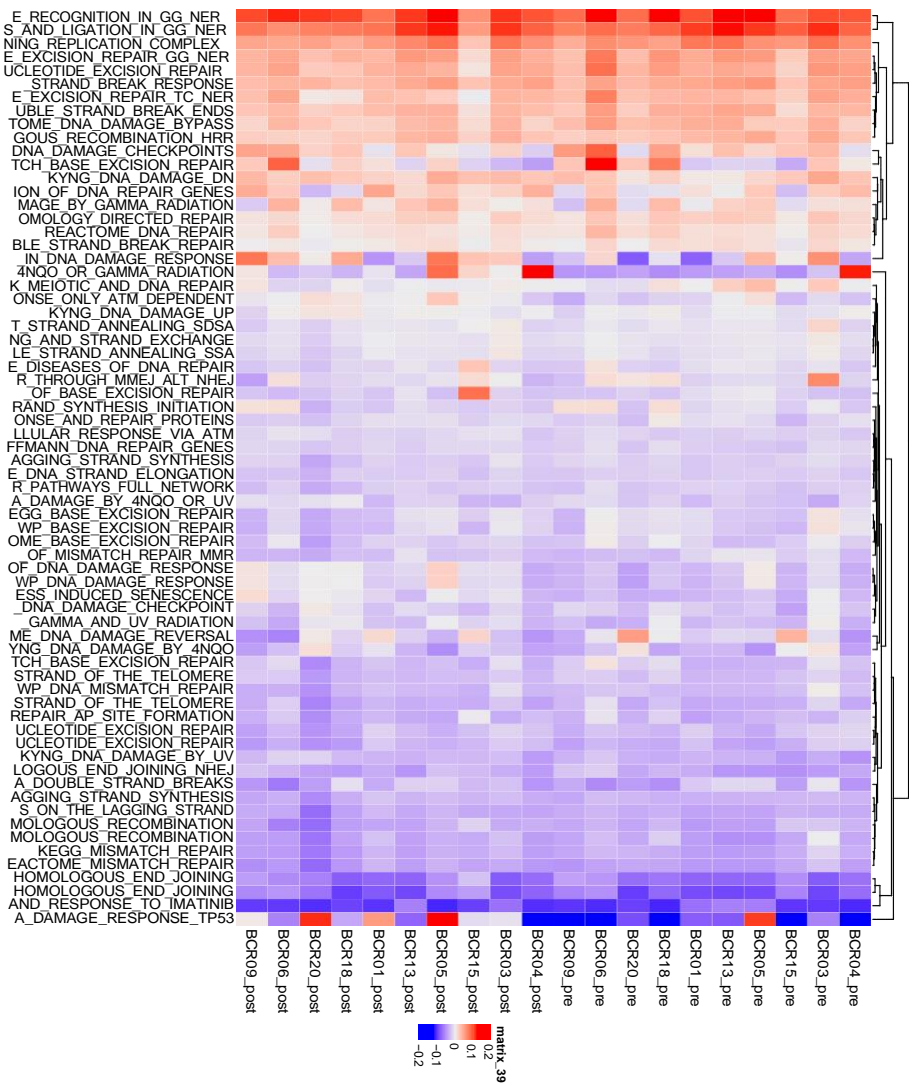


Figure A2.21 : DNA damage pathways

Average score for each patient for all DNA damage and repair related signature from msigdb.

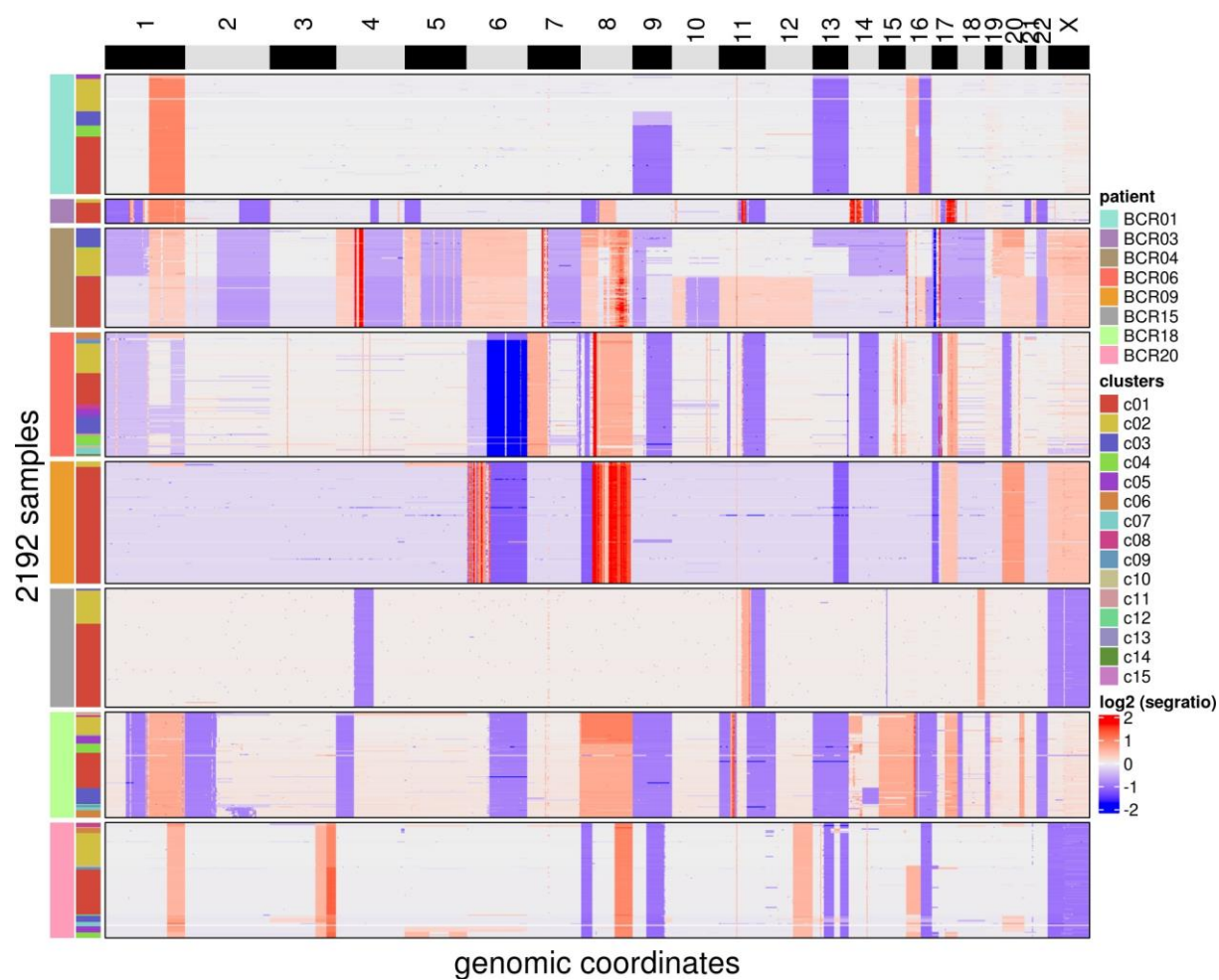


Figure A2.22: Single cell copy number profiles
Pre-treatment single cell copy number profiles for all patients and all clusters.

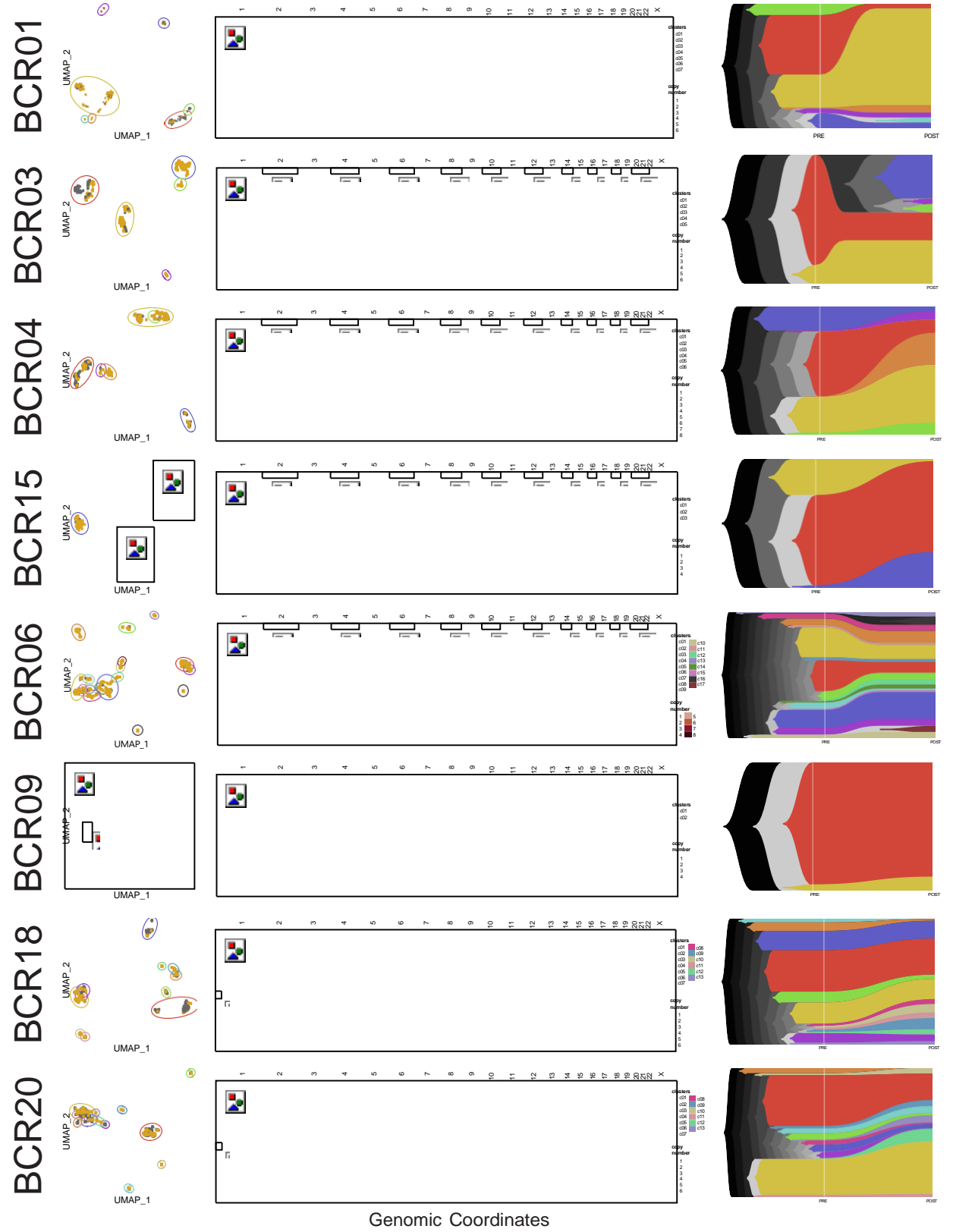


Figure A2.23: Single cell copynumber changes
 UMAP embedding of single cell copy number clusters colored by timepoint and annotated by cluster (left). Integer-scaled single cell copynumber consensus profiles (center) and their frequency changes by timepoint (right). Top four patients represent the high-selection group. Bottom four represent the low-selection group.

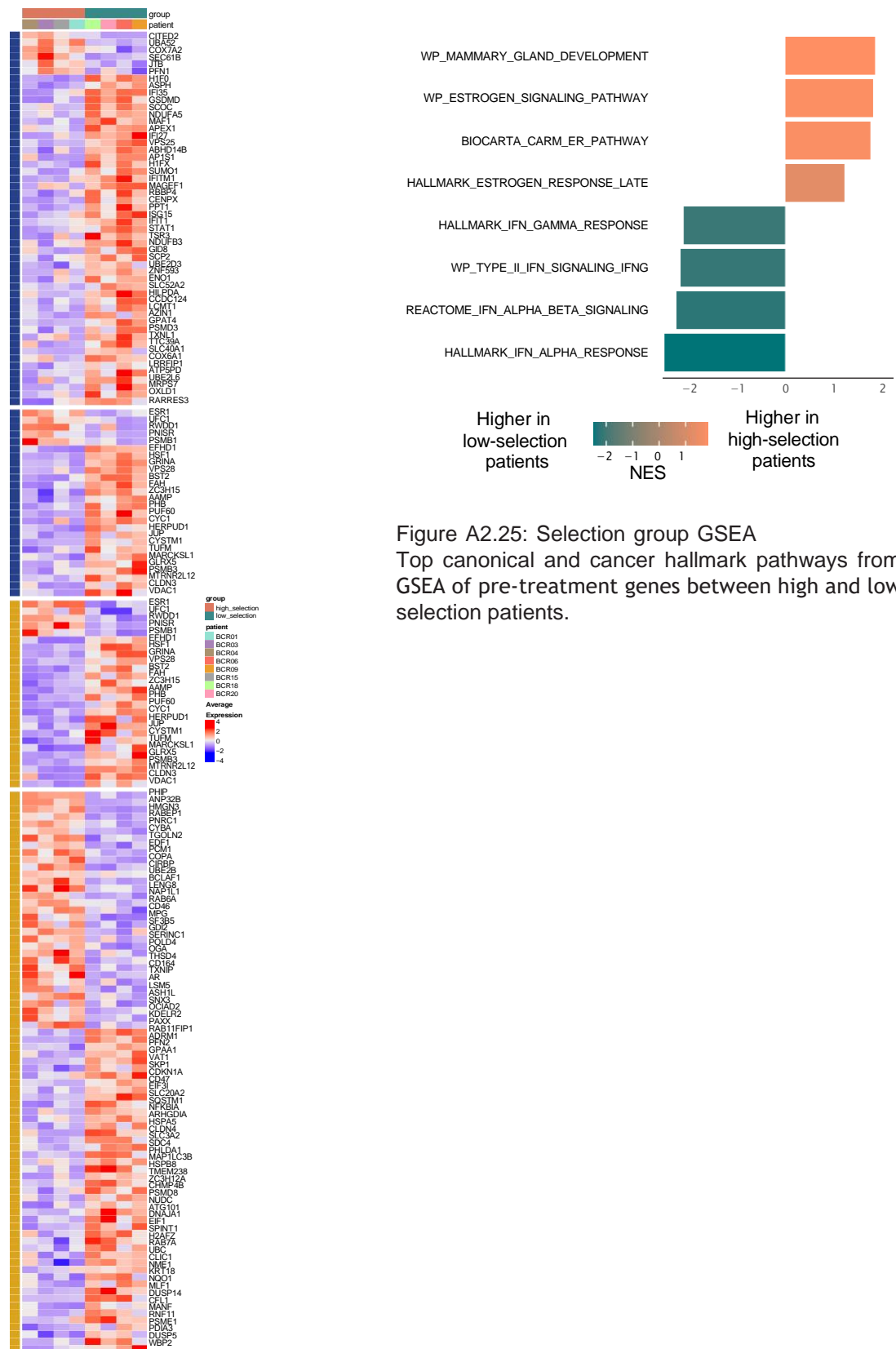


Figure A2.24: Selection group expression differences
Average expression of top genes differentially expressed pre (blue) and post (gold) treatment between tumor cells of the high- and low-selection groups.

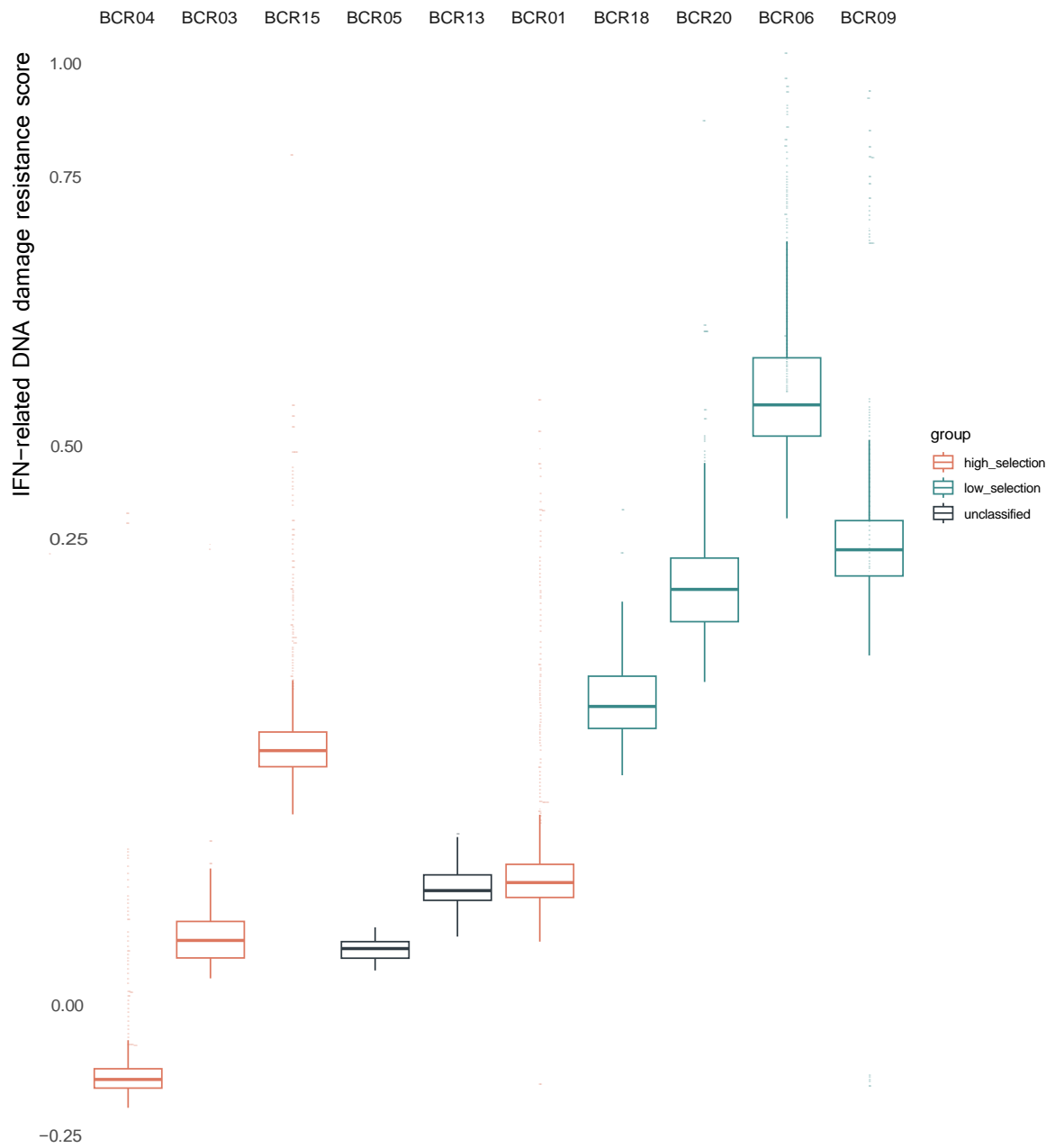
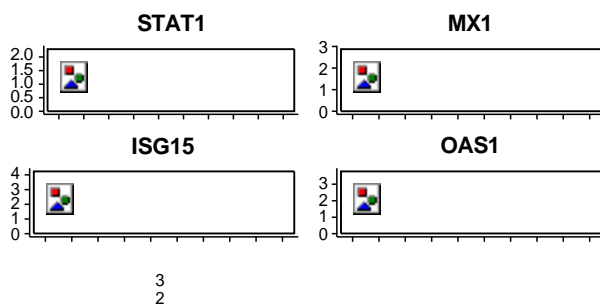


Figure A2.26: IRDS signature
Box plot of distribution of single, pre-treatment tumor cell's scores for the 45 gene IRDS signature.



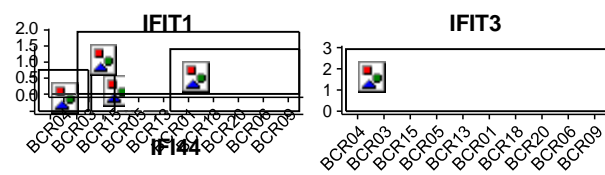


Figure A2.27: IRDS marker genes
Expression of top IRDS marker genes in pre-treatment tumor cells.

References

1. E.F. McCarthy, *The toxins of William B. Coley and the treatment of bone and soft-tissue sarcomas*. The Iowa orthopaedic journal, 2006. **26**: p. 154.
2. J. Larkin, V. Chiarion-Sileni, R. Gonzalez, J.J. Grob, C.L. Cowey, C.D. Lao, D. Schadendorf, R. Dummer, M. Smylie, and P. Rutkowski, *Combined nivolumab and ipilimumab or monotherapy in untreated melanoma*. New England journal of medicine, 2015. **373**(1): p. 23-34.
3. S. Antonia, S.B. Goldberg, A. Balmanoukian, J.E. Chaft, R.E. Sanborn, A. Gupta, R. Narwal, K. Steele, Y. Gu, and J.J. Karakunnel, *Safety and antitumour activity of durvalumab plus tremelimumab in non-small cell lung cancer: a multicentre, phase 1b study*. The lancet oncology, 2016. **17**(3): p. 299-308.
4. M.D. Hellmann, N.A. Rizvi, J.W. Goldman, S.N. Gettinger, H. Borghaei, J.R. Brahmer, N.E. Ready, D.E. Gerber, L.Q. Chow, and R.A. Juergens, *Nivolumab plus ipilimumab as first-line treatment for advanced non-small-cell lung cancer (CheckMate 012): results of an open-label, phase 1, multicohort study*. The lancet oncology, 2017. **18**(1): p. 31-41.
5. R.J. Motzer, B. Escudier, D.F. McDermott, S. George, H.J. Hammers, S. Srinivas, S.S. Tykodi, J.A. Sosman, G. Procopio, and E.R. Plimack, *Nivolumab versus everolimus in advanced renal-cell carcinoma*. New England Journal of Medicine, 2015. **373**(19): p. 1803-1813.
6. G. Erdag, J.T. Schaefer, M.E. Smolkin, D.H. Deacon, S.M. Shea, L.T. Dengel, J.W. Patterson, and C.L. Slingluff, *Immunotype and immunohistologic characteristics of tumor-infiltrating immune cells are associated with clinical outcome in metastatic melanoma*. Cancer research, 2012. **72**(5): p. 1070-1080.

7. S.E. Stanton and M.L. Disis, *Clinical significance of tumor-infiltrating lymphocytes in breast cancer*. Journal for immunotherapy of cancer, 2016. **4**(1): p. 1-7.
8. D.G. DeNardo, D.J. Brennan, E. Rexhepaj, B. Ruffell, S.L. Shiao, S.F. Madden, W.M. Gallagher, N. Wadhvani, S.D. Keil, and S.A. Junaid, *Leukocyte complexity predicts breast cancer survival and functionally regulates response to chemotherapy*. Cancer discovery, 2011. **1**(1): p. 54-67.
9. R.K. Cheung and P.J. Utz, *CyTOF—the next generation of cell detection*. Nature Reviews Rheumatology, 2011. **7**(9): p. 502-503.
10. E. Papalexi and R. Satija, *Single-cell RNA sequencing to explore immune cell heterogeneity*. Nature Reviews Immunology, 2018. **18**(1): p. 35-45.
11. H. Chen, F. Ye, and G. Guo, *Revolutionizing immunology with single-cell RNA sequencing*. Cellular & molecular immunology, 2019. **16**(3): p. 242-249.
12. D. Lähnemann, J. Köster, E. Szczurek, D.J. McCarthy, S.C. Hicks, M.D. Robinson, C.A. Vallejos, K.R. Campbell, N. Beerenwinkel, and A. Mahfouz, *Eleven grand challenges in single-cell data science*. Genome biology, 2020. **21**(1): p. 1-35.
13. S. Liu and C. Trapnell, *Single-cell transcriptome sequencing: recent advances and remaining challenges*. F1000Research, 2016. **5**.
14. O. Stegle, S.A. Teichmann, and J.C. Marioni, *Computational and analytical challenges in single-cell transcriptomics*. Nature Reviews Genetics, 2015. **16**(3): p. 133-145.
15. M.L. Suvà and I. Tirosh, *Single-cell RNA sequencing in cancer: lessons learned and emerging challenges*. Molecular cell, 2019. **75**(1): p. 7-12.
16. G.-C. Yuan, L. Cai, M. Elowitz, T. Enver, G. Fan, G. Guo, R. Irizarry, P. Kharchenko, J. Kim, and S. Orkin, *Challenges and emerging directions in single-cell analy-*

- sis. *Genome biology*, 2017. **18**(1): p. 1-8.
17. R. Elmentaite, C. Domínguez Conde, L. Yang, and S.A. Teichmann, *Single-cell atlases: shared and tissue-specific cell types across human organs*. *Nature Reviews Genetics*, 2022: p. 1-16.
 18. K.A. Janes, *Single-cell states versus single-cell atlases—two classes of heterogeneity that differ in meaning and method*. *Current opinion in biotechnology*, 2016. **39**: p. 120-125.
 19. V. Kumar, K. Ramnarayanan, R. Sundar, N. Padmanabhan, S. Srivastava, M. Koiwa, T. Yasuda, V. Koh, K.K. Huang, and S.T. Tay, *Single-Cell Atlas of Lineage States, Tumor Microenvironment, and Subtype-Specific Expression Programs in Gastric Cancer*. *Cancer discovery*, 2022. **12**(3): p. 670-691.
 20. R.G. Lindeboom, A. Regev, and S.A. Teichmann, *Towards a human cell atlas: taking notes from the past*. *Trends in Genetics*, 2021. **37**(7): p. 625-630.
 21. L. Ma, L. Wang, S.A. Khatib, C.-W. Chang, S. Heinrich, D.A. Dominguez, M. Forgues, J. Candia, M.O. Hernandez, and M. Kelly, *Single-cell atlas of tumor cell evolution in response to therapy in hepatocellular carcinoma and intrahepatic cholangiocarcinoma*. *Journal of hepatology*, 2021. **75**(6): p. 1397-1408.
 22. H. Massalha, K. Bahar Halpern, S. Abu-Gazala, T. Jana, E.E. Massasa, A.E. Moor, L. Buchauer, M. Rozenberg, E. Pikarsky, and I. Amit, *A single cell atlas of the human liver tumor microenvironment*. *Molecular systems biology*, 2020. **16**(12): p. e9682.
 23. P. Nieto, M. Elosua-Bayes, J.L. Trincado, D. Marchese, R. Massoni-Badosa, M. Salvany, A. Henriques, J. Nieto, S. Aguilar-Fernández, and E. Mereu, *A single-cell tumor immune atlas for precision oncology*. *Genome research*, 2021. **31**(10): p. 1913-1926.
 24. D. Osumi-Sutherland, C. Xu, M. Keays, A.P. Levine, P.V. Kharchenko, A. Regev,

- E. Lein, and S.A. Teichmann, *Cell type ontologies of the Human Cell Atlas*. Nature Cell Biology, 2021. **23**(11): p. 1129-1135.
25. S.R. Quake, *A decade of molecular cell atlases*. Trends in Genetics, 2022.
 26. J. Wagner, M.A. Rapsomaniki, S. Chevrier, T. Anzeneder, C. Langwieder, A. Dykgers, M. Rees, A. Ramaswamy, S. Muenst, and S.D. Soysal, *A single-cell atlas of the tumor and immune ecosystem of human breast cancer*. Cell, 2019. **177**(5): p. 1330-1345. e18.
 27. S.Z. Wu, G. Al-Eryani, D.L. Roden, S. Junankar, K. Harvey, A. Andersson, A. Thennavan, C. Wang, J.R. Torpy, and N. Bartonicek, *A single-cell and spatially resolved atlas of human breast cancers*. Nature genetics, 2021. **53**(9): p. 1334-1347.
 28. A.-C. Villani, R. Satija, G. Reynolds, S. Sarkizova, K. Shekhar, J. Fletcher, M. Griesbeck, A. Butler, S. Zheng, and S. Lazo, *Single-cell RNA-seq reveals new types of human blood dendritic cells, monocytes, and progenitors*. Science, 2017. **356**(6335).
 29. M. Sade-Feldman, K. Yizhak, S.L. Bjorgaard, J.P. Ray, C.G. de Boer, R.W. Jenkins, D.J. Lieb, J.H. Chen, D.T. Frederick, and M. Barzily-Rokni, *Defining T cell states associated with response to checkpoint immunotherapy in melanoma*. Cell, 2018. **175**(4): p. 998-1013.
 30. A.M. Van der Leun, D.S. Thommen, and T.N. Schumacher, *CD8⁺ T cell states in human cancer: insights from single-cell analysis*. Nature Reviews Cancer, 2020. **20**(4): p. 218-232.
 31. C.M. Laumont, M.C.A. Wouters, J. Smazynski, N.S. Gierc, E.A. Chavez, L.C. Chong, S. Thornton, K. Milne, J.R. Webb, and C. Steidl, *Single-cell Profiles and Prognostic Impact of Tumor-Infiltrating Lymphocytes Coexpressing CD39, CD103, and PD-1 in Ovarian Cancer*. Clinical Cancer Research, 2021.

32. A. Bassez, H. Vos, L. Van Dyck, G. Floris, I. Arijs, C. Desmedt, B. Boeckx, M.V. Bempt, I. Nevelsteen, and K. Lambein, *A single-cell map of intratumoral changes during anti-PD1 treatment of patients with breast cancer*. Nature Medicine, 2021. **27**(5): p. 820-832.
33. C.M. Laumont, M.C. Wouters, J. Smazynski, N.S. Gierc, E.A. Chavez, L.C. Chong, S. Thornton, K. Milne, J.R. Webb, and C. Steidl, *Single-cell profiles and prognostic impact of tumor-infiltrating lymphocytes coexpressing CD39, CD103, and PD-1 in ovarian cancer*. Clinical Cancer Research, 2021. **27**(14): p. 4089-4100.
34. A. Savino, N. De Marzo, P. Provero, and V. Poli, *Meta-analysis of microdissected breast tumors reveals genes regulated in the stroma but hidden in bulk analysis*. Cancers, 2021. **13**(13): p. 3371.
35. M. Tyler and I. Tirosh, *Decoupling epithelial-mesenchymal transitions from stromal profiles by integrative expression analysis*. Nature communications, 2021. **12**(1): p. 1-13.
36. C. Kim, R. Gao, E. Sei, R. Brandt, J. Hartman, T. Hatschek, N. Crosetto, T. Foukakis, and N.E. Navin, *Chemoresistance evolution in triple-negative breast cancer delineated by single-cell sequencing*. Cell, 2018. **173**(4): p. 879-893. e13.
37. Z.-F. Lim and P.C. Ma, *Emerging insights of tumor heterogeneity and drug resistance mechanisms in lung cancer targeted therapy*. Journal of hematology & oncology, 2019. **12**(1): p. 1-18.
38. F. Chiarini, C. Evangelisti, G. Lattanzi, J.A. McCubrey, and A.M. Martelli, *Advances in understanding the mechanisms of evasive and innate resistance to mTOR inhibition in cancer cells*. Biochimica et Biophysica Acta (BBA)-Molecular Cell Research, 2019. **1866**(8): p. 1322-1337.
39. S. Seth, C.-Y. Li, I.-L. Ho, D. Corti, S. Loponte, L. Sapio, E. Del Poggetto, E.-Y. Yen, F.S. Robinson, and M. Peoples, *Pre-existing functional heterogeneity of tum-*

- origenic compartment as the origin of chemoresistance in pancreatic tumors*. Cell reports, 2019. **26**(6): p. 1518-1532. e9.
40. C.A. Stewart, C.M. Gay, Y. Xi, S. Sivajothi, V. Sivakamasundari, J. Fujimoto, M. Bolisetty, P.M. Hartsfield, V. Balasubramaniyan, and M.D. Chalisehar, *Single-cell analyses reveal increased intratumoral heterogeneity after the onset of therapy resistance in small-cell lung cancer*. Nature Cancer, 2020. **1**(4): p. 423-436.
 41. R.L. Siegel, K.D. Miller, and A. Jemal, *Cancer statistics, 2019*. CA: a cancer journal for clinicians, 2019. **69**(1): p. 7-34.
 42. D.P. Ryan, T.S. Hong, and N. Bardeesy, *Pancreatic adenocarcinoma*. New England Journal of Medicine, 2014. **371**(11): p. 1039-1049.
 43. J. Kleeff, M. Korc, M. Apte, C. La Vecchia, C.D. Johnson, A.V. Biankin, R.E. Neale, M. Tempero, D.A. Tuveson, and R.H. Hruban, *Pancreatic cancer*. Nature reviews Disease primers, 2016. **2**(1): p. 1-22.
 44. S.S. Neelapu, F.L. Locke, N.L. Bartlett, L.J. Lekakis, D.B. Miklos, C.A. Jacobson, I. Braunschweig, O.O. Oluwole, T. Siddiqi, and Y. Lin, *Axicabtagene ciloleucel CAR T-cell therapy in refractory large B-cell lymphoma*. New England Journal of Medicine, 2017. **377**(26): p. 2531-2544.
 45. S.L. Maude, T.W. Laetsch, J. Buechner, S. Rives, M. Boyer, H. Bittencourt, P. Bader, M.R. Verneris, H.E. Stefanski, and G.D. Myers, *Tisagenlecleucel in children and young adults with B-cell lymphoblastic leukemia*. New England Journal of Medicine, 2018. **378**(5): p. 439-448.
 46. S.A. Rosenberg, J.C. Yang, R.M. Sherry, U.S. Kammula, M.S. Hughes, G.Q. Phan, D.E. Citrin, N.P. Restifo, P.F. Robbins, and J.R. Wunderlich, *Durable complete responses in heavily pretreated patients with metastatic melanoma using T-cell transfer immunotherapy*. Clinical cancer research, 2011. **17**(13): p. 4550-4557.

47. M.-A. Forget, C. Haymaker, K.R. Hess, Y.J. Meng, C. Creasy, T. Karpinets, O.J. Fulbright, J. Roszik, S.E. Woodman, and Y.U. Kim, *Prospective analysis of adoptive TIL therapy in patients with metastatic melanoma: response, impact of anti-CTLA4, and biomarkers to predict clinical outcome*. Clinical Cancer Research, 2018. **24**(18): p. 4416-4428.
48. S.A. Rosenberg, B.S. Packard, P.M. Aebbersold, D. Solomon, S.L. Topalian, S.T. Toy, P. Simon, M.T. Lotze, J.C. Yang, and C.A. Seipp, *Use of tumor-infiltrating lymphocytes and interleukin-2 in the immunotherapy of patients with metastatic melanoma*. New England Journal of Medicine, 1988. **319**(25): p. 1676-1680.
49. M.E. Dudley, J.C. Yang, R. Sherry, M.S. Hughes, R. Royal, U. Kammula, P.F. Robbins, J. Huang, D.E. Citrin, and S.F. Leitman, *Adoptive cell therapy for patients with metastatic melanoma: evaluation of intensive myeloablative chemoradiation preparative regimens*. Journal of Clinical Oncology, 2008. **26**(32): p. 5233.
50. M.E. Dudley, J.R. Wunderlich, J.C. Yang, R.M. Sherry, S.L. Topalian, N.P. Restifo, R.E. Royal, U. Kammula, D.E. White, and S.A. Mavroukakis, *Adoptive cell transfer therapy following non-myeloablative but lymphodepleting chemotherapy for the treatment of patients with refractory metastatic melanoma*. Journal of clinical oncology: official journal of the American Society of Clinical Oncology, 2005. **23**(10): p. 2346.
51. D. Sakellariou-Thompson, M.-A. Forget, C. Creasy, V. Bernard, L. Zhao, Y.U. Kim, M.W. Hurd, N. Uraoka, E.R. Parra, and Y.a. Kang, *4-1BB agonist focuses CD8+ tumor-infiltrating T-cell growth into a distinct repertoire capable of tumor recognition in pancreatic cancer*. Clinical Cancer Research, 2017. **23**(23): p. 7263-7275.
52. C.A. Klebanoff, L. Gattinoni, P. Torabi-Parizi, K. Kerstann, A.R. Cardones, S.E. Finkelstein, D.C. Palmer, P.A. Antony, S.T. Hwang, and S.A. Rosenberg, *Central memory self/tumor-reactive CD8+ T cells confer superior antitumor immunity compared with effector memory T cells*. Proceedings of the national academy of

- sciences, 2005. **102**(27): p. 9571-9576.
53. L. Gattinoni, C.A. Klebanoff, D.C. Palmer, C. Wrzesinski, K. Kerstann, Z. Yu, S.E. Finkelstein, M.R. Theoret, S.A. Rosenberg, and N.P. Restifo, *Acquisition of full effector function in vitro paradoxically impairs the in vivo antitumor efficacy of adoptively transferred CD8⁺ T cells*. The Journal of clinical investigation, 2005. **115**(6): p. 1616-1626.
 54. M. Kurachi. *CD8⁺ T cell exhaustion*. in *Seminars in immunopathology*. 2019. Springer.
 55. C.U. Blank, W.N. Haining, W. Held, P.G. Hogan, A. Kallies, E. Lugli, R.C. Lynn, M. Philip, A. Rao, and N.P. Restifo, *Defining 'T cell exhaustion'*. Nature Reviews Immunology, 2019. **19**(11): p. 665-674.
 56. M. Ando, M. Ito, T. Srirat, T. Kondo, and A. Yoshimura, *Memory T cell, exhaustion, and tumor immunity*. Immunological medicine, 2020. **43**(1): p. 1-9.
 57. Y. Ino, R. Yamazaki-Itoh, K. Shimada, M. Iwasaki, T. Kosuge, Y. Kanai, and N. Hiraoka, *Immune cell infiltration as an indicator of the immune microenvironment of pancreatic cancer*. British journal of cancer, 2013. **108**(4): p. 914-923.
 58. J. Li, J. Wang, R. Chen, Y. Bai, and X. Lu, *The prognostic value of tumor-infiltrating T lymphocytes in ovarian cancer*. Oncotarget, 2017. **8**(9): p. 15621.
 59. Y. Togashi, K. Shitara, and H. Nishikawa, *Regulatory T cells in cancer immunosuppression—implications for anticancer therapy*. Nature reviews Clinical oncology, 2019. **16**(6): p. 356-371.
 60. M. Kurachi. *CD8⁺ T cell exhaustion*. Springer.
 61. J.R. Webb, K. Milne, P. Watson, R.J. DeLeeuw, and B.H. Nelson, *Tumor-infiltrating lymphocytes expressing the tissue resident memory marker CD103 are associated with increased survival in high-grade serous ovarian cancer*. Clinical cancer

- research, 2014. **20**(2): p. 434-444.
62. J. Edwards, J.S. Wilmott, J. Madore, T.N. Gide, C. Quek, A. Tasker, A. Ferguson, J. Chen, R. Hewavisenti, and P. Hersey, *Cd103+ tumor-resident cd8+ t cells are associated with improved survival in immunotherapy-naïve melanoma patients and expand significantly during anti-pd-1 treatment*. Clinical Cancer Research, 2018. **24**(13): p. 3036-3045.
 63. A. Pasetto, A. Gros, P.F. Robbins, D.C. Deniger, T.D. Prickett, R. Matus-Nicodem- os, D.C. Douek, B. Howie, H. Robins, and M.R. Parkhurst, *Tumor-and neoanti- gen-reactive T-cell receptors can be identified based on their frequency in fresh tumor*. Cancer immunology research, 2016. **4**(9): p. 734-743.
 64. C. Chougnet and D. Hildeman, *Helios—controller of Treg stability and function*. Translational cancer research, 2016. **5**(Suppl 2): p. S338.
 65. A.M. Magnuson, E. Kiner, A. Ergun, J.S. Park, N. Asinovski, A. Ortiz-Lopez, A. Kil- coyne, E. Paoluzzi-Tomada, R. Weissleder, and D. Mathis, *Identification and vali- dation of a tumor-infiltrating Treg transcriptional signature conserved across spe- cies and tumor types*. Proceedings of the National Academy of Sciences, 2018. **115**(45): p. E10672-E10681.
 66. K.R. Shadidi, T. Aarvak, J.E. Henriksen, J.B. Natvig, and K.M. Thompson, *The chemokines CCL5, CCL2 and CXCL12 play significant roles in the migration of Th1 cells into rheumatoid synovial tissue*. Scandinavian journal of immunology, 2003. **57**(2): p. 192-198.
 67. S. Park, B. Griesenauer, H. Jiang, D. Adom, P. Mehrpouya-Bahrami, S. Chakravorty, M. Kazemian, T. Imam, R. Srivastava, and T.A. Hayes, *Granzyme A–producing T helper cells are critical for acute graft-versus-host disease*. JCI insight, 2020. **5**(18).
 68. E. Cano-Gamez, B. Soskic, T.I. Roumeliotis, E. So, D.J. Smyth, M. Baldrighi, D.

- Willé, N. Nakic, J. Esparza-Gordillo, and C.G.C. Larminie, *Single-cell transcriptomics identifies an effectorness gradient shaping the response of CD4+ T cells to cytokines*. Nature communications, 2020. **11**(1): p. 1-15.
69. E. Azizi, A.J. Carr, G. Plitas, A.E. Cornish, C. Konopacki, S. Prabhakaran, J. Nainys, K. Wu, V. Kisieliovas, and M. Setty, *Single-cell map of diverse immune phenotypes in the breast tumor microenvironment*. Cell, 2018. **174**(5): p. 1293-1308.
 70. C. Zheng, L. Zheng, J.-K. Yoo, H. Guo, Y. Zhang, X. Guo, B. Kang, R. Hu, J.Y. Huang, and Q. Zhang, *Landscape of infiltrating T cells in liver cancer revealed by single-cell sequencing*. Cell, 2017. **169**(7): p. 1342-1356.
 71. L.K. Mackay, M. Minnich, N.A.M. Kragten, Y. Liao, B. Nota, C. Seillet, A. Zaid, K. Man, S. Preston, and D. Freestone, *Hobit and Blimp1 instruct a universal transcriptional program of tissue residency in lymphocytes*. Science, 2016. **352**(6284): p. 459-463.
 72. S.N. Mueller and L.K. Mackay, *Tissue-resident memory T cells: local specialists in immune defence*. Nature Reviews Immunology, 2016. **16**(2): p. 79-89.
 73. E.C. Reilly, K.L. Emo, P.M. Buckley, N.S. Reilly, I. Smith, F.A. Chaves, H. Yang, P.W. Oakes, and D.J. Topham, *TRM integrins CD103 and CD49a differentially support adherence and motility after resolution of influenza virus infection*. Proceedings of the National Academy of Sciences, 2020. **117**(22): p. 12306-12314.
 74. X. Guo, Y. Zhang, L. Zheng, C. Zheng, J. Song, Q. Zhang, B. Kang, Z. Liu, L. Jin, and R. Xing, *Global characterization of T cells in non-small-cell lung cancer by single-cell sequencing*. Nature medicine, 2018. **24**(7): p. 978-985.
 75. S.M. Vareki, *High and low mutational burden tumors versus immunologically hot and cold tumors and response to immune checkpoint inhibitors*. Journal for immunotherapy of cancer, 2018. **6**(1): p. 1-5.

76. P. Bonaventura, T. Shekarian, V. Alcazer, J. Valladeau-Guilemond, S. Valsecia-Wittmann, S. Amigorena, C. Caux, and S. Depil, *Cold tumors: a therapeutic challenge for immunotherapy*. *Frontiers in immunology*, 2019. **10**: p. 168.
77. Y. Zhang, H. Chen, H. Mo, X. Hu, R. Gao, Y. Zhao, B. Liu, L. Niu, X. Sun, and X. Yu, *Single-cell analyses reveal key immune cell subsets associated with response to PD-L1 blockade in triple-negative breast cancer*. *Cancer Cell*, 2021.
78. M. Ashrafizadeh, B. Farhood, A.E. Musa, S. Taeb, and M. Najafi, *Damage-associated molecular patterns in tumor radiotherapy*. *International Immunopharmacology*, 2020. **86**: p. 106761.
79. M. McLaughlin, E.C. Patin, M. Pedersen, A. Wilkins, M.T. Dillon, A.A. Melcher, and K.J. Harrington, *Inflammatory microenvironment remodelling by tumour cells after radiotherapy*. *Nature Reviews Cancer*, 2020. **20**(4): p. 203-217.
80. A. Sharma, B. Bode, R.H. Wenger, K. Lehmann, A.A. Sartori, H. Moch, A. Knuth, L. von Boehmer, and M. van den Broek, γ -Radiation promotes immunological recognition of cancer cells through increased expression of cancer-testis antigens in vitro and in vivo. *PloS one*, 2011. **6**(11): p. e28217.
81. A.B. Sharabi, C.J. Nirschl, C.M. Kochel, T.R. Nirschl, B.J. Francica, E. Velarde, T.L. Deweese, and C.G. Drake, *Stereotactic radiation therapy augments antigen-specific PD-1-mediated antitumor immune responses via cross-presentation of tumor antigen*. *Cancer immunology research*, 2015. **3**(4): p. 345-355.
82. E.A. Reits, J.W. Hodge, C.A. Herberts, T.A. Groothuis, M. Chakraborty, E. K Wansley, K. Camphausen, R.M. Luiten, A.H. de Ru, and J. Neijssen, *Radiation modulates the peptide repertoire, enhances MHC class I expression, and induces successful antitumor immunotherapy*. *Journal of Experimental Medicine*, 2006. **203**(5): p. 1259-1271.
83. X. Wang, L. Yang, F. Huang, Q. Zhang, S. Liu, L. Ma, and Z. You, *Inflammatory*

- cytokines IL-17 and TNF- α up-regulate PD-L1 expression in human prostate and colon cancer cells*. Immunology letters, 2017. **184**: p. 7-14.
84. X. Zhang, Y. Zeng, Q. Qu, J. Zhu, Z. Liu, W. Ning, H. Zeng, N. Zhang, W. Du, and C. Chen, *PD-L1 induced by IFN- γ from tumor-associated macrophages via the JAK/STAT3 and PI3K/AKT signaling pathways promoted progression of lung cancer*. International journal of clinical oncology, 2017. **22**(6): p. 1026-1033.
 85. S. Chen, G.A. Crabill, T.S. Pritchard, T.L. McMiller, P. Wei, D.M. Pardoll, F. Pan, and S.L. Topalian, *Mechanisms regulating PD-L1 expression on tumor and immune cells*. Journal for immunotherapy of cancer, 2019. **7**(1): p. 1-12.
 86. H. Liang, L. Deng, Y. Hou, X. Meng, X. Huang, E. Rao, W. Zheng, H. Mauceri, M. Mack, and M. Xu, *Host STING-dependent MDSC mobilization drives extrinsic radiation resistance*. Nature communications, 2017. **8**(1): p. 1-10.
 87. X. Yang, J. Darling, T. McMillan, J. Peacock, and G. Steel, *Heterogeneity of radio-sensitivity in a human glioma cell line*. International Journal of Radiation Oncology* Biology* Physics, 1992. **22**(1): p. 103-108.
 88. R. Britten, A. Evans, M. Allalunis-Turner, A. Franko, and R. Pearcey, *Intratumoral heterogeneity as a confounding factor in clonogenic assays for tumour radiore-sponsiveness*. Radiotherapy and oncology, 1996. **39**(2): p. 145-153.
 89. T. Nakagomi, T. Goto, Y. Hirotsu, D. Shikata, K. Amemiya, T. Oyama, H. Mochizuki, and M. Omata, *Elucidation of radiation-resistant clones by a serial study of intratumor heterogeneity before and after stereotactic radiotherapy in lung cancer*. Journal of Thoracic Disease, 2017. **9**(7): p. E598.
 90. J. Alfonso and L. Berk, *Modeling the effect of intratumoral heterogeneity of radio-sensitivity on tumor response over the course of fractionated radiation therapy*. Radiation Oncology, 2019. **14**(1): p. 1-12.
 91. J. Yu, J. Yan, Q. Guo, Z. Chi, B. Tang, B. Zheng, J. Yu, T. Yin, Z. Cheng, and X.

- Wu, *Genetic aberrations in the CDK4 pathway are associated with innate resistance to PD-1 blockade in Chinese patients with non-cutaneous melanoma*. Clinical Cancer Research, 2019. **25**(21): p. 6511-6523.
92. J. Boshuizen, D.W. Vredevoogd, O. Krijgsman, M.A. Ligtenberg, S. Blankenstein, B. de Bruijn, D.T. Frederick, J.C. Kenski, M. Parren, and M. Brüggemann, *Reversal of pre-existing NGFR-driven tumor and immune therapy resistance*. Nature communications, 2020. **11**(1): p. 1-13.
 93. N. Navin, J. Kendall, J. Troge, P. Andrews, L. Rodgers, J. McIndoo, K. Cook, A. Stepansky, D. Levy, and D. Esposito, *Tumour evolution inferred by single-cell sequencing*. Nature, 2011. **472**(7341): p. 90-94.
 94. D.C. Minussi, M.D. Nicholson, H. Ye, A. Davis, K. Wang, T. Baker, M. Tarabichi, E. Sei, H. Du, and M. Rabbani, *Breast tumours maintain a reservoir of subclonal diversity during expansion*. Nature, 2021. **592**(7853): p. 302-308.
 95. T. Nguyen-Hoai, M. Pham-Duc, M. Gries, B. Dörken, A. Pezzutto, and J. Westermann, *CCL4 as an adjuvant for DNA vaccination in a Her2/neu mouse tumor model*. Cancer gene therapy, 2016. **23**(6): p. 162-167.
 96. M. De la Fuente López, G. Landskron, D. Parada, K. Dubois-Camacho, D. Simian, M. Martinez, D. Romero, J.C. Roa, I. Chahuán, and R. Gutiérrez, *The relationship between chemokines CCL2, CCL3, and CCL4 with the tumor microenvironment and tumor-associated macrophage markers in colorectal cancer*. Tumor Biology, 2018. **40**(11): p. 1010428318810059.
 97. N. Mukaida, S.-i. Sasaki, and T. Baba, *CCL4 signaling in the tumor microenvironment*. Tumor Microenvironment, 2020: p. 23-32.
 98. S. Dai, H. Zeng, Z. Liu, K. Jin, W. Jiang, Z. Wang, Z. Lin, Y. Xiong, J. Wang, and Y. Chang, *Intratumoral CXCL13+ CD8+ T cell infiltration determines poor clinical outcomes and immunoevasive contexture in patients with clear cell renal cell car-*

- cinoma*. Journal for immunotherapy of cancer, 2021. **9**(2).
99. K.E. Yost, A.T. Satpathy, D.K. Wells, Y. Qi, C. Wang, R. Kageyama, K.L. McNamara, J.M. Granja, K.Y. Sarin, and R.A. Brown, *Clonal replacement of tumor-specific T cells following PD-1 blockade*. Nature medicine, 2019. **25**(8): p. 1251-1259.
 100. J. Chen, Y. Yao, C. Gong, F. Yu, S. Su, J. Chen, B. Liu, H. Deng, F. Wang, and L. Lin, *CCL18 from tumor-associated macrophages promotes breast cancer metastasis via PITPNM3*. Cancer cell, 2011. **19**(4): p. 541-555.
 101. I.U. Schraufstatter, M. Zhao, S.K. Khaldoyanidi, and R.G. DiScipio, *The chemokine CCL18 causes maturation of cultured monocytes to macrophages in the M2 spectrum*. Immunology, 2012. **135**(4): p. 287-298.
 102. L. Lin, Y.-S. Chen, Y.-D. Yao, J.-Q. Chen, J.-N. Chen, S.-Y. Huang, Y.-J. Zeng, H.-R. Yao, S.-H. Zeng, and Y.-S. Fu, *CCL18 from tumor-associated macrophages promotes angiogenesis in breast cancer*. Oncotarget, 2015. **6**(33): p. 34758.
 103. M.L. Pinto, E. Rios, A.C. Silva, S.C. Neves, H.R. Caires, A.T. Pinto, C. Duraes, F.A. Carvalho, A.P. Cardoso, and N.C. Santos, *Decellularized human colorectal cancer matrices polarize macrophages towards an anti-inflammatory phenotype promoting cancer cell invasion via CCL18*. Biomaterials, 2017. **124**: p. 211-224.
 104. H.M. Mohan, C.M. Aherne, A.C. Rogers, A.W. Baird, D.C. Winter, and E.P. Murphy, *Molecular pathways: the role of NR4A orphan nuclear receptors in cancer*. Clinical cancer research, 2012. **18**(12): p. 3223-3228.
 105. H. Wu, J. Bi, Y. Peng, L. Huo, X. Yu, Z. Yang, Y. Zhou, L. Qin, Y. Xu, and L. Liao, *Nuclear receptor NR4A1 is a tumor suppressor down-regulated in triple-negative breast cancer*. Oncotarget, 2017. **8**(33): p. 54364.
 106. B. Zhu, J.-R. Yang, Y. Jia, P. Zhang, L. Shen, X.-L. Li, J. Li, and B. Wang, *Over-expression of NR4A1 is associated with tumor recurrence and poor survival in non-small-cell lung carcinoma*. Oncotarget, 2017. **8**(69): p. 113977.

107. E.D. Adamson and D. Mercola, *Egr1 transcription factor: multiple roles in prostate tumor cell growth and survival*. Tumor biology, 2002. **23**(2): p. 93-102.
108. M. Yang, W. Teng, Y. Qu, H. Wang, and Q. Yuan, *Sulforaphene inhibits triple negative breast cancer through activating tumor suppressor Egr1*. Breast cancer research and treatment, 2016. **158**(2): p. 277-286.

Vitae

Aislyn Pamela Schalck is the daughter of Becky Lea Dow and Richard Lancy Schalck. After completing her work at Amesbury High School, Amesbury, Massachusetts in 2009, she entered the Massachusetts Institute of Technology in Cambridge, Massachusetts. She received a degree of Bachelor of Science with a major in Bioengineering from MIT in June, 2013. For the next two years, she worked as a research technician in the Department of Medical Oncology at Massachusetts General Hospital. In August of 2015 she entered The University of Texas MD Anderson Cancer Center UTHealth Graduate School of Biomedical Sciences.

Permanent address:

918 W 30th St

Houston, Texas 77018